Monopile upending workability and techniques

G. A. van der Veen

Juli 2019

TU Delft

Monopile upending workability and techniques

by

G. A. van der Veen

to obtain the degree of Master of Science
at the Delft University of Technology,
to be defended publicly on Friday Juli 19, 2019 at 9:00 AM.

Student number:	4285298	
Project duration:	December 10, 2018 – Juli 19, 2019	
Thesis committee:	dr. A. J. Laguna,	TU Delft, supervisor
	Prof. A. Metrikine,	TU Delft
	Ir. K. van der Heiden,	Jumbo Maritime

An electronic version of this thesis is available at `http://repository.tudelft.nl/`.

TU Delft

Preface

This research has been conducted at Jumbo Maritime to obtain a masters degree in Offshore & Dredging Engineering at the Delft University of Technology. The assignment is a consequence of the growing offshore wind industry. During my research I got help from a lot of people who I would like to thank for their time and understanding.

First I want to thank Jumbo Maritime to be able to do my master thesis at an interesting and innovative company in Schiedam. I would also like to thank my daily supervisor Kasper van der Heiden for his help, guidance and the freedom he gave me during my master thesis.

The help and support from the Delft University of Technology was also unmissable. Therefor I would like to thank Antonio Jarquin Laguna as my daily supervisor for his fast and help-full answers to my questions. Finally I would like to thank my graduation chairman Andrei Metrikine for his very usefull and to the point questions and remarks during our meetings and for taking his time to answer my questions despite his full agenda.

G. A. van der Veen
Delft, Juli 2019

Abstract

To respond to the growing offshore industry Jumbo Maritime has designed a new vessel to expand its offshore fleet: The Stella Synergy. The vessel will be able to install monopiles for the offshore wind and oil and gas industry. The main objective of this thesis is: Making a model that is able to predict the motions of the vessel as well as the forces induced by the monopile on the vessel during the monopile installation process.

The most suitable upending technique has been chosen by comparing different upending methods. The techniques that are possible for the Stella Synergy are: A separate upending frame, Upending in water, Upending using multiple hooks and upending with the gripper. The different techniques are analysed using a multi criteria analysis. Upending with the gripper turned out to be the best choice. The gripper design has been chosen in the same way. The designs possible on the Stella Synergy are: Linear two arm gripper, linear four or more arm gripper rotating two arm gripper and a subsea frame. The criteria used are: Workability, easy of use for upending, versatility and cost. The two rotating arm and linear four arm grippers score the highest , there for one of these two grippers is advised.

The best upending location is chosen using the vessels motions. The $\boldsymbol{A}$, $\boldsymbol{B}$ and $\boldsymbol{H_{FZ}}$ matrices are obtained using AQWA and imported into matlab where the RAOs of the vessel are calculated. These are compared with the measured RAOs by Marin and are almost similar. When the crane hoisting curve is taken into account only two possible upending locations remain: $x = 42m$ and $x = 70m$. Both locations are on the starboard side of the vessel. At the location $x = 70m$ the motions are far less severe. A disadvantage of this location is that only monopiles up to 100 m can be placed into the gripper without coming to close to the secondary crane.

The forces on the crane and gripper during upending and the workability of upending have been examined using a model in Matlab. The upending process is split up in six phases. Because the monopile is partly under water during four of the six phases the wave forces, added mass and damping that act on the monopile are obtained using AQWA. The viscous damping is calculated using the drag coefficient of a cylinder. The dynamic forces are the biggest during phase 3. The static forces during phase 1 to 5 are really low. Therefor the workability of upending in phase six is computed, the workability is: 34.3%.

The workability of the vessel while it is hoisting a monopile from a barge onto the gripper is investigated using a ten degree of freedom model: six degree of freedom of the vessel, the lower and upper offlead angles and the lower and upper sidelead angles. The natural frequencies of the model are calculated and compared with the RAO plots. The total workability for a hoisting cable length of 64m is: 29.9% and for 80m it is: 27.9%. Increasing the offlead angle from one to two degrees will increase the workability to: 44.0% for 80m and 36.7% for 64m. It is advised to look into increasing the maximum offlead angle of the crane.

Contents

Nomenclature

Abbreviations

CoG	Center of Gravity
DAF	Dynamic amplification factor
DP	Dynamic positioning
$JONSWAP$	Joint North Sea Observation Project
MCA	Multi Criteria Analysis
MPM	Most Probable Maximum

Symbols

$\boldsymbol{A}$	Added mass matrix	
$\boldsymbol{B_{add}}$	viscous damping matrix	
$\boldsymbol{B}$	Damping matrix	
$\boldsymbol{CoG}$	Center of gravity	
$\boldsymbol{C}$	Stiffness matrix	
$\boldsymbol{F_D}$	Diffraction forces vector	
$\boldsymbol{F_W}$	Undisturbed wave forces vector	
$\boldsymbol{H_{fz}}$	Undisturbed and diffraction wave forces divided by wave height	
$\boldsymbol{L}$	RAO transformation matrix	
$\boldsymbol{M}$	Mass matrix including added mass	
$\boldsymbol{m}$	Mass matrix excluding added mass	
$\boldsymbol{RAO}$	Response Amplitude Operator matrix	
$\boldsymbol{X}$	displacement vector	
ϵ	Phase angle	rad
Γ	Wave spreading factor	
λ	eigenvalues of system	
μ	Wave direction	$^\circ$
∇	volume displacement	m^3
ν	Kinematic viscosity	$m^2 s$
ω	Angular velocity	$\frac{rad}{s}$
ϕ	Roll of vessel	rad
ϕ_{c1}	Upper hoisting angle in ϕ direction	rad

ϕ_{c2}	Lower hoisting angle in ϕ direction	rad
ψ	Yaw of vessel	rad
ρ	density	$\frac{kg}{m^3}$
θ	Pitch of vessel	rad
θ_u	upending angle	$^\circ$
θ_{c1}	Upper hoisting angle in θ direction	rad
θ_{c2}	Lower hoisting angle in θ direction	rad
ζ_a	Wave amplitude	m
A	Surface area	m^2
a	Distance from CoG to point in x direction	m
$a_{i,j}$	Added mass	kg
A_{wp}	waterplane surface area	m^2
acc	acceleration	$\frac{m}{s^2}$
b	Distance from CoG to point in y direction	m
$b_{i,j}$	Damping	$\frac{Ns}{m}$
BM	Distance CoB to metacenter in z direction	m
c	Distance from CoG to point in z direction	m
C_D	Drag coefficient	
c_{cable}	Cable stiffness	Nm
$c_{i,j}$	Stiffness	$\frac{N}{m}$
CoB	Center of Buoyancy	m
CoF	Center of Flotation	m
D	Distribution of wave energy over directions	
d	Water depth	m
E	Directional wave spectrum	
E	Youngs modulus	Pa
F	total Force	N
F_b	Buoyancy force	N
F_d	Diffraction forces	N
F_r	Radiation forces	N
F_s	Hydro-static forces	N
F_w	Undisturbed incoming wave forces	N
F_x	Force on vessel in x direction	N

F_y	Force on vessel in y direction	N
F_z	Force on vessel in z direction	N
g	gravitational constant of earth	$\frac{m}{s^2}$
GM_L	Longitudal Metacentric height	m
GM_T	Transverse Metacentric height	m
H	Individual wave height	m
H_r	Root mean square of wave height	m
Hs	Significant wave height	m
I_L	Longitudinal buoyancy moment of inertia	m^4
I_T	Transverse buoyancy moment of inertia	m^4
I_{xx}	Moment of inertia around the x axis	m^2kg
I_{yy}	Moment of inertia around the y axis	m^2kg
I_{zz}	Moment of inertia around the z axis	m^2kg
k	Wave number	
KB	Distance from keel to center of buoyancy in z direction	m
KC	Keulegan and Carpenter number	
KG	Distance from keel to CoG in z direction	m
L	Characteristic length	m
l_1	length of total hoisting cable	m
l_2	length of lower hoisting cable	m
l_c	length between hook and crane	m
l_w	length between waterline and $z = 0$	m
l_{mp}	Length of monopile	m
$l_{submerged}$	Submerged length of monopile	m
l_{total}	total hoisting cable length	m
l_{w2}	length between bottom of monopile and waterline	m
m	Mass	kg
$m0$	Zeroth moment	
M_b	Buoyancy moment	Nm
M_x	Moment on vessel around x direction	Nm
M_y	Moment on vessel around y direction	Nm
M_z	Moment on vessel around z direction	Nm
N	Correction factor of D	
n	Number of waves that passes	m

n_f	number of falls	
OL	Offlead angle	$^\circ$
$r_{ballast}$	Distance in x direction from CoG to CoG of ballast	m
r_{xx}	Radius of gyration around the x axis	m
r_{yy}	Radius of gyration around the y axis	m
r_{zz}	Radius of gyration around the z axis	m
RAO	Response Amplitude Operator	$\frac{m}{m}$
RAO_{amp}	Amplitude of the Response Amplitude Operator	$\frac{m}{m}$
Re	Reynolds number	
S_ζ	Directionless wave spectrum	
S_z	Response spectrum for heave	
SL	Sidelead angle	$^\circ$
T	Kinetic energy	J
T_{total}	Total installation time	s
Tp	Peak wave period	s
Tz	Zero crossing wave period	s
u_a	flow velocity amplitude	$\frac{m}{s}$
V	Potential energy	J
V	Velocity	$\frac{m}{s}$
v	eigenvector of system	
x	Surge of vessel	m
y	Sway of vessel	m
z	Heave of vessel	m
z_a	Heave amplitude	m

List of Figures

List of Tables

1 Introduction

1.1. Company Introduction

Jumbo is a heavy lift shipping and offshore transportation and installation contractor. Jumbo was founded in 1948 by Hans Kahn, his motto was: Not everything can be transported inside a shipping container. In 1956 the company bought its first ship and started transporting bulky and heavy loads. The ship had four 12 ton cranes. The first ship was a success and soon more ships were ordered. Every next iteration off ships became stronger, more efficient or faster. In 2003 Jumbo entered a new industry: The offshore installation industry.

Jumbo is currently planning to build a new vessel: the Stella Synergy, a multi purpose offshore installation vessel with a length of 185.4m. The vessel will be able to install equipment for the oil and gas industry as well as monopiles and other parts for the offshore wind industry. It has a main crane that is capable of lifting 2500 tons and an auxiliary crane that can lift 600 tons. It will be able to work in arctic conditions and will be the biggest ship that utilizes an axe bow. The vessel will use a dual fuel system, which makes it capable of using LNG as a fuel, making it a more environmentally friendly vessel. It will be equipped with a class 2 Dynamic Positioning system.

Figure 1.1: Render of the Stella Synergy

1.2. Background Information

To reduce the cost of green energy wind turbines are getting bigger every generation. Especially the offshore windturbines are growing substantially. The new 12 MW offshore wind turbine of General Electrics will be 260 meter tall and the monopile will have a diameter of 10 m.[General-electric, 2018]
The increasing size of windturbines from 2015 to 2020 can be seen in Table 1.1.

Table 1.1: Changing wind turbine and monopile dimension over time [Buitendijk, 2016]

Year	2015	2017	2020	
Turbine capacity	4	8	12	MW
Rotor diameter	130	165	200	m
Water depth	30	40	50	m
Monopile length	65	80	90	m
Monopile diameter	7	8	10	m
Monopile weight	800	1300	2200	ton

Installing these huge monopiles requires bigger ships. Also the oil and gas industry is using monopiles more often for small and more automated oil and gas fields like the one M7-A tower which Oranje Nassau Energy is using in the M07-A field north of Terschelling. [van der Steen, 2017] The Stella Synergy will be capable of installing these monopiles. To remain flexible and be able to install the bigger future monopile sizes Jumbo wants the vessel to be able to install monopiles with a size range from six to twelve meters in diameter and weights from 1000 to 2500 metric tonnes.

The installation of a modern offshore windturbine consists of the following steps:

1 Monopile installation

2 Transition piece installation

3 Tower installation

4 Nacelle installation

5 Blades installation

The Stella Synergy will be able to install the monopiles, the transition pieces and the bottom parts of the towers. To install the higher parts of the wind-turbine a bottom-founded ship is needed like a jack up. A collaboration with Mammoet is being considered to combine the Stella Synergia with a climbing crane that can install the top part of the tower as well as the nacelle and the blades. The climbing crane will be installed on the bottom part of the tower using the crane of a Jumbo ship. The focus of this thesis will be on step one: The monopile installation. The Stella Synergy has to do the following steps to install monopiles for wind turbines:

1 Loading of monopiles onto ship

2 Transit

3 Arrival and start of station keeping using DP or moorings

4 Monopile upending

5 Lowering of monopile to the seabed

6 Installing noise mitigation screen

7 Installing of the hammer

8 Driving of monopile and correcting for tilt

[ir. Joost den Haan, 2018]

1.3. Problem Analysis

The building process of the Stella Synergy will start soon. Jumbo has not jet decided on the equipment and techniques for step four until six: A gripper during the driving of the piles and an upending device to support the monopile during upending. The method used and the position of the upending device and the gripper that will be used during the driving of the piles are also not determined yet. The monopile installation process and equipment must be designed in such a way that:

- The operation goes as fast as possible, this most of the time means that the method with the least amount of lifts is the best. Reattaching the monopile to the crane hook and lifting are very slow processes.
- The workability must be as high as possible, when the vessel is able to install monopiles with rougher weather the vessel can work more days a year and therefor do more work in a year. The motions of the vessel can be to severe to be able to install a monopile. The position of the gripper is really important because motions have different amplitudes at different locations on the vessel.
- It must be as versatile as possible, being able to install short monopiles in shallow water and long monopiles in deep water as well as monopiles with small and large diameters. The vessel must be able to install the huge monopiles of the future
- The installation is done as safe and with the least amount of negative environmental impact as reasonably possible.

1.4. Objectives

The main objective of this master thesis is to build a model that is able to calculate the motions of the vessel as well as the forces induced by the monopile during monopile installation. The sub-objectives are: Choosing an upending technique and gripper design for the Stella Synergy, a location on the vessel where the device will be used and calculating the workability for installing a certain monopile size on a location in the central north sea.

1.5. Approach and scope

In this section the approach to complete the objectives as well as the scope of the master thesis are discussed.

1.5.1. Comparing current techniques

Comparing monopile upending methods that are currently being used or being developed. After all options have been examined a multi criteria analysis (MCA) will be done to decide which method would be the best option for the Stella Synergy. When the method is chosen different types of equipment needed for the method are compared and the best type is selected using a MCA.

1.5.2. Calculating ship motions

Calculating ship motions and comparing possible positions for the gripper and upending device. To have the highest workability the motions of the gripper need to be as small as possible during the monopile installation. To calculate the motions a linear model in the frequency domain is used. The hydrodynamic variables are calculated using Aqwa from Ansys. These are then used in MATLAB to calculate the ships motions because of incoming waves. The RAOs are calculated for different wave frequencys and wave directions. When the RAOs are know the most probable maxima (MPM) of the vessels motions can be calculated and compared at the different possible locations on the vessel, afterwards the best location is chosen, also taking into account the crane load curve of the Stella Synergy.

1.5.3. Calculating forces exerted by monopile during upending

Calculating the forces on the monopile and gripper during upending. First the upending process is split up into six phases. The vessel with monopile next to it is modeled in Aqwa for the phases where the monopile is partly under water. Using the hydrodynamic parameters from Aqwa a model is made in Matlab to calculate the forces on the gripper as well as the crane during upending. With these forces the workability of upending for a curtain size monopile can be calculated so that it will not exceed the maximum lifting capability of the crane.

1.5.4. Calculating forces exerted by monopile during lifting

Calculating the forces on the crane and motions of the monopile and vessel during hoisting. A ten degree of freedom model is made in Matlab. Using this model the motions of the monopile are calculated. The forces on the crane are calculated using these forces. The workability for hoisting a monopile can then be calculated using the vessel motions and forces on the crane.

1.6. Structure

The chapters of this master thesis are build up the following way:

- **Chapter 1**: Introduction

  In the introduction the Company is introduced and the background information that is used for this master thesis is discussed, afterwards the problem is analysed and the Objectives for the master thesis are displayed. The approach to get to these objectives is described and finally the structure of the thesis is discussed.

- **Chapter 2**: Gripper and upending methods and equipment

  In this chapter upending methods are described and the most suitable for the Stella Synergy is chosen. Afterwards a gripper that can be combined with this upending technique is chosen.

- **Chapter 3**: Vessel motions

  In this chapter the motions of the vessel are calculated. These motions are needed to choose the best location for the monopile upending device and gripper. The motions must be as small as possible at the location of the upending device to allow the vessel to have as high workability as possible. The motions of the vessel are calculated in the frequency domain by describing it as a mass spring damper system. The obtained results are compared with data from experiments done by Marin.

- **Chapter 4**: Upending forces and workability

  In this chapter the forces on the gripper and crane are calculated using a model made in Matlab. Because the monopile will be partly submerged during some phases of the upending process the hydrodynamic and hydrostatic forces on the monopile are also taken into account. The viscous damping forces of the monopile are calculated using the drag coefficient of a cylinder. The hydrostatic and hydrodynamic parameters are then used to calculate the vessels motions. The workability of upending is calculated using a wave scatter for a location in the central North Sea.

- **Chapter 5**: Hoisting forces and workability

  In this chapter the motions of the monopile and forces acting on the crane during the hoisting of the monopile are calculated. This is done by modeling the vessel and monopile in a ten degree of freedom linear system. The motions are then used to calculate the workability of hoisting a monopile.

- **Chapter 6**: Conclusion and recomendations

  The result of Chapter 1 to 5 are discussed and advice is given for future research.

2

Gripper and upending methods and equipment

In this chapter monopile upending techniques and gripper designs that are currently being used or being developed are compared. After all options have been examined a gripping mechanism and upending technique are chosen for the Stella Synergy using a multi criteria analysis.

2.1. Upending techniques

The monopiles will be transported on a barge or on one of Jumbos shipping vessels towards the installation site. The Stella Synergy must will be able to pick up the monopile from the barge or vessel. The monopile is in a longitudinal position with the open ends of the monopile pointing towards the stern and bow of the vessel. The monopile must then be rotated in some way so that the open ends are pointing towards the sea bed and the sky. This procedure is called up-ending. The Stella Synergy must be able to up-end monopiles with diameters from six to twelve meter and with weights from 1000 to 2500 ton. The possible upending techniques that are compared in the following subsections are:

- Upending using separate upending frame
- Upending in water
- Upending using multiple hooks
- Upending using gripper

2.1.1. Upending using Separate upending frame

Conventionally a separate upending frame is used to up-end the monopiles. The monopile is first lifted into the upending frame then it is up-ended and finally it is lifted from the upending frame into the gripper. The upending device consists most of the time of a steel frame which is hinged to allow for the rotation of the monpile during upending. An example of an upending frame can be seen in figure 2.1 The advantages of using a separate upending frame are:

- The separate upending tool can be a really simple device and is therefor reliable and not expensive
- Monopiles weighing up to the maximum lifting capability of the crane can be up-ended

The disadvantages are:

- The monopile needs to be transfered from the upending device to the gripper, therefor the cycle time will be longer then other methods.
- extra deck space is needed for the upending device
- upending frames are not versatile, so one upending frame is needed for every monopile size.

Figure 2.1: A monopile upending frame

2.1.2. upending in water

Because of the continuously increasing size of the windturbines their masses are increasing drastically as well. What was considered as a future proof heavy lift windturbine installation vessel ten years ago now can not even install the biggest monopiles anymore. Monopile weight also is dependent on the waterdepth. The new windfarms are planned in deeper waters, therefor the new monopiles are getting even heavier. The monopiles for the currently used vestas V164-8.0 MW windturbine for water depths of 15m to 50m already weigh 800t to 2700t respectively.[University-Strathclyde, 2015]

The costs of making a monopile are a big part of the total costs for a wind turbine, to reduce the costs of the monopiles other materials are being suggested. Concrete monopiles can cut a big part of the cost of the monopile, but there is one main disadvantage; they are a lot heavier. A concrete variant of a 6.5m diameter monopile for a 3-4MW windturbine has a weight of around 1450t[4c offshore, 2013] compared to the 900t[University-Strathclyde, 2015] variant of the steel version for the same water depth. The main reason why concrete monopiles are not used as often as steel monopiles is because the cranes on the installation vessels are not able to handle the weight of monopiles. To be able to install these big sized monopiles they can be up-ended in water. The monopiles are plugged on both sides so they will float. then they are towed from a dock to the installation site. There the main crane of the installation vessel is attached to one side of the monopile and the crane starts lifting the monopile. Because the monopile is filled with air the crane only has to lift a small portion of the weight normally required to install the monopile. When the monopile is staight up it can be placed in a gripper alongside the installation vessel and the seals at the bottom and top of the monopile are punctured or removed slowly in such a way that the crane can lower the monopile until it hits the ground without being overloaded. The crane can then be removed and the driving hammer can be installed.[J.B.Crol, 2015]

The advantages of upending in water are:

- heavier monopiles than the maximum lifting capability of the vessel can be installed.
- no extra deck equipment and space is required to up-end the monopiles

The disadvantages are:

- Special plugs have to be made to fit on the ends of the monopile
- The plugs have to be removed carefully during the installation or else a dangarous situaiton can occur because the crane can get overloaded.
- The monopiles have to be towed to the installation location

2.1.3. upending using multiple hooks

When a vessel has multiple separately controlled main hooks on its crane it is possible to up-end monopiles using the main crane only. On each end of the monopile one of the hooks is installed using an adapter,

afterwards the monopile is lifted from the barge and the barge sails away. One end of the monopile is lowered into the water. After up-ending the lower hook can be released and the monopile can be placed directly in the gripper. The advantages are:

- Fast upending process
- No upending equipment is needed on deck

the disadvantages are:

- The maximum weight monopile is lower then the maximum lifting capability of the crane because the cables are under an angle and the monopile is hanging on one hook completely after upending.
- less controlled and more dangerous then using an upending device on deck, especially in rough weather conditions.

Stella Synergy will have a main crane with three hooks installed which can lift a maximum of 1250t each with a total maximum of 2500t. The third hook will be installed on the higher end of the monopile when using this upending technique. The total load will than hang on two hooks when upended, therefor the monopile can be heavier than when using only two hooks. The monopile can still not be as heavy as the total lifting capacity of the crane because the hoisting cables are not going straight down from the crane to the monopile, this increases the load on the cables.

2.1.4. upending using gripper

Most grippers on installation vessels can be retracted when they are not in use. This is sometimes done by rotating the gripper upwards. This movement can also be used to upend a monopile when the gripper is strengthened. The monopile is placed in the gripper directly from the barge. The gripper will have an extra support point where it holds the monopile. The crane then picks up one side of the monopile and upends it. The gripper only guides the monopile, the crane causes the upending by lifting one side of the monopile. When the monopile is straight up the crane hook will be detached from the monopile and the hammering tool can be installed. The advantages are:

- The installation process is shorter because the monopile only needs to be lifted ones.
- The upending is done securely and unwanted movements of the monopile are restricted.
- Less deck space is needed then when using a separate upending frame.

The disadvantages are:

- An extra mount needs to be installed on the gripper.
- The gripper needs to be strengthened to be able to handle the forces induced by the monopile during upending.

2.2. Multi Criteria Analysis

To evaluate which upending technique and gripper design would be the best for the Stella Synergy a MCA is done. The criteria that are important for an upending technique are:

- Workability: The percentage of days in a year this technique can be used without being influenced to much by weather conditions.
- Cycle time: How long it takes to up-end a monopoile using this technique
- Versatility: The difference in monopile sizes the technique can handle as well as the maximum size and weight it can handle. More versatile is better.
- Cost: The cost of the equipment needed for the technique.
- Safety: The safety of using the technique.

All the criteria are given an importance score, so that the total importance of all the criteria added up is one. The higher the importance score the more important this aspect of the upending technique is for Jumbo. Every concept is given a score from one to ten for all the criteria. The higher the score the better the technique is in that criterion, afterwards all the scores are multiplied with the importance of that criterion and then added up to give the total score. The technique with the highest total score is the best option for the Stella Synergy.

Table 2.1: MCA upending technique

	Workability	cylce time	versatility	cost	safety	total score
Importance	0.25	0.25	0.15	0.15	0.2	1
Separate upending frame	7	4	4	7	6	5.6
Upending in water	6	5	10	7	8	6.9
Using Multiple hooks	6	9	7	9	3	6.8
Upending with gripper	8	8	8	6	9	7.9

Although systems can rank relatively high in the MCA they still can have their limitations. The final method sugested to Jumbo is therefor not simply the highest scoring technique in the MCA. One of these limitations is the maximum monopile weight. When a monopile is up-ended using the gripper (subsection 2.1.4) the monopile has to be lifted into the gripper and therefor the monopile has a maximum weight.

Jumbo is suggested to use a gripper on their vessel that is capable of gripping monopiles as well as upending them. This gripper will be used until the monpile excerts bigger forces on the crane then allowed. In chapter 4 the maximum dynamic and static forces on the crane during upending are discussed. When heavier monopiles need to be installed the upending in water technique can be used (subsection 2.1.2). This will allow the vessel to upend monopiles for future wind turbines with extreme sizes as well as the heavier concrete monopiles.

2.3. gripper designs

Now that the upending method is known the equipment for holding the monopile while driving it into the ground is compared.

The gripper must keep the monopile straight up while the hammer is installed on top of the monopile and while the monopile is being driven into the ground. The monopile gripper must be able to grip monopiles with different diameters and must be strong enough to handle the forces that are induced on the gripper by the motions of the ship in waves. The monopile is supported using rollers or low friction material so it can move freely in z direction through the gripper. This is necessary to allow the hammer to drive the pile down and to allow for heave motions of the vessel. After the monopile is driven to a depth where the hammer will start hitting the gripper, the gripper must be able to open and make space for the hammer. It must also be able to open quickly in case of an emergency. The monopile gripper is also being used for up-ending the monopile (see section 2.1) it must be able to hold the monopile securely during the upending procedure.

2.3.1. two arm linear gripper

The two arm linear gripper design has two opposing arms holding the monopile as seen in figure 2.2. This system is not ideal for gripping and up-ending. When used for upending there will be huge moments and shear stresses inside the arms, therefor the arms will have to be made a lot stronger compared to other designs of grippers. This is the least stable way of gripping a monopoile that is compared. When it is used for multiple sizes of monopiles the gripper will need different types of clamps for every size of monopile (only the part that touches the monopile). The two arms can simply be moved apart to create enough space for the hammer to drive the monopile the last part and for emergency release. Because of its simple design the two arm linear gripper is relatively affordable.

Figure 2.2: A two arm linear gripper

2.3.2. four or more arm liniear gripper

The four linear arm gripper design has two extra arms square to the other two arms. The four arm gripper will suport the monpile a lot better then when using only two. There is almost no shear stress in the arms. This will make the four arm design a lot more viable to be used for gripping as well as up-ending. Having extra arms will make the system more expensive but because they are all only loaded in compression they can be made lighter. Using four arms will make the system much more capable of installing variable sizes of monopiles. The arms need to be made long enough to be able to grip the small monopiles. To allow the monopile to exit the gripper when the final part is driven into the ground or when an emergency release is necessary the gripper should be made so that it can open. Adding more then four arms will spread the load across the monopile more evenly and will therefore damage the monopile less likely. This is the most stable way of gripping a monopile. Also there will be more redundancy during the operation. If the hydraulics of one cylinder fails the monopile will still be supported and operation might even continue. The extra arms do add extra weight and costs.

Figure 2.3: A four arm linear gripper

2.3.3. two rotating arm gripper

The two arm gripper has two arms that rotate instead of a linear motion. This allows for easy and quick release of the monopile when needed. The two arm gripper can be designed in such a way that it is capable of gripping multiple sizes of monopiles as seen in figure 2.4. The wo arm gripper can be designed so that it is capable of upending monopiles as well.

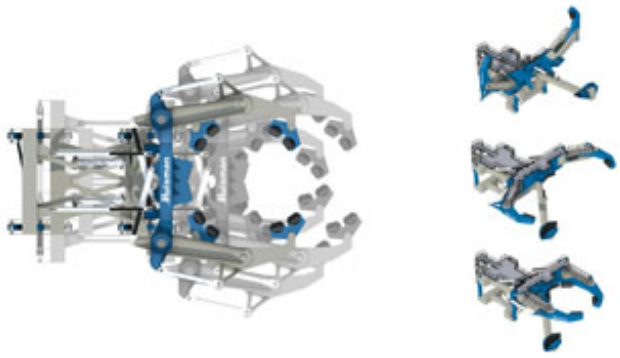

Figure 2.4: A two rotating arm gripper

2.3.4. Subsea frame

As an alternative to using a gripper to hold the monopile in position during driving it a subsea frame can be used. This is a steal frame that is placed at the seabed and carefully leveled. The monopile is placed inside the frame and then driven into the ground. Afterwards the frame is removed. The frames can be installed and removed using a separate ship. When using two frames the main installation vessel can continuously install monopiles without waiting on the placement of a frame on the seabed.

The advantages of using a subsea frame are:

- When the monopile is placed in the gripper it is not dependent on ship movement
- No deck space is needed for the gripper and upending device
- No size limitations after upending

The disadvantages are:

- The subsea frames need to be installed, removed and transported from turbine to turbine.
- The seabed needs to be carefully inspected before placing of the frames
- The frames need to be placed within tolerances

2.4. MCA gripper

The criteria that are important for the gripper design are:

- Workability: The ammount of days in a year this gripper can be used without being influenced by weather conditions
- Upending: How easy it is to use this gripper design for upending.
- Versatility: The difference in monopile sizes the gripper can handle as well as the maximum size and weight it can handle
- Cost: The cost of the gripper

Table 2.2: MCA gripper design

	Workability	upending	versatility	cost	total score
Importance	0.31	0.31	0.19	0.19	1
linear two arm	6	3	5	8	5.3
linear four or more arm	7	7	8	6	6.8
two arm	7	8	7	7	7.0
subsea frame	8	1	3	9	5.1

2.5. Motion compensated grippers

The installation of monopiles is a really precise job, most of the time the monopile has to be installed with a maximum distance of one meter from the desired location. Even more important is the angle of the monopile, it must almost be exactly straight up with a difference of maximum half a degree. The rotation of the monopile is also important because the wiring holes in the monopile must face a certain direction. To be able to achieve these tolerances it is really important that the monopile is moved as less as possible while it is driven into the ground. Until now this has been done by using a vessel that has a Jack-up system. This Jacks up the whole vessel above the water using legs. This has the advantage that the vessel is almost completely motionless during the installation. A big disadvantage is that the seabed first needs to be surveyed and that the jack-up process takes a lot of time, also the load per jack-up leg is limited and with the increasing size of the monopiles it is getting harder to design a vessel that is still capable of using this system.

Another way of installing monopiles is using a floating vessel with mooring lines like the Oleg Strashnov from Seaway Heavy Lifting. The vessel is positioned at the right locations using mooring lines and handling tugs to place the anchors. [Bosch, 2018] This requires less precise seabed surveillance and is not limited to the maximum load per jack-up leg. However in waves the vessel will move and handling tugs are needed to place the anchors. To stay within tolerances the vessel will only be able to operate in calm conditions. The workability is most of the time smaller than using a jack-up system. The anchor laying is a time consuming process that has to be redone fore every monopile.

A dynamically Positioned vessel like the Stella Synergy will overcome the need for anchor handling tugs and will significantly improve the installation time compared to the moored and jack-up vessels. Unfortunately the vessel will never be able to install the monopiles within tolerances using a standard gripper. The dynamic positioning system is not capable to keep the vessel within such a small area and the vessel experiences a lot more roll and pitch compared to the jack-up and moored vessel. To overcome this problem a dynamically positioned monopile gripper is suggested. This gripper can, when properly integrated with the ships DP system, compensate for the motions of the ship. The biggest disadvantages of this system are that they have not been proven on a floating vessel and are a lot more expensive than conventional grippers.
The motion compensated gripper can also be used to get the monopile within tolerances when it is being driven into the ground. The system can exerts forces on the monopile so it will go straight into the ground.

2.6. gripper design

The motion compensated gripper from Huisman that is capable of upending monopiles seems to be the perfect gripper for the Stella Synergy when looking at the MCA, however When the crane lifting diagram is taken into account it can be concluded that it is impossible to use the Huisman gripper at the selected location decided on in chapter 3. The monopile must be placed with one end at the end of the gripper. When the monopile is longer then 70m it is out of reach from the main hoist. When a shorter monopile is being installed the crane needs to lift around half of the monopile weight at a range of almost the monopile length away from the crane. The crane will not be able to lift such loads at a big distance. Also when up-ended the center of gravity of the monopile is really high, influencing the stability of the ship negatively. Another reason why the upending tool from Huisman is limiting the maximum length of the monopile that can be upended is that the end of the monopile will be really high above the deck when lifting. The crane of the Stella Synergy will have maximum lifting height of around 87 m so the end of the monopile can not exceed this height during upending. This makes this upending device a not practically usable option for the Stella Synergy.

To be able to upend monopiles with lenghts of 100 m and longer the upending tool and gripper should be redesigned. The CoG should be placed close to the point where the monopile rotates around. This will not only decrease the distance from the crane center to the end of the monopile but also reduces the forces needed for up-ending a lot. A two arm rotating gripper or a four or mour arm linear gripper is adviced.

3

Vessel motions

In this chapter the motions of the vessel are examined to determine the best location for the monopile upending device. Other aspects of the vessel that have influence on the best location of the upending device are taken into account like the crane lift curve. First the RAOs of the vessel are computed in chapter 3.2 then the ship motions are computed in chapter 3.5 and finally the location of the gripper is decided on in chapter 3.6.

3.1. Coordinate system

In a three dimensional space objects have six degrees of freedom. For a ship these degrees of freedom are defined as:

- Surge: translation along X axis
- Sway: translation along Y axis
- Heave: translation along Z axis
- Roll: rotation around X axis
- Pitch: rotation around Y axis
- Yaw: rotation around Z axis

Table 3.1: The motions and rotations of a ship

Translation			
	Surge	Sway	Heave
Positon	x	y	z
Velocity	$\dot{x}$	$\dot{y}$	$\dot{z}$
Acceleration	$\ddot{x}$	$\ddot{y}$	$\ddot{z}$
Rotation			
	Roll	Pitch	Yaw
Angle	ϕ	θ	ψ
Angular velocity	$\dot{\phi}$	$\dot{\theta}$	$\dot{\psi}$
Angular acceleration	$\ddot{\phi}$	$\ddot{\theta}$	$\ddot{\psi}$

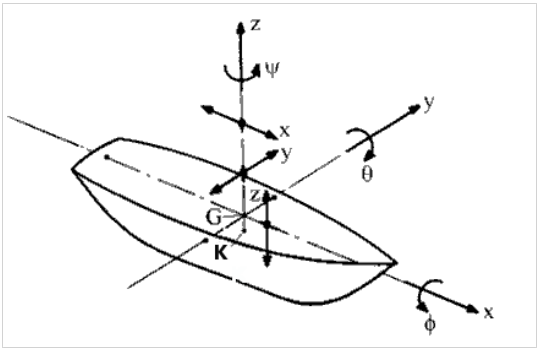

Figure 3.1: The six degrees of freedom of a ship

3.2. RAOs

To obtain the vessels motions newtons second law is used:

$$F = m * acc \tag{3.1}$$

where the Force can be split up in multiple parts:

$$\sum F = F_r + F_w + F_d + F_s \tag{3.2}$$

Where:

- F_r are the radiation forces
- F_w are the incoming wave forces
- F_d are the diffraction forces
- F_s are the hydrostatic buoyancy forces

3.2.1. Mass matrix

To obtain the vessels motions first the mass matrix off the vessel must be known. The design displacement is used to calculate the mass of the vessel. When the vessel accelerations are computed in chapter 4 the mass matrix is edited for different phases in the monopile upending process.

Because it is a six dimensional system the mass matrix $\boldsymbol{m}$ will be a $6x6$ matrix:

$$\boldsymbol{m} = \begin{bmatrix} m & 0 & 0 & 0 & 0 & 0 \\ 0 & m & 0 & 0 & 0 & 0 \\ 0 & 0 & m & 0 & 0 & 0 \\ 0 & 0 & 0 & I_{xx} & 0 & 0 \\ 0 & 0 & 0 & 0 & I_{yy} & 0 \\ 0 & 0 & 0 & 0 & 0 & I_{zz} \end{bmatrix} \tag{3.3}$$

Where: m is the mass of the vessel and I_{xx}, I_{yy} and I_{zz} are the moments of inertia and can be calculated using:

$$I_{xx} = mr_{xx}^2; \quad I_{yy} = mr_{yy}^2; \quad I_{zz} = mr_{zz}^2 \tag{3.4}$$

where r_{xx}, r_{yy} and r_{zz} are the radii of gyration of the vessel. They given by Ulstein, they use a 3D model of the vessel with the weight distribution in it.

3.2.2. hydrostatic buoyancy forces

The hydrostatic restoring forces are the buoyancy forces acting on the vessel. For example if the vessel is pulled down one meter into the water the extra restoring force will be the volume of water that is displaced compared to the neutral position times the density of water times g. The hydro-static restoring forces act like a spring on the vessel. The restoring forces for surge and sway are zero because the ships displacement does not change when the vessel is translated in one of these directions. The roll and pitch hydrostatic restoring moments can be computed using GM, which is the distance between the center of gravity and the metacentrum of the vessel. It can be calculated using:

$$GM_T = KB + BM - KG = KB + \frac{I_T}{\nabla} - KG \tag{3.5}$$

$$GM_L = KB + BM - KG = KB + \frac{I_L}{\nabla} - KG \tag{3.6}$$

The restoring yaw moment is zero as well because there is no change in displacement when the vessel is rotated around the z axis. The restoring stiffness for small translations and rotations are described in the $\boldsymbol{C}$ matrix:

$$\boldsymbol{C} = \begin{bmatrix} 0 & 0 & 0 & 0 & 0 & 0 \\ 0 & 0 & 0 & 0 & 0 & 0 \\ 0 & 0 & \rho g A_{wp} & 0 & -\rho g A_{wp}(CoF - CoB) & 0 \\ 0 & 0 & 0 & \rho g \nabla GM_T & 0 & 0 \\ 0 & 0 & -\rho g A_{wp}(CoF - CoB) & 0 & \rho g \nabla GM_L & 0 \\ 0 & 0 & 0 & 0 & 0 & 0 \end{bmatrix} \tag{3.7}$$

3.2.3. radiation forces

The radiation forces are forces due to the movement of the ship: When the vessel starts accelerating it also accelerates water around the vessel, therefor an added mass term is needed in the model. This added mass term is frequency dependent: $\boldsymbol{M} = \boldsymbol{m} + \boldsymbol{A}(\omega)$ The system is not just a mass spring system but also has damping. The hydrodynamic damping is caused by the waves the vessel generates when it moves because of the incoming waves,the damping is represented in the $\boldsymbol{B}$ matrix. The a and b coefficients are frequency dependent so to solve the motion equation it is written in frequency domain. The coupled motion equation becomes:

$$\left\{-\omega^2 \begin{vmatrix} m+a_{11} & a_{12} & a_{13} & a_{14} & a_{15} & a_{16} \\ a_{21} & m+a_{22} & a_{23} & a_{24} & a_{25} & a_{26} \\ a_{31} & a_{32} & m+a_{33} & a_{34} & a_{35} & a_{36} \\ a_{41} & a_{42} & a_{43} & I_{xx}+a_{44} & a_{45} & a_{46} \\ a_{51} & a_{52} & a_{53} & a_{54} & I_{yy}+a_{55} & a_{56} \\ a_{61} & a_{62} & a_{63} & a_{64} & a_{65} & I_{zz}+a_{66} \end{vmatrix} + i\omega \begin{vmatrix} b_{11} & b_{12} & b_{13} & b_{14} & b_{15} & b_{16} \\ b_{21} & b_{22} & b_{23} & b_{24} & b_{25} & b_{26} \\ b_{31} & b_{32} & b_{33} & b_{34} & b_{35} & b_{36} \\ b_{41} & b_{42} & b_{43} & b_{44} & b_{45} & b_{46} \\ b_{51} & b_{52} & b_{53} & b_{54} & b_{55} & b_{56} \\ b_{61} & b_{62} & b_{63} & b_{64} & b_{65} & b_{66} \end{vmatrix} + \right.$$

$$\left. \begin{vmatrix} c_{11} & c_{12} & c_{13} & c_{14} & c_{15} & c_{16} \\ c_{21} & c_{22} & c_{23} & c_{24} & c_{25} & c_{26} \\ c_{31} & c_{32} & c_{33} & c_{34} & c_{35} & c_{36} \\ c_{41} & c_{42} & c_{43} & c_{44} & c_{45} & c_{46} \\ c_{51} & c_{52} & c_{53} & c_{54} & c_{55} & c_{56} \\ c_{61} & c_{62} & c_{63} & c_{64} & c_{65} & c_{66} \end{vmatrix} \right\} \begin{vmatrix} x \\ y \\ z \\ \phi \\ \theta \\ \psi \end{vmatrix} = \begin{vmatrix} F_x \\ F_y \\ F_z \\ M_x \\ M_y \\ M_z \end{vmatrix} \tag{3.8}$$

Velocity potentials are used to obtain the added mass and damping coefficients. This is explained in Appendix A.1. In this master thesis these coëficcients are obtained using a model in Aqwa (subsection 3.2.6).

3.2.4. undisturbed incoming wave and diffraction forces

The undisturbed wave and diffraction forces can be measured by holding a model of the vessel restrained in an undisturbed wave and measuring the forces and moments that act on it. How these forces can be calculated is described in Appendix A.2.

The undisturbed wave and diffraction forces are obtained using a model in Aqwa (subsection 3.2.6).

3.2.5. viscous damping

Using the panel method the damping because of waves generated by the vessel can be calculated, this does not take into account the viscous damping. Therefor another damping matrix needs to be added to get more realistic results. The viscous damping is generated by: skin friction, roll resistance of appendages and vortices (eddy shedding) [Himeno, 1981]. The viscous damping will have the biggest influence on the roll motions of the vessel. The viscous damping for yaw, sway, heave, sway and surge are neglected. In Marin the viscous damping has been measured. The total equation of motion becomes:

$$(-\omega^2(\boldsymbol{m}+\boldsymbol{A}) + i\omega(\boldsymbol{B}+\boldsymbol{B_{add}}) + \boldsymbol{C})\boldsymbol{X} = \boldsymbol{F_W} + \boldsymbol{F_D} \tag{3.9}$$

The added damping matrix $\boldsymbol{B_{add}}$ is frequency independent and is:

$$\boldsymbol{B_{add}} = \begin{bmatrix} 0 & 0 & 0 & 0 & 0 & 0 \\ 0 & 0 & 0 & 0 & 0 & 0 \\ 0 & 0 & 0 & 0 & 0 & 0 \\ 0 & 0 & 0 & B_{add} & 0 & 0 \\ 0 & 0 & 0 & 0 & 0 & 0 \\ 0 & 0 & 0 & 0 & 0 & 0 \end{bmatrix} \tag{3.10}$$

where $B_{add} = 130 \frac{MNm}{rad/s}$ [Marin, 2018].

3.2.6. panel method

The panel method from Aqwa is used to analyse the hydrodynamic parameters of the Stella Synergy. How the panel method works is explained in Appendix A.3.

To use Aqwa a 3D model of the vessel is edited. The bow thruster tunnels and some other detailes are removed from the vessel because they will have little influence on the diffraction, radiation and incoming wave forces and will make the program a lot slower. The viscous damping of the removed parts is taken into account in the added damping matrix. The 3D model is then imported into Aqwa and a mesh is generated. The program is first tested using a very big grid size to reduce the time needed to run the program. After the program works succesfully the program is run with smaller mesh sizes until the results converge as seen in Table 3.2

Table 3.2: Mesh size influence on RAO heave

Mesh size (m)	RAO heave (m/m)
5	0.0252
4	0.0245
3	0.0241
2	0.0238
1	0.0238

The RAO heave becomes constant from a mesh size of 2m and smaller. To keep the model as fast and precise as possible a mesh size of 2m is used. A mesh of the Stella Synergy can be seen in Figure 3.2. In Aqwa the model is ran for a total of 100 wave frequencies from $0.1\frac{rad}{s}$ to $1.58\frac{rad}{s}$ and a total of 32 wave directions from -180° to 180°.

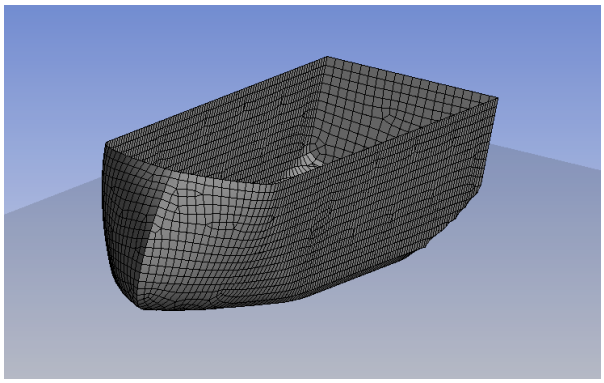

Figure 3.2: A mesh of the Stella Synergy generated by Aqwa

To be able to adjust the model and CoG of the model quickly the RAOs are not directly used from Aqwa. As long as the vessel has the same draft and stays straight up (as is assumed, see chapter 4.3.3)the added mass matrices, damping matrices and incoming wave forces stay the same. Therefor $\boldsymbol{A}(\omega)$ and $\boldsymbol{B}(\omega)$ are obtained from the Aqua output file for every frequency and the incoming wave forces $H_{fz}(\omega,\mu)$ are obtained for every frequency and every direction. $H_{fz}(\omega,\mu)$ is the transfer function between the wave height and the forces on the vessel because of the incoming undisturbed wave and diffraction: chapter 3.2.4:

$$\boldsymbol{H_{fz}} = \frac{\boldsymbol{F_D} + \boldsymbol{F_W}}{\zeta_a} \tag{3.11}$$

To obtain the boundry conditions for the model in Aqwa the water depth needs to be known. The chosen waterdepth is 50 m because a lot of future windfarms are planned at this depth. [NorthSee, 2018]

3.2.7. RAOs

The full equation of motion is now known, so the RAOs can be computed. The vessels RAOs are dependent on: The frequency of the incoming wave and the direction of the incoming wave. The RAOs are calculated for every degree of freedom of the vessel:

$$RAOSurge = \frac{x_a}{\zeta_a} \tag{3.12}$$

$$RAOSway = \frac{y_a}{\zeta_a} \tag{3.13}$$

$$RAOHeave = \frac{z_a}{\zeta_a} \tag{3.14}$$

$$RAORoll = \frac{\phi_a}{\zeta_a} \tag{3.15}$$

$$RAOPitch = \frac{\theta_a}{\zeta_a} \tag{3.16}$$

$$RAOYaw = \frac{\psi_a}{\zeta_a} \tag{3.17}$$

The RAOs can be calculated using the following formula:

$$\boldsymbol{RAO}(\omega,\mu) = \frac{\boldsymbol{H_{fz}}(\omega,\mu)}{-\omega^2(\boldsymbol{m}+\boldsymbol{A}(\omega))+i\omega(\boldsymbol{B}(\omega)+\boldsymbol{B_{add}})+\boldsymbol{C}} \tag{3.18}$$

The amplitude of the RAOs can be calculated using:

$$RAO_a = \sqrt{Re(RAO)^2 + Im(RAO)^2} \tag{3.19}$$

The phase angles of the RAOs can be calculated using:

$$\epsilon = \arctan\left(\frac{Im(RAO)}{Re(RAO)}\right) \tag{3.20}$$

The RAOs for all six degrees of freedom at the CoG of the vessel are obtained for different directions (μ) and different angular frequencies (ω) and are plotted in Figure 3.3 until Figure 3.8.

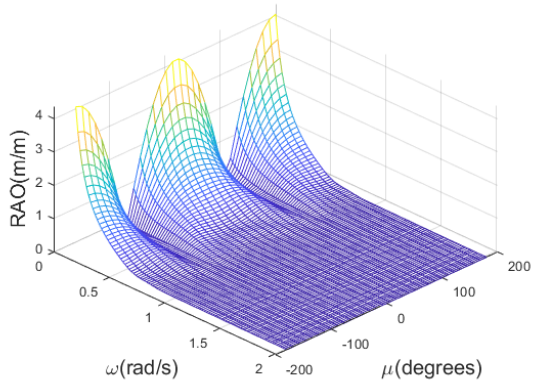

Figure 3.3: The surge RAOs of the CoG for different angular frequencies and directions

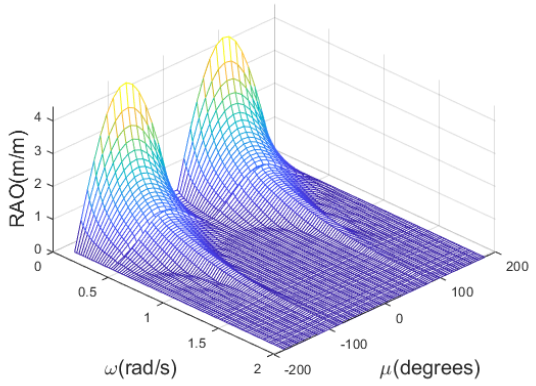

Figure 3.4: The sway RAOs of the CoG for different angular frequencies and directions

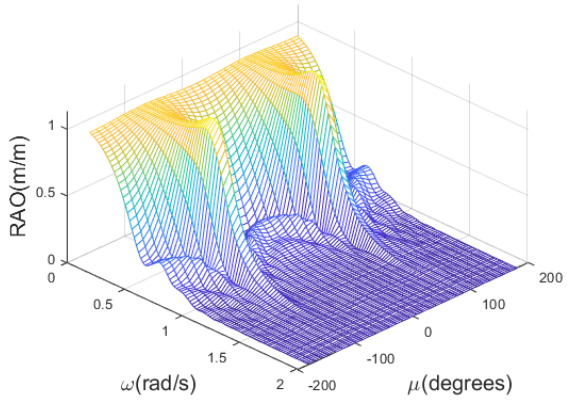

Figure 3.5: The heave RAOs of the CoG for different angular frequencies and directions

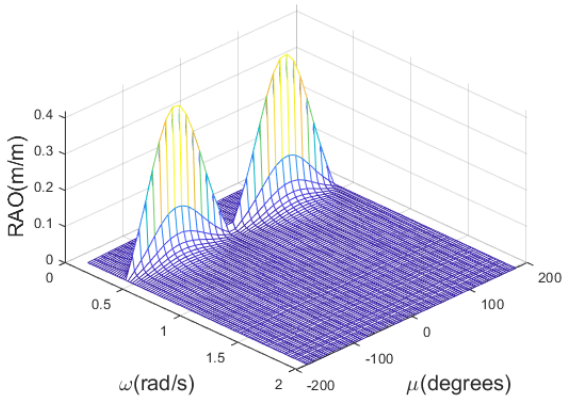

Figure 3.6: The roll RAOs of the CoG for different angular frequencies and directions

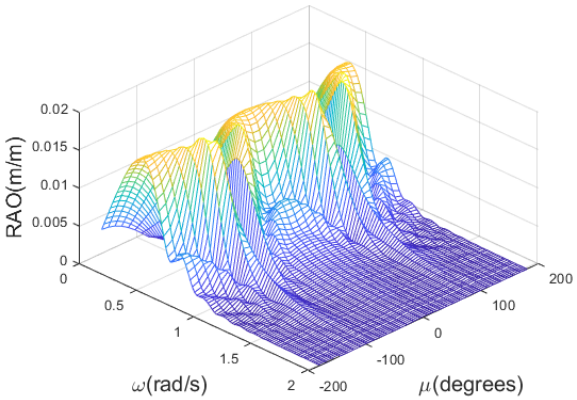

Figure 3.7: The pitch RAOs of the CoG for different angular frequencies and directions

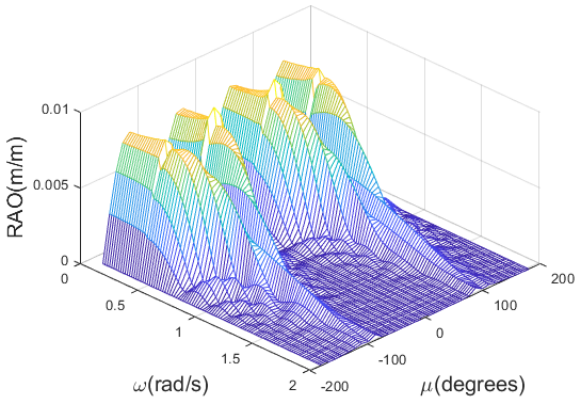

Figure 3.8: The yaw RAOs of the CoG for different angular frequencies and directions

3.2.8. comparing RAOs with Marin measurements

To verify the RAOs from the model the data is compared with the measured RAOs from Marin. The RAOs have been meassured in Marin for different sea states. The theoretical RAOs are the same for every wave height but the wave frequency, wave direction and GM do influence the theoretical RAOs. The measured RAOs are slightly different for different wave heights and periods. After the response spectrum (S_U) is measured by marin the RAOs are computed by marin using:

$$RAO = \sqrt{\frac{S_u}{S_\zeta}} \tag{3.21}$$

Where S_z is the wave spectrum that is used during the measurements. The RAOs are meassured in Marin for deep water. Therefor the waterdepth in Aqwa is set to deep water as well. The draft of the vessel is set to 8 meters which is the same as the tests in Marin.[Marin, 2018] In figures 3.9, 3.10 and 3.11 the Calculated and measured RAOs at the CoG are plotted. In Tables 3.3, 3.4 and 3.5 the legends of the figures are displayed.

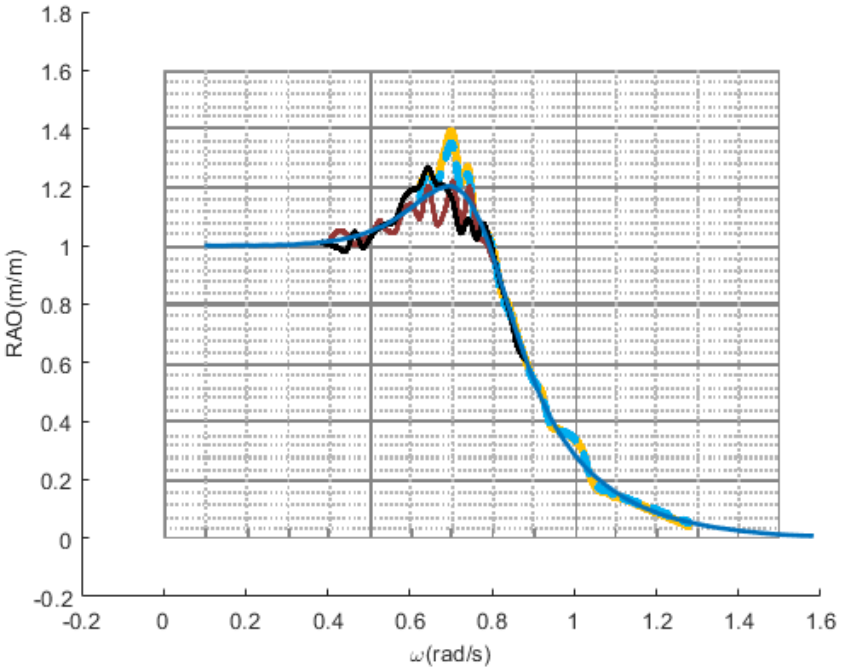

Figure 3.9: Calculated heave RAOs compared to Meassured heave RAOs from Marin

Table 3.3: Legend of Heave RAOs measured by Marin and the theoretical calculated RAOs in MATLAB

	Meassured by marin				**Theoretical**	
color	yellow	blue dashed	brown	black	blue	
Hs	2.5	2.5	2.5	1	-	m
GM	2	7	7	7	7	m
Tp	8	8	12	12	-	s
μ	90	90	90	90	90	degrees

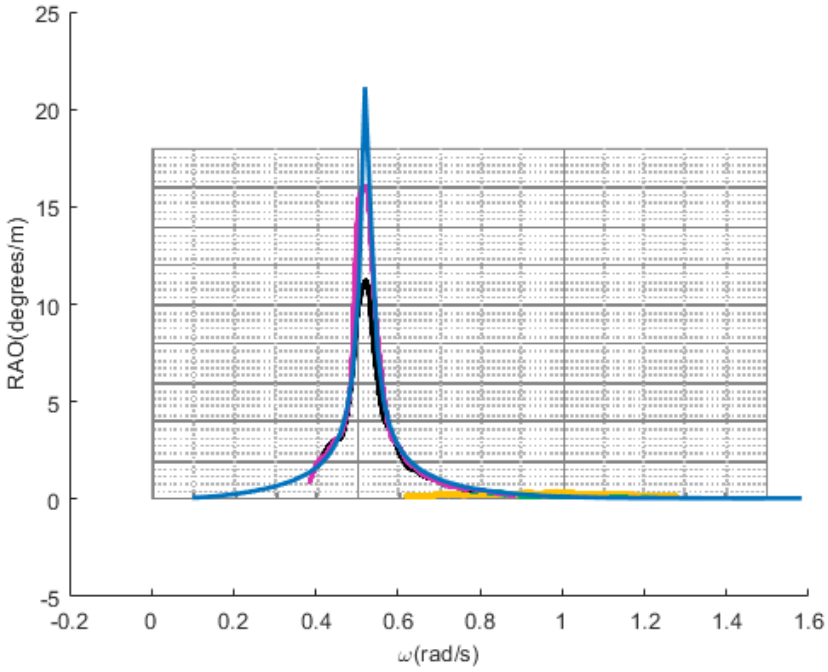

Figure 3.10: Calculated roll RAOs compared to Meassured roll RAOs from Marin

Table 3.4: Legend of Roll RAOs measured by Marin and the theoretical calculated RAOs in MATLAB

	Meassured by marin				**Theoretical**	
color	yellow	green dashed	black	purple	blue	
Hs	2.5	2.5	2.5	1	-	m
GM	2	7	7	7	7	m
Tp	8	8	12	12	-	s
μ	90	90	90	90	90	degrees

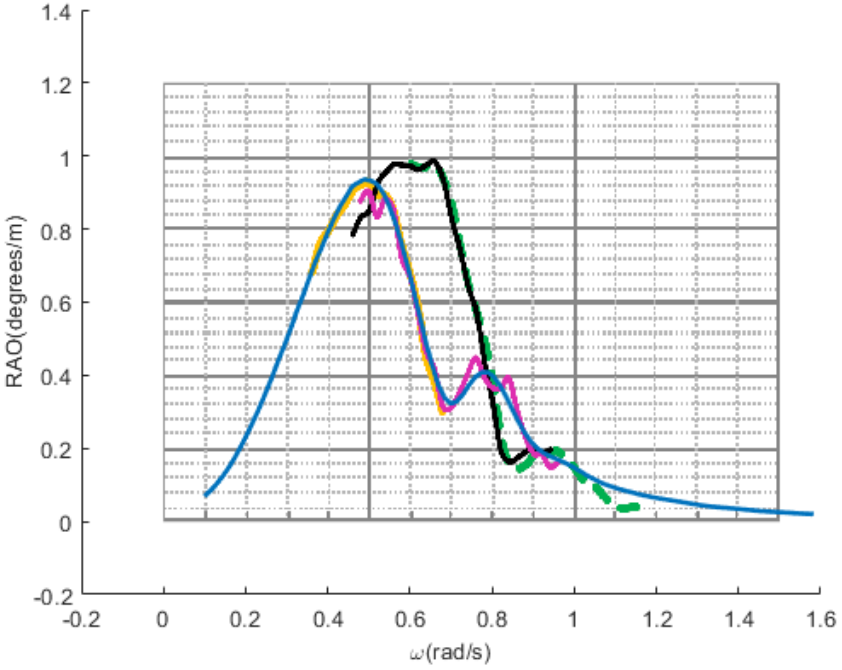

Figure 3.11: Calculated pitch RAOs compared to Meassured pitch RAOs from Marin

Table 3.5: Legend of Pitch RAOs measured by Marin and the theoretical calculated RAOs in MATLAB

	Meassured by marin				**Theoretical**	
color	yellow	green dashed	black	purple	blue	
Hs	2	3	1.5	2	-	m
GM	2	2	2	2	2	m
Tp	14	8	10	10	-	s
μ	180	135	315	0	0	degrees

The theoretical heave and pitch RAOs are almost completely the same as the measured RAOs. The theoretical roll RAOs are except for the peak at around $0.52\frac{rad}{s}$ really similar to the real roll RAOs. When the viscous damping in the model is increased the Theoretical and measured RAOs are exactly the same. This can be because viscous damping is assumed to be linear in the model. The viscous roll damping that is used is linearised by Marin (subsection 3.2.5). [Haver, 2016].

Because the roll RAOs have such a skinny peak it is analysed if no information is missing between two frequency steps. The maximum amount of frequencies that can be used in Aqwa is 100. To get more frequency steps in the region of the peak the model is rerun with a smaller frequency range and still 100 frequencies. The results are compared and almost the same as using the bigger frequency range. Therefor using 100 frequencies over the chosen frequency range is accurate enough.

3.3. RAO transformation

Transforming the RAOs for one location of the vessel to RAOs of another location of the vessel can be done using two methods:

- During the calculation of the RAO using a transformation matrix
- After the RAOs have been calculated using the amplitudes and face angles of the RAOs at the CoG

Both methods have been used in this master thesis. For both methods small angles are assumed.

3.3.1. RAO transformation using transformation matrix

To transform the RAOs from the Center of gravity to a location p with coordinates compared to the CoG: a,b and c. The coordinates of point p are described by:

$$x_p = x_{CoG} + c\theta_{CoG} - b\psi_{CoG} \tag{3.22}$$

$$y_p = y_{CoG} - c\phi_{CoG} + a\psi_{CoG} \tag{3.23}$$

$$z_p = z_{CoG} + b\phi_{CoG} - a\theta_{CoG} \tag{3.24}$$

The vessel is assumed to be infinetly stiff and therefor the rotation at location p are the same as at the CoG:

$$\phi_p = \phi_{CoG} \tag{3.25}$$

$$\theta_p = \theta_{CoG} \tag{3.26}$$

$$\psi_p = \psi_{CoG} \tag{3.27}$$

This can be combined into matrix $\boldsymbol{L}$:

$$\begin{vmatrix} x_p \\ y_p \\ z_p \\ \phi_p \\ \theta_p \\ \psi_p \end{vmatrix} = \begin{bmatrix} 1 & 0 & 0 & 0 & c & -b \\ 0 & 1 & 0 & -c & 0 & a \\ 0 & 0 & 1 & b & -a & 0 \\ 0 & 0 & 0 & 1 & 0 & 0 \\ 0 & 0 & 0 & 0 & 1 & 0 \\ 0 & 0 & 0 & 0 & 0 & 1 \end{bmatrix} \begin{vmatrix} x_{CoG} \\ y_{CoG} \\ z_{CoG} \\ \phi_{CoG} \\ \theta_{CoG} \\ \psi_{CoG} \end{vmatrix} \tag{3.28}$$

where x_p ... ψ_p are the coordinates of the the point p in the global coordinate system and x_{CoG} ... ψ_{CoG} are the coordinates of the CoG in the global coordinate system. The RAOs at point p can then be computed using:

$$\boldsymbol{RAO}(\omega,\mu) = \frac{\boldsymbol{L}^T H_{FZ}(\omega,\mu)}{\boldsymbol{L}^T(-\omega^2(\boldsymbol{m}+\boldsymbol{A}(\omega)) + i\omega(\boldsymbol{B}(\omega)+\boldsymbol{B_{add}}) + \boldsymbol{C})\boldsymbol{L}} \tag{3.29}$$

3.3.2. RAO transformation using phase and amplitude

The RAOs can also be transformed from the CoG of the vessel to a desired location of the vessel (p) by using the RAOs and phase angles:

$$x = x_a \cos(\omega t + \epsilon_{x\zeta}) \tag{3.30}$$

$$y = y_a \cos(\omega t + \epsilon_{y\zeta}) \tag{3.31}$$

$$z = z_a \cos(\omega t + \epsilon_{z\zeta}) \tag{3.32}$$

$$\phi = \phi_a \cos(\omega t + \epsilon_{\phi\zeta}) \tag{3.33}$$

$$\theta = \theta_a \cos(\omega t + \epsilon_{\theta\zeta}) \tag{3.34}$$

$$\psi = \psi_a \cos(\omega t + \epsilon_{\psi\zeta}) \tag{3.35}$$

Where x_a ... ψ_a are the amplitudes and $\epsilon_{x\zeta}$ ... $\epsilon_{\psi\zeta}$ are the phase angles. For example $\frac{z_p}{\zeta_a}$ can then be computed as follows:

$$\frac{z_p}{\zeta_a} = \frac{z_{a,p}}{\zeta_a}\cos(\omega t + \epsilon_{z,p}) = \frac{z_{a,CoG}}{\zeta_a}\cos(\omega t + \epsilon_{z,CoG}) + b\frac{\phi_{a,CoG}}{\zeta_a}\cos(\omega t + \epsilon_{\phi,CoG}) - a\frac{\psi_{a,CoG}}{\zeta_a}\cos(\omega t + \epsilon_{\psi,CoG})$$

$$= \frac{z_{a,CoG}}{\zeta_a}\left(\cos(\omega t)\cos(\epsilon_{z,CoG}) - \sin(\omega t)\sin(\epsilon_{z,CoG})\right) + b\frac{\phi_{a,CoG}}{\zeta_a}\left(\cos(\omega t)\cos(\epsilon_{\phi,CoG}) - \sin(\omega t)\sin(\epsilon_{\phi,CoG})\right)...$$

$$... - a\frac{\theta_{a,CoG}}{\zeta_a}\left(\cos(\omega t)\cos(\epsilon_{\theta,CoG}) - \sin(\omega t)\sin(\epsilon_{\theta,CoG})\right)$$

$$= A\cos(\omega t) - B\sin(\omega t) \tag{3.36}$$

where A and B are:

$$A = \frac{z_{a,CoG}}{\zeta_a}(\cos(\epsilon_{z,CoG}) + b\frac{\phi_{a,CoG}}{\zeta_a}\cos(\epsilon_{\phi,CoG}) - a\frac{\theta_{a,CoG}}{\zeta_a}\cos(\epsilon_{\theta,CoG}) \tag{3.37}$$

$$B = \frac{z_{a,CoG}}{\zeta_a}(\sin(\epsilon_{z,CoG}) + b\frac{\phi_{a,CoG}}{\zeta_a}\sin(\epsilon_{\phi,CoG}) - a\frac{\theta_{a,CoG}}{\zeta_a}\sin(\epsilon_{\theta,CoG}) \tag{3.38}$$

From this we find that:

$$\frac{z_{a,p}}{\zeta_a} = \sqrt{A^2 + B^2} \tag{3.39}$$

$$\epsilon_{z,p} = \arctan\left(\frac{A}{B}\right) \tag{3.40}$$

Using the same method the RAOs for x and y at point p can be computed.

3.4. waves

The sea surface elevation can be split up in two main types of waves: Locally generated waves and swell. On a windless day on the Atlantic ocean the waves follow an almost sinusoidal shape. This is because only really few waves are combined here. This is swell and is generated at a different location. Locally generated waves are generated mainly by wind at or close to the location of the wave. The North sea has mainly locally generated waves but also some swell. Combining multiple waves gives a sea state like in figure 3.12.[Krogstad and Arntsen, 2000]

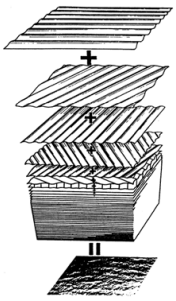

Figure 3.12: A sea-state is a combination of random waves

Therefor the surface of a sea or ocean can be described by the sum of different waves with each different height, period, direction and shape. To describe an ocean surface first the wave shape must be described using a model. Which model is most accurate is dependent on the relative water depth and steepness of the wave. In figure 3.13 the different wave theories are compared using the wave steepness: $\frac{H_s}{gT_p^2}$ and relative water depth: $\frac{d}{gT_p^2}$, where g is the gravitational acceleration, H_s is the significant wave height, T_p is the wave period and d is the water depth.

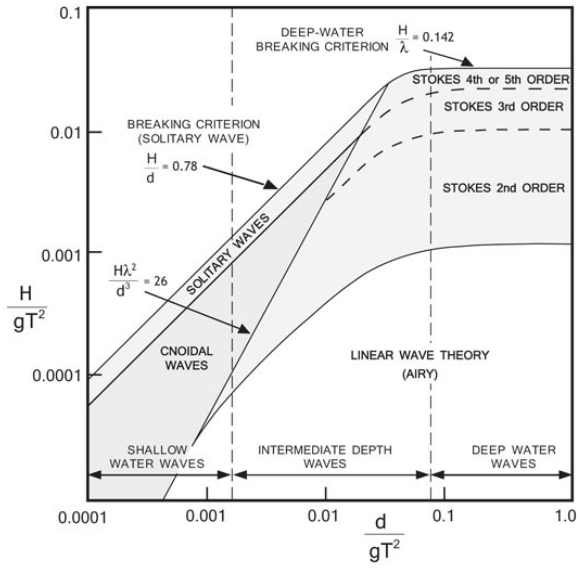

Figure 3.13: The wave models that are used for different wave conditions

The installations of monopiles will be done mainly in a waterdepths of around 50m with relatively small waves with short periods. So the waves that will be used are linear or Stokes second order waves. Using the waterdepth Aqwa decides if it will use stokes or linear waves [May, 2012]. Using the linear wave theory a wave can be described using the following parameters:

- wave amplitude ζ_a
- the angular frequency $\omega = \frac{2\pi}{Tp}$
- wave direction μ
- phase angle ϵ

One wave can be described as:

$$\zeta = \zeta_a \cos(kx - \omega t) \tag{3.41}$$

The surface elevation of a location in the ocean can then be described by summing a lot of these waves.

$$\zeta = \sum \zeta_{a,n} \cos(k_n x - \omega_n t + \epsilon_n) \tag{3.42}$$

where k is the wave number and is obtained using:

$$\omega^2 = k \arctan(kd) \tag{3.43}$$

Wave spectra are used to describe the energy the ocean has for a certain frequency range. From the wave spectrum the wave height at a certain frequency can be obtained using:

$$\frac{1}{2}\zeta_a^2 = S_\zeta(\omega)\Delta\omega \tag{3.44}$$

Using the same formula a wave spectrum can be made from measured data. This is done in many locations and conditions. The result are the two most commonly used wave spectra: the Pierson-Moskowitz spectrum and the Joint Northsea Wave Project (JONSWAP) spectrum as seen in figure 3.14.

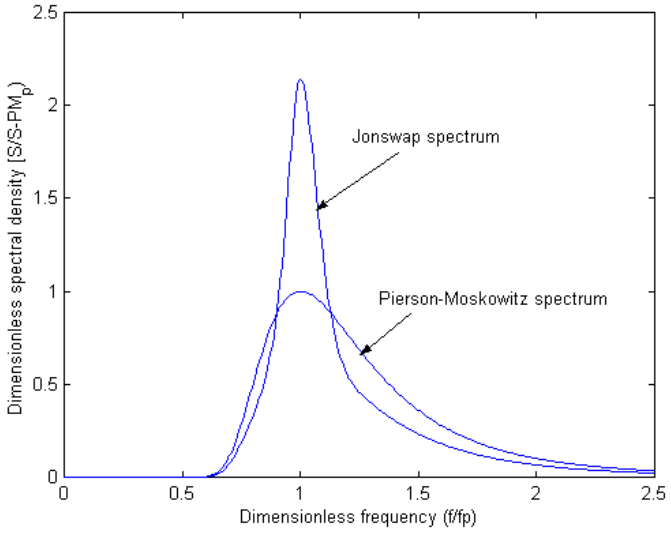

Figure 3.14: Comparison JONSWAP and Pierson-Moskowitz

The JONSWAP is based on a large database of measurements in the north sea. Since the Stella Synergy will mostly be installing monopiles in the north sea the JONSWAP spectrum is used in this thesis.

A JONSWAP spectrum is only accurate when:

$$3.6 < \frac{T_p}{\sqrt{H_S}} < 5 \tag{3.45}$$

The JONSWAP spectrum can be described using:

$$S_{JONSWAP} = \frac{320 H_s^2}{T_p^4} \omega^{-5} exp\left(\frac{1950\omega^{-4}}{T_p^4}\right) \gamma^{exp\left(-\left(\frac{\frac{\omega}{\omega_p}-1}{\sigma\sqrt{2}}\right)^2\right)} \tag{3.46}$$

From the north sea measurements the following parameters were obtained:
$\gamma = 3.3$
$\sigma = 0.07$ when: $\omega \leq \omega_p$
$\sigma = 0.09$ when: $\omega \geq \omega_p$

The wave spectrum shown in Figure 3.14 is unidirectional. This means that the waves come from one direction only. Using this unidirectional JONSWAP spectrum will make the data generated by the model less accurate, because in the north sea the waves do not come from one direction. The Stella Synergy will be able to rotate itself in any direction using its DP system. The Unidirectional waves will all come at ab angle of 0 °towards the ship leading to different motions as the realistic scenario where waves come from multiple directions.

Therefor a directional spectrum is used:

$$E(\mu, f) = S_\zeta(f) D(\mu, f) \tag{3.47}$$

Where $D(\mu, f)$ is the distribution of wave energy over the directions μ for a given frequency. Note that:

$$\int_{\mu=0}^{2\pi} D(\mu, f)\, d\mu = 1 \tag{3.48}$$

where:

$$D(\theta, f) = N(s) cos^{2s}\left(\frac{\theta - \theta_1}{2}\right) \tag{3.49}$$

Where N(s) makes sure the integral of D stays 1

$$N(s) = \frac{1}{\pi} 2^{2s-1} \frac{\Gamma^2(s+1)}{\Gamma(2s+1)} \tag{3.50}$$

where $\Gamma(s+1) = s!$ and s describes how much the waves are spread out over the directions. So for higher s the spectrum will become more concentrated on a single direction. In the locations Jumbo is going to use the vessel s is almost always around four.

Jumbo has an internal rule in which they assume the DP system is able to point the vessel straight into the waves with a deviation of 15°. In the model it is assumed that the waves are coming with a main direction of 15°. In figure 3.15 a directional JONSWAP spectrum made in MATLAB can be seen with a main wave direction of 15°

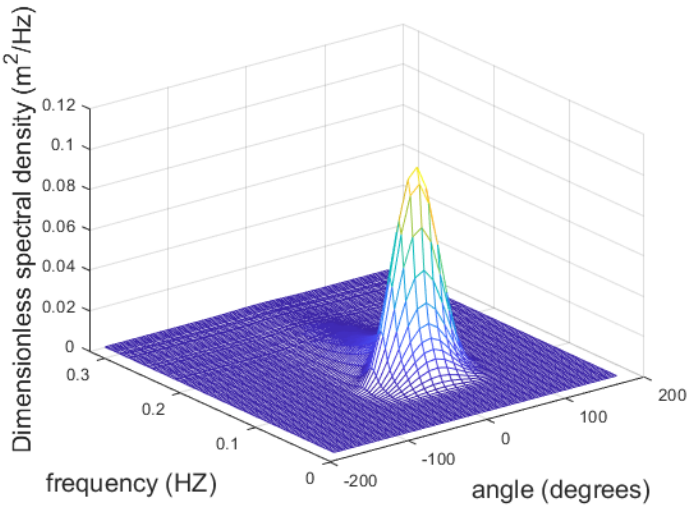

Figure 3.15: A directional Jonswap spectrum made in MATLAB

3.5. ship motions

Now that the vessels RAOs and the wave spectra are known the motions of the vessel can be looked at. The heave motions are taken as an example:

$$S_z = \left(\frac{z_a}{\zeta_a}\right)^2 S_\zeta \tag{3.51}$$

Where S_z is the motion spectrum of the ship. The significant heave amplitude ($z_{a,s}$) can then be calculated.

$$z_{a,s} = 4\sqrt{m_0(S_z)} \tag{3.52}$$

where:

$$m_0 = \int_0^\infty S_z(\omega)\, d\omega \tag{3.53}$$

Waves have a narrow spectrum and are Gaussian, because of this the probability distribution of wave height follows a Rayleigh distribution.[Charles, 1964]

$$P(H) = 1 - e^{\left(\frac{H}{H_r}\right)^2} \tag{3.54}$$

where: H_r is the root mean square of the wave height and H is an individual wave height. The most probable maximum (MPM) wave height can be defined as:

$$H_{MPM} = \frac{1}{2} z_{a,s} \sqrt{ln(n)} \tag{3.55}$$

where n is the number of waves that pas during the operation where the MPM is calculated for. For this project it is been estimated by:

$$n = \frac{T_{total}}{T_z} \tag{3.56}$$

where T_{total} is the total time over which the MPM is calculated and T_z is zero crossing wave period and is obtained with: $\frac{T_p}{0.777}$

3.6. location of upending device

Not only the motions of the monopile are important, but also the distance from the crane center to the hoisting point is important. Cranes have a load diagram in which the maximum load compared to the distance from the crane center is displayed. When the load gets further away from the crane center it will induce a bigger moment on the crane therefor the maximum lifting capability becomes less when the load is further away from the crane.

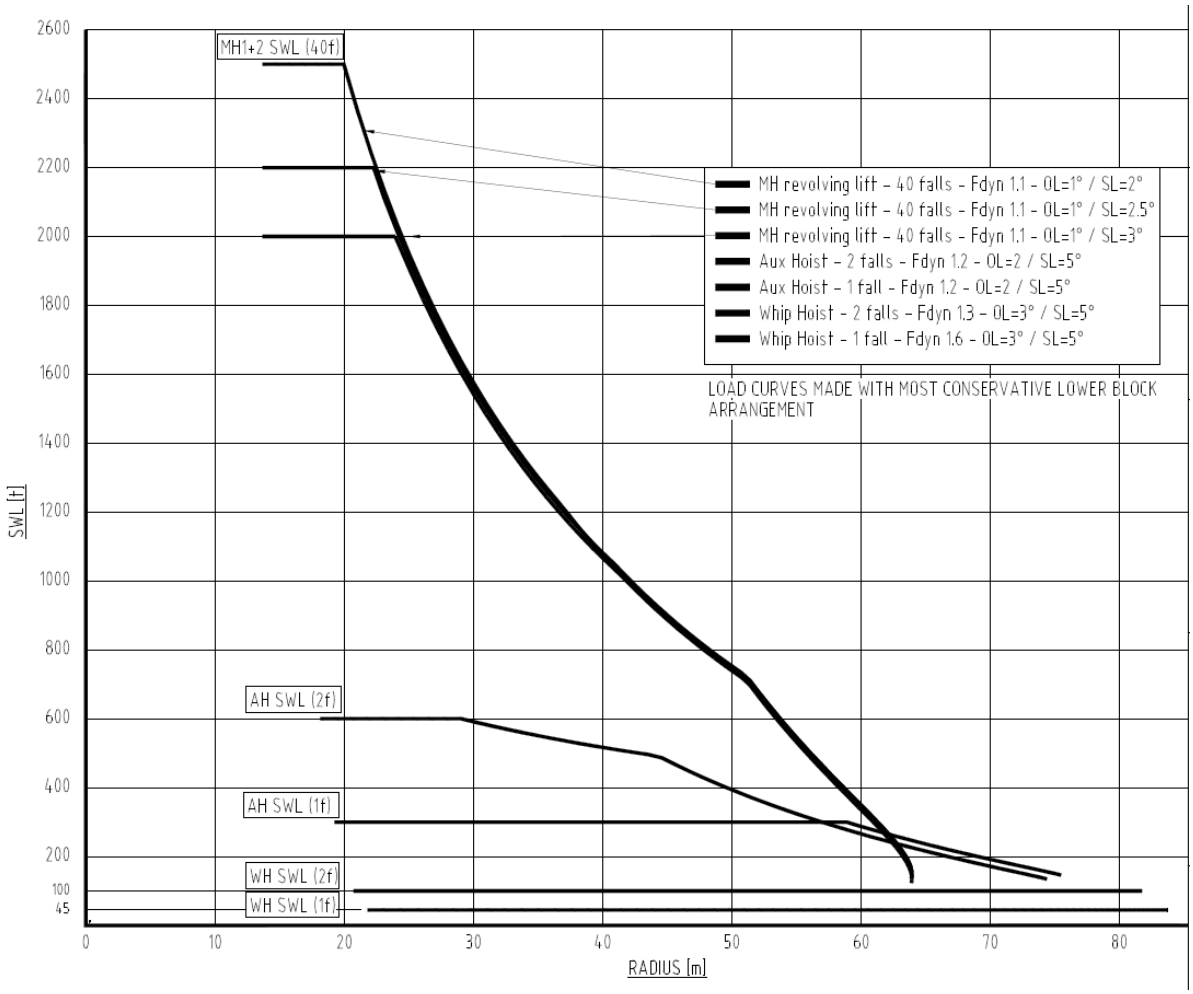

Figure 3.16: Crane load curve of the Stella Synergy[Jumbo-maritime, 2018]

In figure 3.16 it can be seen that the crane of the Stella Synergy can lift the maximum of 2500 tons between 13.5 and 20 meters away from the center of the crane. 13.5 meters is the minimum radius from which the crane can hoist, 20 meters is the maximum distance at which the crane has its full lifting capacity. To be able to install the heaviest monopiles the position of the gripper must be chosen in such a way that the monopile is lifted into the gripper within this range. This only leaves two ranges of locations for the monopile gripper: 13.5-20 m to the stern, or 13.5-20 m to the bow of the vessel compared to the center of the crane.
The end of the monopile where the crane hook is attached will follow a path with a constant x coordinate

when it is being upended. These paths are displayed in figure 3.17 with red and blue lines. The lines are for a 100m long monopile. The most important locations are highlighted with stars. The upper stars on the red and blue lines display the locations of the CoG of the monopile when it is laying flat in the gripper. This is where the crane will be attached to the monopile when it is lifting the monopile into the gripper. The lower two stars display the location of the monopile when it is straight up and the full weight will be hanging on the crane instead of on the gripper and the crane. The stars must be within the 13.5 - 20 m radius so that the crane will be able to lift as heavy monopiles as possible with this crane.

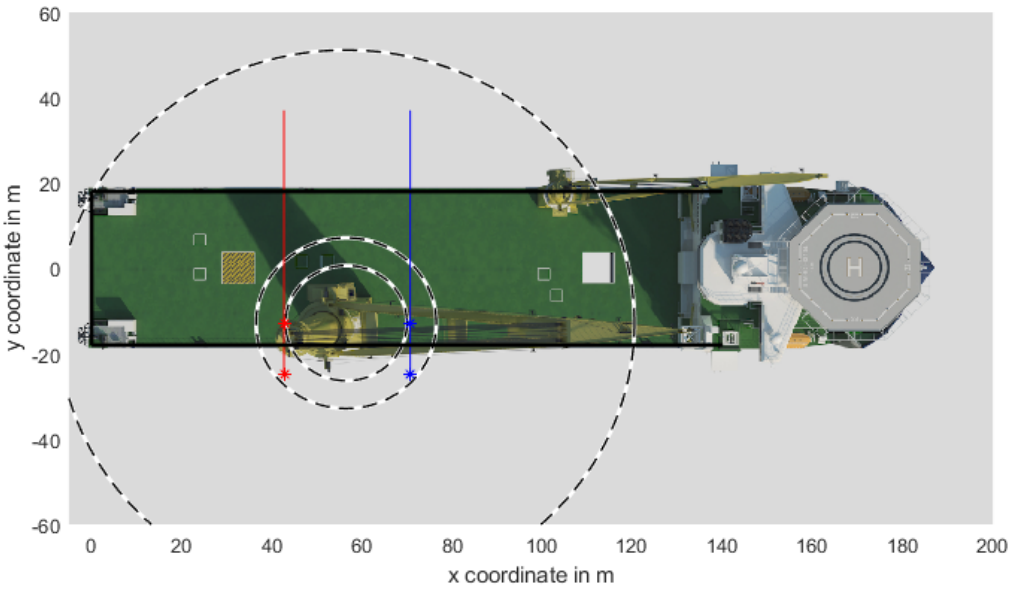

Figure 3.17: The two possible upending locations(red and blue lines) and crane lifting capabilities (dashed circles) plotted over the vessel.

The x locations of the gripper has been chosen in such a way that when the monopile increases in size slightly or the distance between the edge of the deck and the gripper becomes a bit larger the monopile will be within 20 meter radius of the center of the crane. The distance between the CoG of the monopile and center of the crane in x direction has been chosen to be 14 meters so that the lifting point will always stay easily outside of the minimum lifting radius of 13.5 meters. So the x coordinates for the two options become: $x = 42$ m and $x = 70$ m.

The loads on the crane during the upending process are the highest when the monopile is straight up and completely hanging on the crane. The y Coordinate of a 10 meter diameter monopile with 2 meter offset of the vessel is: $y = -25$ m. To choose between the two locations the motions of the ship are analysed at: $(42, -25)$ and $(70, -25)$. Not only the motions in z direction are important at the location of the gripper, but also the motions in x and y direction. The MPM of vessel motions have been analysed for common wave conditions in the central north sea from the scatter diagram (subsection 4.5.1) at $y = -16$ m. In figures 3.18, 3.19 and 3.20 the MPM of ship motion in sway, surge and heave directions are plotted against the x coordinate of the ship. In table 3.7 the legend of the figures are shown and in table 3.6 the wave data used to make the figures is shown.

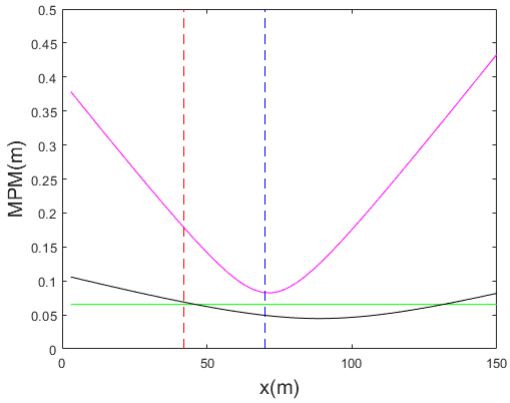

Figure 3.18: MPMs of ship motions at $y = -16m, T_p = 5$ and $H_{m0} = 1$

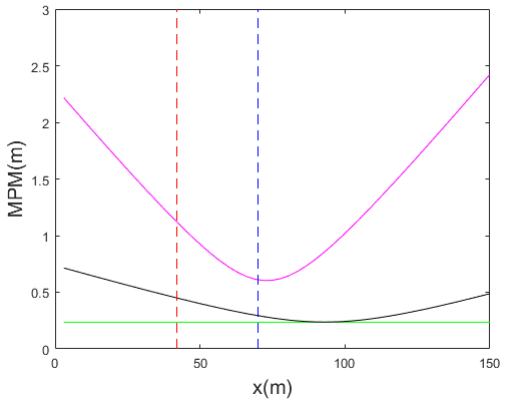

Figure 3.19: MPMs of ship motions at $y = -16m, T_p = 7$ and $H_{m0} = 1.5$

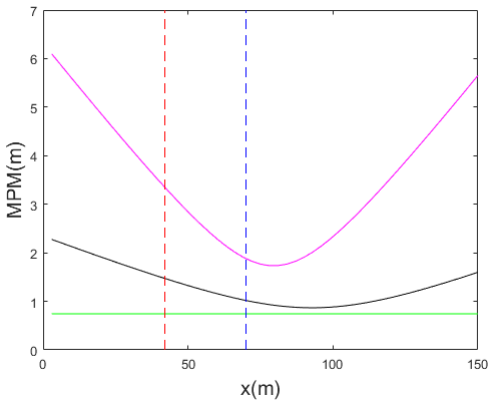

Figure 3.20: MPMs of ship motions at $y = -16m, T_p = 9$ and $H_{m0} = 2$

Table 3.6: Wave data used in figures 3.18, 3.19 and 3.20

figure	3.18	3.19	3.20	
T_p	5	7	9	s
H_{m0}	1	1.5	2	m
μ	15	15	15	degrees

Table 3.7: Legend of figures 3.18, 3.19 and 3.20

blue	Heave MPM
black	Sway MPM
green	Surge MPM
red dashed	position 1 ($x = 42$ m)
blue dashed	position 2 ($x = 70$ m)

From figures 3.18, 3.19 and 3.20 it is clear that the MPM of surge motions is the same for both locations which is logical because it is not dependent on the x location. The sway and especially heave motions are a lot smaller in position one then in position two in all three sea states. Position one is therefor a better location for upending as well as gripping the monopile while it is driven into the ground.

A disadvantage of position one is that when the monopile is lifted from a barge and rotated into the gripper it needs to pass the secondary crane of the vessel. The maximum size of monopile that can be loaded on the gripper safely is 105 m. When the CoG of the monopile is not in the center of the monopile the maximum length can become smaller, like with tapered monopiles. As seen insection 4.1 a monopile with a length of 100m and diameter of 10m will already weigh around 2500t (the maximum lifting capacitiy of the Stella Synergy) and therefor there are not a lot of monopiles above 100m that can be installed with the Stella Synergy.

Because on location one the motions are a lot less severe then on location two the upending device is advised to be placed at location one for monopiles up to 105 m. When longer monopiles need to be installed the upending device can be removed and installed at location two. The gripper will be easily removable because it also needs to be removed when different offshore equipment (not monopiles) need to be installed.

4

Upending forces and workability

In this chapter the forces on the crane and gripper during upending are modeled. First the motions of the vessel with monopile on it are modeled, then the forces on the gripper and crane during upending are modeled and finally the workability of upending with the crane of the Stella Synergy is computed.

4.1. simplifications and assumptions

First the dimensions of the monopile are obtained. The monopile will have a diameter of 10m and a length of 100m. According to:[Vicente Negro, 2015] the monopile wallthickness should be around 0.1m for this size of monopile. When the weight of the monopile is calculated for a monopile with these sizes it turns out to be 2500 tons. Which is the maximum lifting capacity of the Stella Synergy.

To check if the hoisting cable can be assumed to be infinitely stiff the eigenfrequency has been calculated:

$$f = \frac{1}{2\pi}\sqrt{\frac{c_{cable}}{m_{mp}}} \tag{4.1}$$

where c_{cable} is the stiffness of the hoisting cable. The hoisting cable of the Stella Synergy for heavy lifting is $n_f = 40$ fall, therefor the stiffness is calculated as follows:

$$c_{cable} = \frac{n_f^2 EA}{l_{total}} \tag{4.2}$$

the stiffness is multiplied by n_f^2 because when the cable stretches one meter the crane hook only goes down by $\frac{1}{n_f}$ meter and the load on the cable is $\frac{1}{n_f}$ of the load on the crane. l_{total} is the total length of the hoisting cable which is:

$$l_{total} = n_f l_c + c \tag{4.3}$$

where c is the z coordinate of the crane tip which is included because the cable goes back from the crane tip to the winch. Only the z coordinate is included because the crane is almost straight up when hoisting a heavy monopile (see crane lift curve Figure 3.16).

Using this the naturalfrequency is: $f = 1.13\ Hz$ when the crane hook is highest in the upending process and $f = 0.81\ Hz$ when the crane hook is lowest (when the monopile is lowered). Waves with this frequency do not excite the motions of the vessel and and therefor will not excite the naturalfrequency. In the other faces of upending there is much less load on the crane and therefor the naturalfrequency is even higher. Because the naturalfrequency of the system is not excited the crane cable is infenetly stiff. The following assumptions are made as well:

- The vessel, crane, monopile and gripper are infinetly stiff.
- The upending speed is so low it does not influence the motions of the vessel.

4.2. Phases in upending process

In the upending process the following phases are analysed:

Table 4.1: Different phases in monopile upending

Phase	θ_u (°)	Forces in z act on:	Displayed in:
1	0	gripper only	Figure 4.1
2	0	gripper and crane	Figure 4.2
3	30	gripper and crane	Figure 4.3
4	60	gripper and crane	Figure 4.4
5	90	gripper only	Figure 4.5
6	90	crane only	Figure 4.6

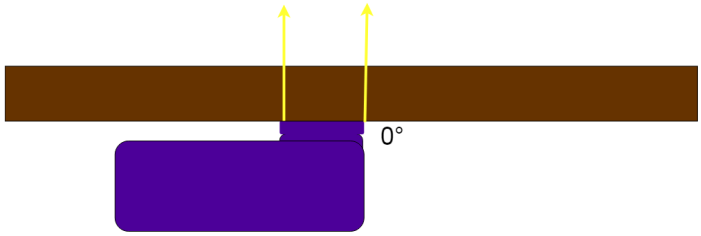

Figure 4.1: Phase 1: forces only on gripper, upending angle: 0°

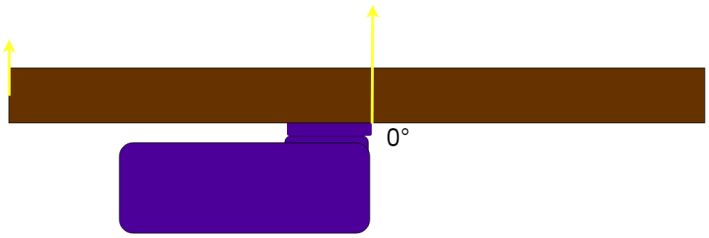

Figure 4.2: Phase 2: forces on gripper and crane, upending angle: 0°

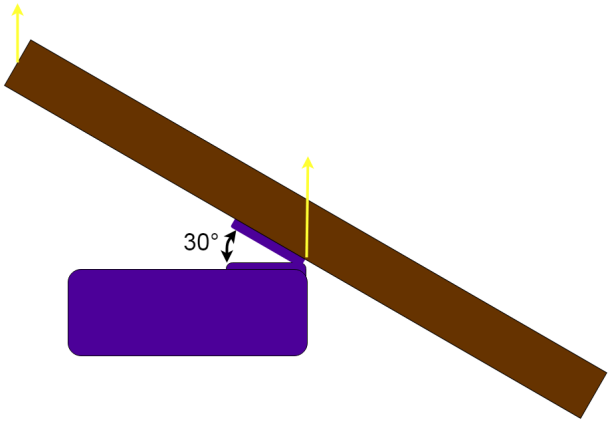

Figure 4.3: Phase 3: forces on gripper and crane, upending angle: 30°

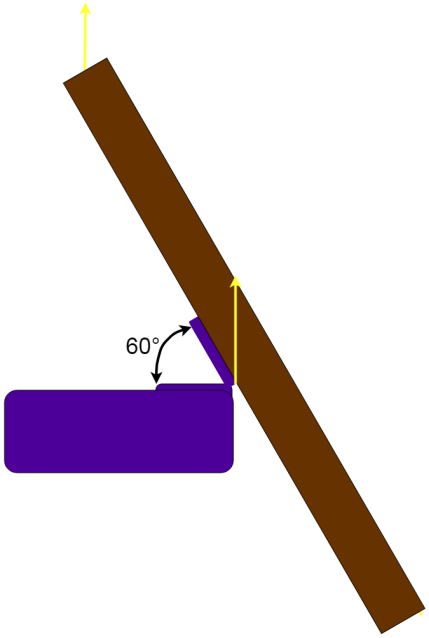

Figure 4.4: Phase 4: forces on gripper and crane, upending angle: 60°

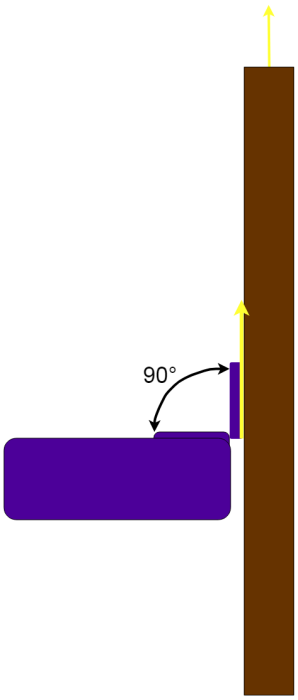

Figure 4.5: Phase 5: forces on gripper and crane, upending angle: 90°

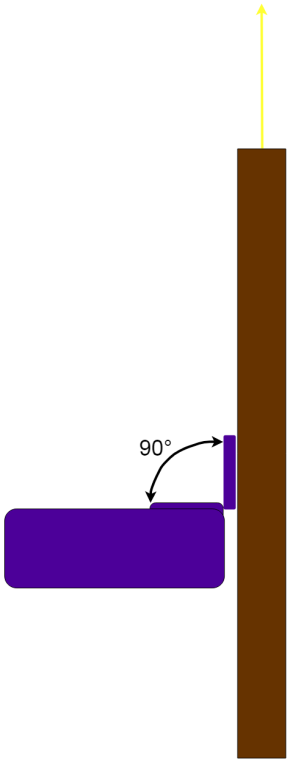

Figure 4.6: Phase 6 : forces on gripper and crane (z direction forces only on crane), upending angle: 90°

4.3. motions of vessel with monopile

In this section the motions of the vessel with the monopile connected to it are modeled for the six phases described in section 4.2.

4.3.1. coordinate system of monopile

The local coordinate system of the monopile has been chosen in such a way that when it is fully up-ended (phase 6: $\theta_u = 90°$) the coordinate system aligns with the global coordinate system.

Because the monopile is rotated when going from phase to phase, the local coordinate system changes compared to the global coordinate system. The monopile rotates around the global x axis. To transform motions from the local to the global coordinate system a rotation matrix has been made:

$$\boldsymbol{\Theta_u} = \begin{bmatrix} 1 & 0 & 0 & 0 & 0 & 0 \\ 0 & \sin(\theta_u) & \cos(\theta_u) & 0 & 0 & 0 \\ 0 & -\cos(\theta_u) & \sin(\theta_u) & 0 & 0 & 0 \\ 0 & 0 & 0 & 1 & 0 & 0 \\ 0 & 0 & 0 & 0 & \sin(\theta_u) & 0\cos(\theta_u) \\ 0 & 0 & 0 & 0 & -\cos(\theta_u) & \sin(\theta_u) \end{bmatrix} \tag{4.4}$$

Where θ_u is the upending angle.
By multiplying the $\boldsymbol{\Theta_u}$ matrix with motions in the local system it gives the motions or global coordinate system.

4.3.2. mass matrix monopile

To caclulate the accelerations a mass matrix for the monopile is made. This is done the same way as the mass matrix of the vessel in subsection 3.2.1:

$$\boldsymbol{m_{mp}} = \begin{bmatrix} m_{mp} & 0 & 0 & 0 & 0 & 0 \\ 0 & m_{mp} & 0 & 0 & 0 & 0 \\ 0 & 0 & m_{mp} & 0 & 0 & 0 \\ 0 & 0 & 0 & I_{xx,mp} & 0 & 0 \\ 0 & 0 & 0 & 0 & I_{yy,mp} & 0 \\ 0 & 0 & 0 & 0 & 0 & I_{zz,mp} \end{bmatrix} \tag{4.5}$$

where m_{mp} is the mass of the monopile and $I_{xx,mp}$, $I_{yy,mp}$ and $I_{zz,mp}$ are the moments of inertia of the monopile. It is assumed that the wall thickness of the monopile is infinitely thin during the moment of inertia calculations. The moments of inertia can therefor be calculated as follows:

$$I_{xx} = \frac{1}{2} m_{mp} r^2 + \frac{1}{12} m_{mp} l^2 \tag{4.6}$$

$$I_{yy} = \frac{1}{2} m_{mp} r^2 + \frac{1}{12} m_{mp} l^2 \tag{4.7}$$

$$I_{zz} = m_{mp} r^2 \tag{4.8}$$

where l is the length of the monopile and r is the radius of the monopile. $I_{xx} = I_{yy}$ because of symmetry.

The weight of the monopile lifting tool has also been taken into account. A 100 ton lifting tool is used. The lifting tool will be attached to the end of the monopile and is the connection between the monopile and the crane hook. The lifting tool is modeled as a point mass at the end of the monopile.

To include the weight of the monopile lifting tool into the model it is added to the $\boldsymbol{m_{mp}}$ matrix, this results in:

$$m_{mp+lt} = m_{mp} + m_{lt} \tag{4.9}$$

$$\boldsymbol{CoG_{mp+lt}} = \frac{\boldsymbol{CoG_{mp}} m_{mp} + \boldsymbol{CoG_{lt}} m_{lt}}{m_{mp+lt}} \tag{4.10}$$

$$I_{xx,mp+lt} = I_{xx,mp} + m_{mp}(CoG_{mp+lt,z} - CoG_{mp,z})^2 + m_{lt}(CoG_{mp+lt,z} - CoG_{lt,z})^2 \tag{4.11}$$

$$I_{yy,mp+lt} = I_{yy,mp} + m_{mp}(CoG_{mp+lt,z} - CoG_{mp,z})^2 + m_{lt}(CoG_{mp+lt,z} - CoG_{lt,z})^2 \tag{4.12}$$

$$I_{zz,mp+lt} = I_{zz,mp} \tag{4.13}$$

Where $_{lt}$ is related to the lifting tool, $_{mp}$ is related to the monopile and $_{mp+lt}$ is related to them combined. The CoG_z coordinates are in the local coordinate system for the monopile.The results are filled into the $\boldsymbol{m_{mp}}$ matrix. The lifting tool is assumed to be a point mass so I_{zz} does not change.

4.3.3. stability and balasting

The draft during upending is determined in such a way that the vessel will have a $GM > 2.5$m during the whole monopile installation process so that the draft of the vessel will not have to be changed during upending. When the vessel is hoisting the monopile from the barge the GM is the lowest. When the vessel heels the monopile will go further away from the vessel increasing the moment it excerts on the vessel. The CoG_{mp} is taken at the tip of the crane when computing GM, as explained in section 5.3. A deeper draft will result in a higher GM

$$GM_{hoisting} = GM - CoG_{ves,z} + \frac{CoG_{ves,z} m_{ves} + z_{ct} m_{mp}}{m_{ves} + m_{mp}} \tag{4.14}$$

GM is only bigger then 2.5m with a draft of 8m, therefor the draft of the vessel is chosen to be 8m during the whole monopile installation process. In the model discussed in chapter 4 the vessel is assumed to keep the same draft throughout the monopile installation process using the ballasting system. To maintain the same draft the mass of the vessel decreases by removing ballast when the monopile and lifting tool are in the gripper or on the crane.

Because of the removed ballast the CoG_z changes:

$$CoG_{vb,z} = \frac{CoG_{ves,z} m_{total} - z_{ballast} m_{mp+lt}}{m_{total} - m_{mp+lt}} \tag{4.15}$$

where $_{vb}$ stands for the vessel after ballasting adjustment and $z_{ballast}$ is the z coordinate of the ballast. The ballast is assumed to be at the same x coordinate as the CoG_{vessel} so the x coordinate of the CoG stays the same after the ballasting adjustment. The ballast tanks are at a radius: $r_{ballast}$ away from the middle of the vessel.The moments of inertia of the vessel with adjusted balasting are:

$$I_{xx,vb} = I_{xx,vessel} - \left(z_{ballast}^2 + r_{ballast}^2\right) m_{mp} \tag{4.16}$$

$$I_{yy,vb} = I_{yy,vessel} - z_{ballast}^2 m_{mp} \tag{4.17}$$

$$I_{zz,vb} = I_{zz,vessel} - r_{ballast}^2 m_{mp} \tag{4.18}$$

To compose the mass matrix $\boldsymbol{M_{total}}$ of the vessel, the monopile and the monopile lifting tool combined the same method is used as combining the monopile and lifting tool. For every phase in the upending process analysed there is a separate $\boldsymbol{M_{total}}$ matrix, because the CoG of the monopile changes. The mass matrices of the monopile under angle θ_u are computed using the $\boldsymbol{\Theta_u}$ from subsection 4.3.1 [J. Peraire, 2008]

$$\boldsymbol{m_{mp+lt,\theta_u}} = \boldsymbol{\Theta_u} \boldsymbol{m_{mp+lt}} \boldsymbol{\Theta_u}^T \tag{4.19}$$

The total CoG is then given by:

$$CoG_{total} = \frac{CoG_{vessel} m_{vb} + CoG_{mp+lt} m_{mp+lt}}{m_{total}} \tag{4.20}$$

where m_{vb} is the weight of the ballasted vessel without the monopile and lifting tool.

$$I_{xx,total} = I_{xx,vb} + I_{xx,mp+lt,\theta_u} + m_{mp+lt}\left(CoG_{mp+lt,y} - CoG_{vessel,y}\right)^2 + m_{mp+lt}\left(CoG_{mp+lt,z} - CoG_{vessel,z}\right)^2 \tag{4.21}$$

$$I_{yy,total} = I_{yy,vb,\theta_u} + I_{yy,mp+lt} + m_{mp+lt}\left(CoG_{mp+lt,x} - CoG_{vessel,x}\right)^2 + m_{mp+lt}\left(CoG_{mp+lt,z} - CoG_{vessel,z}\right)^2 \tag{4.22}$$

$$I_{zz,total} = I_{zz,vb,\theta_u} + I_{zz,mp+lt} + m_{mp+lt}\left(CoG_{mp+lt,y} - CoG_{vessel,y}\right)^2 + m_{mp+lt}\left(CoG_{mp+lt,x} - CoG_{vessel,x}\right)^2 \tag{4.23}$$

Where I_{xx,mp,θ_u}, I_{yy,mp,θ_u} and I_{zz,mp,θ_u} are from the $\boldsymbol{m_{mp+lt,\theta_u}}$ matrix. The $\boldsymbol{M_{total}}$ matrices can then be filled in for every phase of the upending process. The moments of inertia are around the CoG of the vessel when the monopile is not on it because we know the damping and added mass matrices for this point. All movements modeled will be around this point unless mentioned separately.
Jumbo has an internal rule that the GM value of the vessel should stay above 2.5 m during the installation process to ensure stability. GM will change for every phase in the upending process because of the change in height of the CoG of the monopile. GM is checked the following way:

$$GM_{total} = GM_{vessel} - CoG_{vessel,z} + CoG_{total,z} \tag{4.24}$$

Table 4.2: The GM of the vessel during different phases in the upending process.

Phase	θ_u (°)	GM (m)
1	0	5.73
2	0	5.73
3	30	5.62
4	60	5.61
5	90	5.76
6	90	5.76

The new GM is filled in the stiffness matrix from subsection 3.2.2 for every fase in the upending process. This is the only variable that changes in the $\boldsymbol{C}$ matrix. So only $\boldsymbol{C}(4,4)$ and $\boldsymbol{C}(5,5)$change.

The ballasting system of the vessel will keep the vessel straight up during the monopile upending process. The required ballast that needs to be released from one side of the vessel and added to the other side is calculated for every phase in the upending process using:

$$\Delta m_{ballast} = \frac{1}{2}\frac{m_{total} CoG_{total,y}}{r_{ballast}} \tag{4.25}$$

The half is because the mass is removed from one side and added to the other to remain at the same draft. The ballasting needed is:

Table 4.3: Ballast that needs to be placed from one side of the vessel to the other during the different phases in the monopile upending process.

Phase	θ_u (°)	ballast (tons)
1	0	883
2	0	883
3	30	1248
4	60	1672
5	90	2043
6	90	2043

4.3.4. radiation, diffraction and undisturbed wave froces of monopile

In phases three to six of the upending process the monopile is partly under water, because of this there are wave forces acting on the monopile. To obtain the diffraction, radiation and undisturbed wave forces of the monopile next to the vessel first a 3D model of the monopile has to be made. This is done in Solidworks using the dimensions as described in section 4.1. The 3D model of the monopile is then imported into Ansys Aqwa. There the monopile is placed next to the hull of the Stella Synergy. When they are next to each other they influence each other and the incoming waves. This is taken into account in Aqwa. For every phase where the monopile is partly under water a new 3D model is made in which the monopile is placed differently on the vessel. Then a Matlab model is made for every phase. A mesh of the Stella Synergy with monopile can be seen in Figure 4.7

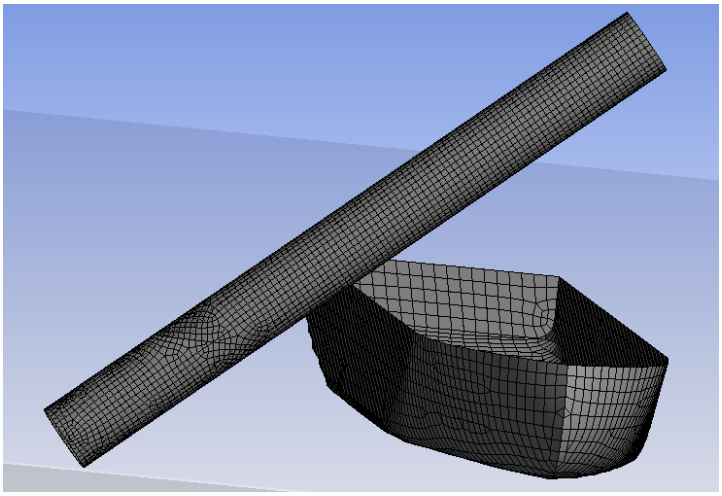

Figure 4.7: The mesh of the Stella Synergy with monopile

4.3.5. viscous damping of monopile

The viscous roll and pitch damping of the monopile during upending are calculated using the resistance of a cylinder in water. The disadvantage of this is that the viscous effects of the water at the end of the monopile will be ignored. The drag coefficient C_D is read out of Figure 4.8 [Wenjun Gao, 2018]. The Reynolds number (Re) is calculated using:

$$Re = \frac{VL}{\nu} \tag{4.26}$$

Where L is the specific length which is the diameter of the monopile in this case, V is the velocity of the fluid going over the object and ν is the kinematic viscosity of the sea water. The Reynolds number of the monopile on the vessel is around 10^7 and therefor the drag coefficient C_D is around 1 as seen in figure Figure 4.8. The new monopile has no sea growth on it during installation and is therefor assumed to be a smooth cylinder.

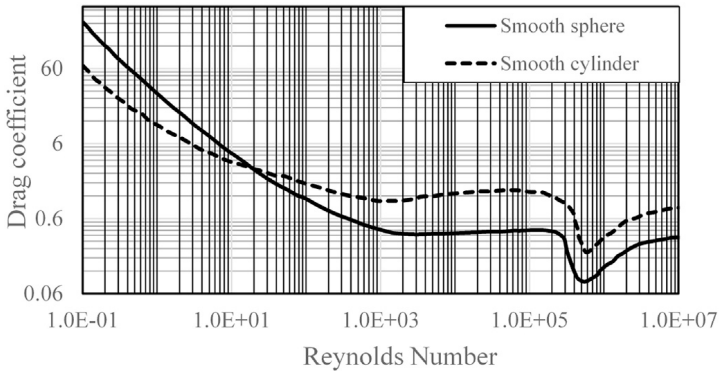

Figure 4.8: C_D of a cylinder for different Reynolds numbers

Keulegan and Carpenter discovered that the drag coefficient of a oscillating object is dependent on a different number; this is called the Keulegan Carpenter number [G.H. Keulegan, 1985]. The KC number is defined as:

$$KC = \frac{u_a T}{L} \tag{4.27}$$

Where u_a is the flow velocity amplitude. For sinusoidal waves the KC number can be defined as:

$$KC = \pi \frac{H_{m0}}{L} \tag{4.28}$$

For all wave conditions analysed and a specific length of $L = 10m$ the KC number does never exceed ten. When the C_D for a smooth cylinder with a KC of lower then ten is evaluated in Figure 4.9 C_D is 1 again. So for this size of cylinder in the analysed conditions using KC and Reynolds give the same results.

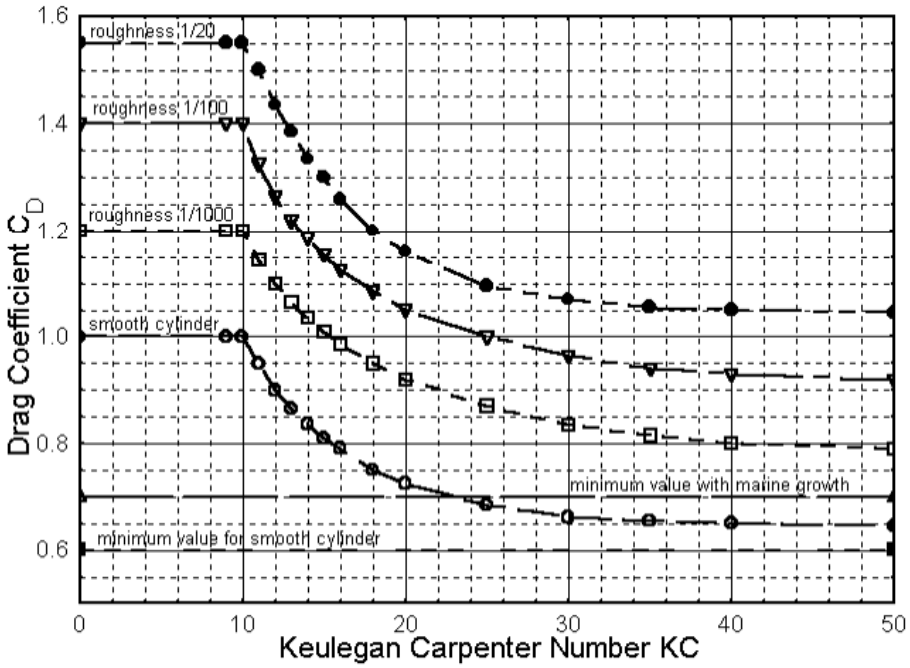

Figure 4.9: C_D of a cylinder for different KC numbers

Using this drag coefficient the resistance of the monopile while it is moving through water can be computed using:

$$F_r = \frac{1}{2}\rho V^2 C_D A \tag{4.29}$$

Where A is the frontal surface area of the monopile, ρ is the sea water density and F_r is the resistance force. The drag formula depends on V^2 and is therefor not linear. To be able to use the calculated viscous damping in the frequency domain it needs to be liniearised. Stochastic linearisation is used.[Y. Drobyshevski, 2018]

$$B|\dot{\phi}|\dot{\phi} = \left(B\sqrt{\frac{8}{\pi}}rms(\dot{\phi}_{spectrum})\right)\dot{\phi} = B_{lin}\dot{\phi} \tag{4.30}$$

Where rms is the root mean square of the motion: $= \sqrt{m_{0\zeta}}$ and is obtained using iterations. First an estimation is done for $rms(\dot{x}_{spectrum})$ then the model computes the new value of $rms(\dot{x}_{spectrum})$ and that is then filled in in the model again until it converges. This means that the $rms(\dot{x}_{spectrum})$ that is filled into the model is the same as the model computes it to be.

The viscous damping is only modeled for roll and pitch and only motions square to the local z axis of the monopile are taken into account. B_{add} is calculated using:

$$M_{x/y} = \int_{l_1}^{l_2} \frac{1}{2}\rho D(\dot{\phi}l)^2 l C_D dl = \frac{\rho D\dot{\phi}^2 C_D(l_2^4 - l_1^4)}{8} \tag{4.31}$$

where l_1 is the distance from the water line to the z = 0 and l_2 is the distance from the waterline to the bottom of the monopile and D is the diameter of the monopile.

From this we can conclude that:

$$B_{add} = \frac{M_{x/y}}{\dot{\phi}^2} = \frac{\rho D C_D(l_2^4 - l_1^4)}{8} \tag{4.32}$$

B_{add} is then linearised to get B_{lin} using stochastic liniearisation. This is done for every phase in the upending process. The results are:

Table 4.4: The linearised angular roll velocity and viscous drag of the monopile for the different upending phases

Phase	$\dot{\phi}_{spectrum}$ (rad/s)	$\dot{\theta}_{spectrum}$ (rad/s)	$B_{\phi,lin}$ (MNm)	$B_{\theta,lin}$ (MNm)
1	-	-	-	-
2	-	-	-	-
3	0.0166	0.0142	300	4.28
4	0.0073	0.0128	96	7.86
5	0.0048	0.0129	27.7	74.5
6	0.0048	0.0129	27.7	74.5

The optimization has been done for a wave with : $H_{m0} = 1.5m$ and $T_p = 8s$ which is a conditions that occurs regularly on the north sea as seen in subsection 4.5.1.

4.3.6. RAOs

The ships RAOs and phase angles are modeled for every phase in the upending process. This is done the same way as in chapter 3:

$$\boldsymbol{RAO}(\omega,\mu) = \frac{\boldsymbol{L}^T\left(\boldsymbol{H_{FZ,ves}} + \boldsymbol{H_{FZ,mp}}\right)}{\boldsymbol{L}^T\left(-\omega^2(\boldsymbol{M_{total}} + \boldsymbol{A_{ves}} + \boldsymbol{A_{mp}}) + i\omega(\boldsymbol{B_{ves}} + \boldsymbol{B_{mp}} + \boldsymbol{B_{add,ves}} + \boldsymbol{B_{add,mp}}) + \boldsymbol{C_{ves}} + \boldsymbol{C_{mp}}\right)\boldsymbol{L}} \tag{4.33}$$

Where $\boldsymbol{ves}$ referes to the vessel. The wave forces, added mass, damping and added damping of the monopile are compared to the CoG of the vessel, so that the forces and moments act on and around the CoG of the vessel. The $\boldsymbol{M}$, $\boldsymbol{A}$, $\boldsymbol{B}$, $\boldsymbol{B_{add}}$ $\boldsymbol{C}$ and $\boldsymbol{L}$ matrices change for every phase in the upending process. So for every phase a separate set of RAOs is created. The L matrix is adjusted so that the RAOs are modeled for the CoG of the monopile. In subsection 3.3.1 is explained how the L matrix is filled in. This will make the calculation of the forces later easier.

4.4. Forces on monopile

4.4.1. Force RAO

The forces on the monopile are obtained using the force RAOs. Rewriting the RAO formula leads to:

$$\boldsymbol{RAO}\left(-\omega^2(\boldsymbol{M_{ves}} + \boldsymbol{M_{mp}} + \boldsymbol{A_{ves}} + \boldsymbol{A_{mp}}) + i\omega(\boldsymbol{B_{ves}} + \boldsymbol{B_{mp}} + \boldsymbol{B_{add,ves}} + \boldsymbol{B_{add,mp}}) + \boldsymbol{C_{ves}} + \boldsymbol{C_{mp}}\right) = \boldsymbol{H_{FZ,ves}} + \boldsymbol{H_{FZ,mp}} \tag{4.34}$$

From this we find that:

$$\frac{\boldsymbol{F_{mp}}}{\boldsymbol{\zeta_a}} = \boldsymbol{RAO}\left(-\omega^2(\boldsymbol{M_{mp}} + \boldsymbol{A_{mp}}) + i\omega(\boldsymbol{B_{mp}} + \boldsymbol{B_{add,mp}}) + \boldsymbol{C_{mp}}\right) - \boldsymbol{H_{FZ,mp}} \tag{4.35}$$

In this equation the forces, added mass and damping are filled in for the coordinate system of the monopile. So moments and forces on and around the CoG of the monopile. This will result in a force per meter of wave height. This is then squared and multiplied with the wave spectrum. Now that the response spectrum of the forces is known the MPM of forces can be computed as explained in section 3.5. The forces that act on the monopile must be transfered directly to the vessel because the connection is assumed to be infinitely stiff.

4.4.2. buoyancy of monopile

During the upending process the monopile will get partly submerged. This will generate buoyancy forces and moments which are different for every phase in the upending process. The buoyancy force works in positive z direction and acts in the center of the submerged part of the monopile.

The submerged part of the monopile for all phases is:

$$l_{submerged}(\theta_u) = \frac{\sin(\theta_u)(\frac{l_{mp}}{2} - l_{dCoG}) - \cos(\theta_u)(d_{mp} + l_{\theta_u,gripper}) - l_{\theta_u}}{\sin(\theta_u)} \tag{4.36}$$

Where l_{dCoG} is the distance from the point where the monopile rotates around to the center of the CoG of the monopile in z direction (measured when θ_u is 90 °), $l_{\theta_u,gripper}$ is the height of the gripper that rotates with the monopile and l_{θ_u} is the length from the point where the monopile rotates around to the water. The negative submerged lengths are made zero. The total buoyancy force can then be calculated using:

$$F_b = g m_{mp} \frac{\rho_w l_{submerged}}{\rho_s l_{mp}} \tag{4.37}$$

The moment the buoyancy generates around the CoG of the monopile is:

$$r_b = cos(\theta_u) \frac{l_{mp} + l_{submerged}}{2} \tag{4.38}$$

$$M_b = r_b F_b \tag{4.39}$$

The results at the CoG of the monopile are:

Table 4.5: Buoyancy forces and moments

Phase	θ_u(°)	$l_{submerged}$	$F_b(MN)$	$M_b(MNm)$
1	0	0	0	0
2	0	0	0	0
3	30	17.7	0.55	19.7
4	60	32.2	1.01	17.0
5	90	37.4	1.17	0
6	90	37.4	1.17	0

In phase 1 to 2 the monopile is still out of the water therefor the buoyancy force and moment are zero. In phase 5 and 6 the monopile is straight up and therefor the buoyancy force does not generate any moment around the CoG of the monopile.

4.4.3. results

The forces on the gripper and crane are modeled by combining the buoyancy with the gravitational and dynamic forces on the monopile. Then the forces are balanced between the gripper and the crane. During phase 1 and 5 it is assumed that all forces act on the gripper. During phase 6 the gripper is locked into its position and the monopile clamps are loosened so it can move in z direction, therefor all forces in z direction act on the crane and all other forces and moments on the gripper. During the other phases the moment around the x axis and the forces in z direction are divided over the gripper and crane. The forces on crane are:

$$F_{crane} = \frac{l_{dCoG} F_{mp,z} + \dfrac{M_{mp,x}}{\cos(\theta_u)}}{l_{dCoG} + \dfrac{l_{mp}}{2}} \tag{4.40}$$

In this thesis the dynamic forces that act on the monopile are assumed to be linear proportional to the wave height. Therefor the dynamic forces are displayed as a function of the wave height $\left(\frac{F_{mp}}{\zeta_a}\right)$ and the static forces are displayed separately. The static forces on the crane and gripper are calculated by combining the buoyancy and the gravitational forces on the monopile:

Table 4.6: Static forces on monopile and gripper

Phase	$F_c(MN)$	$F_z(MN)$
1	0	25.5
2	2.3	23.2
3	2.7	22.3
4	2.8	21.7
5	0	24.3
6	24.3	0

Where F_c is the force on the crane cable in z direction and F_z is the the force on the gripper in z direction. The static forces and moments in other directions are zero. Note that the monopile with the gripping tool together weigh 2600 tons, but because of buoyancy the vessel is capable of upending a 2500 ton monopile. When the monopile is being lifted from a barge onto the gripper the monopile is not partly submerged and therefor there is no buoyancy during this operation. No monopile lifting tool as needed for upending is needed to lift the monopile from the barge. See chapter 5 for more information on the monopile lifting process.

The dynamic forces are displayed for every phase in the upending process. In phase 1 the forces on the crane are zero, so these are not displayed. The forces and moments during phase 1 dependent on the wave period are displayed in Appendix B.1.1.

In phase 2,3 and 4 the gripper can not resist moments around the x axis, since it can freely rotate around the x axis and is modeled as a hinge. Therefor the graph of the moment around the x axis is not shown and instead the force on the crane is plotted. The moment around the x axis and forces in z direction work partly on the crane and partly on the gripper. The forces and moments during phase 2,3 and 4 per meter wave amplitude dependent on the wave period are displayed in: Appendix B.1.2, Appendix B.1.3 and Appendix B.1.4.

In phase 5 all forces caused by the monopile act on the gripper, therefor the forces on the crane are not displayed here. Because the monopile is symmetric in the xz and yz plane when it is straight up the wave forces do not cause a moment around the z axis of the monopile during phase 5 and 6. The dynamic moments around the z axis are not displayed. The forces and moments during phase 5 per meter wave amplitude dependent on the wave period are displayed in Appendix B.1.5.

In phase 6 the gripper is blocked so it can not rotate around the x axis. Therefor the moments around the x axis act on the gripper. The clamps of the gripper are released so that the monopile can slowly be lowered by the crane. The forces in z direction on the gripper are zero, these forces act on the crane. Therefor the forces in z direction are not displayed and instead the forces on the crane in z direction are displayed. The forces and moments during phase 6 per meter wave amplitude dependent on the wave period are displayed in Appendix B.1.6.

The difference between the dynamic forces that the monopile exerts on the vessel varies a lot from phase to phase. The biggest differences are of course because in phase 1 and 5 all forces are exerted on the gripper and during the other phases the forces partly work on the crane. The next biggest difference in forces is between phase 2 and 3. The reason of this big change is that in phase 2 the monopile is not submerged at all so only acceleration forces work on it and in phase 3 the monopile is partly submerged so also hydrodynamic and hydrostatic forces work on it. The other differences can mainly be explained by the difference in the submerged length of the monopile between phases. This changes the dynamical forces on the monopile as well as the buoyancy forces. Also the distance from the part of the monopile that is under water to the center of rotation of the vessel changes drastically. Because of this the velocities of the submerged part of the monopile changes and therefor the dynamical moments and forces are larger. This extra distance will also increase the dynamical moments as well as the buoyancy moments the monopile exerts on the gripper, this is because the forces have a bigger lever arm. The difference between the phases is so big that it is assumed that the calculation of the forces and moments on the gripper and crane for more phases in between phase 2 and phase 5 is necessary. This is done in subsection 4.4.4. Although having more data would be critical for doing a precise analysis of the forces on the crane and gripper some interesting results are still visible: From between phase 4 and phase 5 the dynamical forces in x and y direction are really similar, the peak at 18 seconds in the forces in z direction is also seen in both phases, the moments around the y axis are also really similar, only the longer periods have a higher amplitude in phase 5.

4.4.4. Extra phases

To be able to understand the results better two extra phases are added: Phase 3.5 with an angle of $\theta_u = 45°$ and Phase 4.5 with an upending angle of $\theta_u = 75°$. These phases are exactly in the middle between phase 3 and 4 and between phase 4 and 5. The phases are first build in Aqwa and then a model in matlab for both phases is made.

The static forces for phase 3.5 and phase 4.5 are:

Table 4.7: Static forces on monopile and gripper

Phase	$F_c(MN)$	$F_z(MN)$
3.5	2.8	21.9
4.5	2.9	21.5

During phase 3.5 and 4.5 the moments around the x axis are not displayed for the same reason as for phase 2,3 and 4. The dynamical forces and moments of phase 3.5 and 4.5 per meter wave amplitude dependent on the wave period are displayed in: Appendix B.1.7 and Appendix B.1.8

Then the forces and moments of all phases are compared. Only phase 3, 3.5, 4, 4.5 and 6 are included because phase 5 has the same forces and moments as phase 6 only differently distributed over the crane and gripper and during phase 1 and 2 the monopile is not submerged. Comparing the forces in x direction results in:

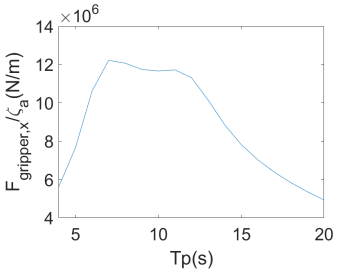

Figure 4.10: Phase 3: forces on gripper in x direction per meter wave height

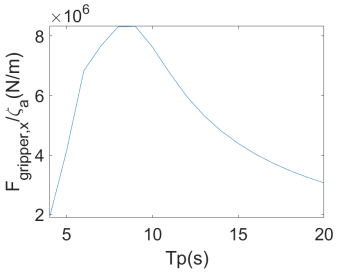

Figure 4.11: Phase 3.5: forces on gripper in x direction per meter wave height

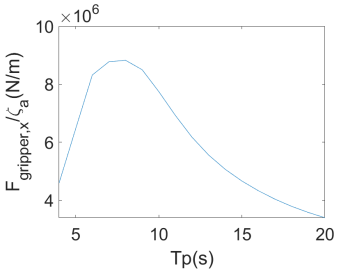

Figure 4.12: Phase 4: forces on gripper in x direction per meter wave height

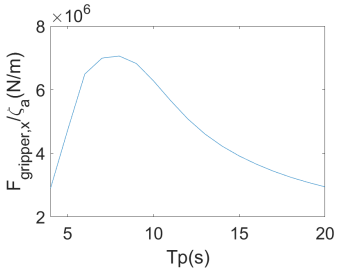

Figure 4.13: Phase 4.5: forces on gripper in x direction per meter wave height

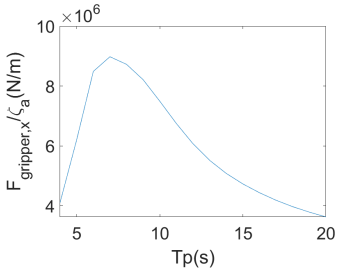

Figure 4.14: Phase 6: forces on gripper in x direction per meter wave height

It can clearly be seen that the dynamic forces in x direction on the gripper decrease from phase 3 to phase 3.5 and then stay more constant. During phase 3 the part of the monopile that is under water is the furthest away from the center of rotation in y direction and therefor the x direction forces because of pitch and yaw motions of the vessel will be the biggest during phase 3. During phase three the peak also has a different shape. For the later phases the surge motions will have a bigger influence because the monopile is further submerged.

Comparing the forces in y direction results in:

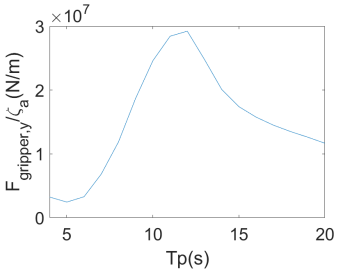

Figure 4.15: Phase 3: forces on gripper in y direction per meter wave height

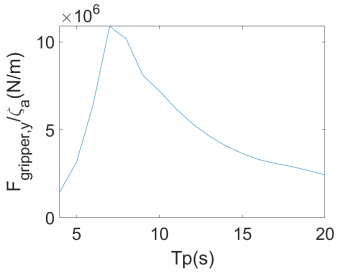

Figure 4.16: Phase 3.5: forces on gripper in y direction per meter wave height

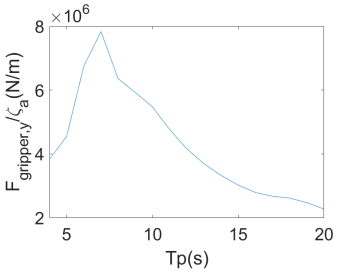

Figure 4.17: Phase 4: forces on gripper in y direction per meter wave height

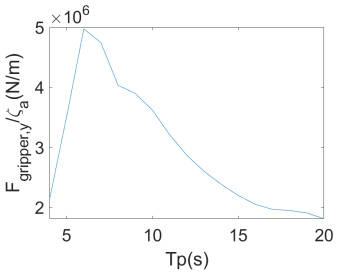

Figure 4.18: Phase 4.5: forces on the crane in y direction per meter wave height

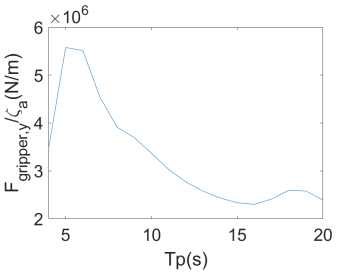

Figure 4.19: Phase 6: forces on the crane in y direction per meter wave height

During this phase it can again be seen that phase 3 has a different curve shape compared to the other phases. The amplitude of the dynamic forces decreases when going from phase 3 to phase 3.5, 4 and 4.5 and then increases again slightly to phase 6. The amplitude of motions of the submerged part of the monopile because of roll motions is a lot bigger during phase 3. This results in a decrease in force on the gripper when going from phas 3 to face 3.5 etc.. The monopile will get further submerged when going from phase 3 to phase 6 which has the opposite effect, this explains the increase in force when going from phase 4 to phase 6.

When comparing the forces on the crane only phases 3 to 4.5 are compared since the other phases have a different distribution between the forces on the crane and on the gripper as explained in section 4.2. Comparing the dynamic forces on the crane results in:

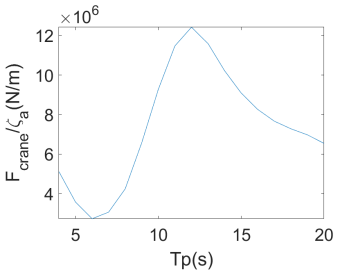

Figure 4.20: Phase 3: forces on the crane in z direction per meter wave height

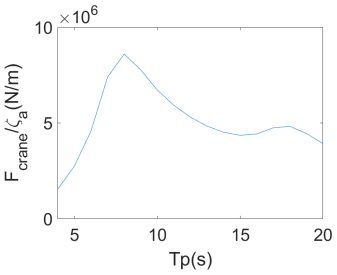

Figure 4.21: Phase 3.5: forces on the crane in z direction per meter wave height

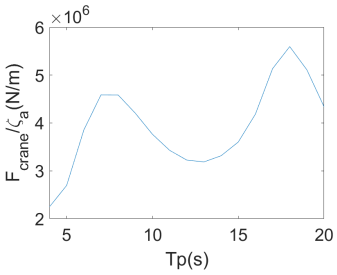

Figure 4.22: Phase 4: forces on the crane in z direction per meter wave height

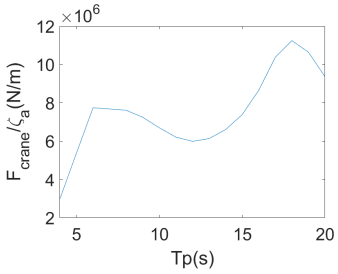

Figure 4.23: Phase 4.5: forces on the crane in z direction per meter wave height

When comparing the forces on the crane it needs to be taken into account that these forces are caused by two things: The force in z direction of the monopile and the moment around he x axis of the monopile. Two clear distinctive peaks can be seen in phases 3.5 to 4.5. Especially the peak at high frequencies can cause problems, because the monopile will mostly be installed in the North Sea where short period waves are more common. The high frequency peak mainly exists because the added mass of the monopile is really high for periods of around 8 seconds during phases 3.5 to 6. The second peak is the roll natural-frequency off the vessel with the monopile attached to it. Here the motions of the monopile are the highest and therefor the forces as well. The high added mass is more extreme for phases 3 and 3.5 and therefor they have the highest peak at higher frequencies.

Comparing the moments around the z axis results in:

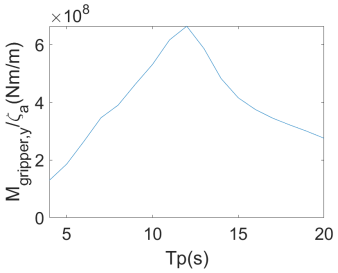

Figure 4.24: Phase 3: moments on gripper around the y axis per meter wave height

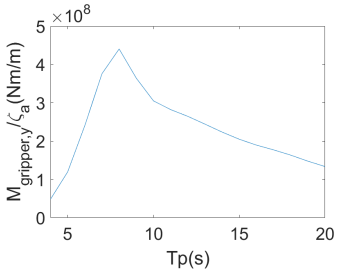

Figure 4.25: Phase 3.5: moments on gripper around the y axis per meter wave height

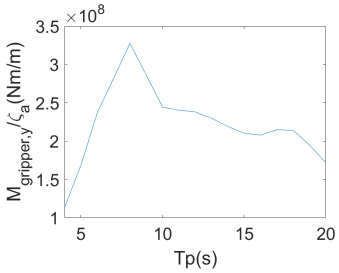

Figure 4.26: Phase 4: moments on gripper around the y axis per meter wave height

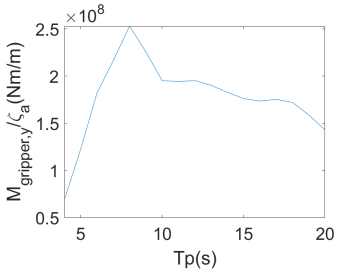

Figure 4.27: Phase 4.5: moments on gripper around the y axis per meter wave height

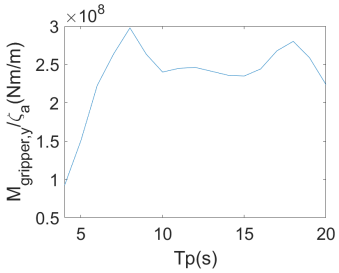

Figure 4.28: Phase 6: moments on gripper around the y axis per meter wave height

For pitch motions the same can be seen as for roll motions because the monopile is symmetric, therefor the added mass is also a lot higher at low frequencies in pitch motions of the vessel. This generates a bigger moment around the y axis. The high frequency added mass is also higher during the first phases then during the later phases.

Comparing the moments around the z axis results in:

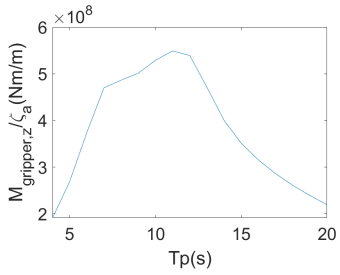

Figure 4.29: Phase 3: moments on gripper around the z axis per meter wave height

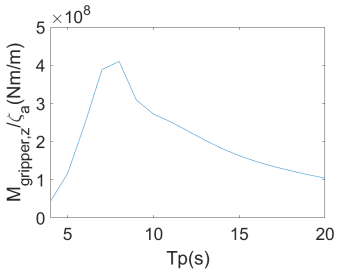

Figure 4.30: Phase 3.5: moments on gripper around the z axis per meter wave height

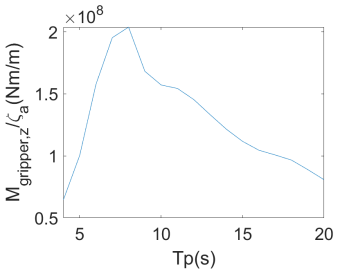

Figure 4.31: Phase 4: moments on gripper around the z axis per meter wave height

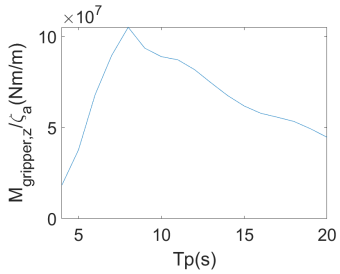

Figure 4.32: Phase 4.5: moments on gripper around the z axis per meter wave height

The moment around the z axis of the grippper decreases substantially from phase 3 to phase 6. This is mainly explained by the less severe motions the monopile undergoes when it is less far away from the center of rotation. Also the forces that work on the end of the monopile have a longer arm around the z axis in the first phases.

After examining the forces it becomes clear that the dynamic forces and moments in every direction are the biggest during phase 3. The graph shape of phase 3 is also the most different from other phases.

Comparing the static forces of phase 1 to 5 results in:

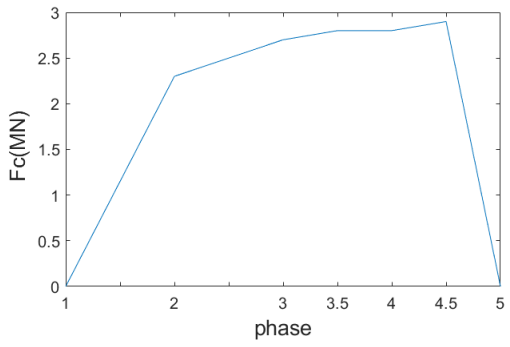

Figure 4.33: The static forces on the crane from phase 1 to 5

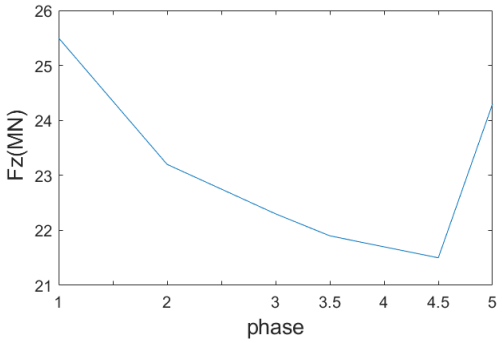

Figure 4.34: The static forces on the gripper in z direction from phase 1 to 5

The decrease in arm the buoyancy forces have and the decrease in arm the crane and gripper have to counteract the buoyancy moment are linear proportional, therefor the difference in the force on the crane and gripper is caused by the change in the ammount of monopile that is submerged during the upending process. This leads to a higher force on the crane during the later upending phases and a lower force on the gripper since the gripper gives a force in opposite direction as the crane does to counteract the buoyancy moment. The gravity forces on the monopile and the buoyancy moments and forces on the monopile partly

cancel each other out. The total static force exerted by the monopile are:

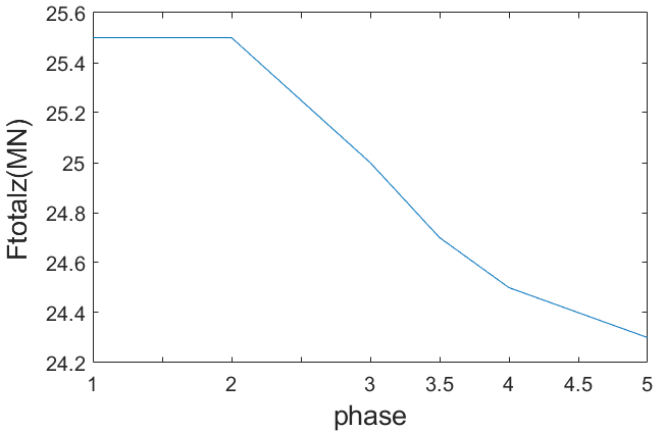

Figure 4.35: The total static forces exerted by the monopile from phase 1 to 5

The total force is the same as the weight of the monopile with the lifting tool times g minus the buoyancy forces. The forces that counteract the buoyancy moment exerted on the gripper and crane cancel each other out.

4.5. Workability

To know how many days in a year the Stella Synergy will be able to upend monopiles a workability analysis is done using the maximum dynamic load that the crane can handle. For the maximum load of 2500t the maximum dynamic amplification factor (DAF): F_{dyn} = 1.1. This means that the dynamic loads caused by waves may not exceed 10% of 2500t when an object of 2500t is lifted. The crane also has a maximum off-lead and side-lead angle, but because the monopile is fixed at the vessel and the crane will move in such a way that it stays straight above the hoisting point of the monopile the off-lead and side-lead angles will remain zero. The workability is only computed for phase 6, because all other faces have a static load with a factor 10 lower. This are really low loads for the main crane and therefor the DAF will be much higher, making phase six the limiting phase for workability.

4.5.1. Wavescatter

A wave scatter is used to obtain the workability. A wave scatter is given available by Jumbo for the Central North Sea. This is also the location where many future wind farms are planned. In the wavescatter the probability of having a certain wave condition (Tp and Hs) is displayed. So if the table gives a certain percentage this is the chance of having that wave condition on a day. The data is averaged over a year so in summer you can have smaller waves then in winter, but on average over the whole year this will be the chance to have these wave conditions. The wave scatter diagram is made using measured data from the past. The wavescatter used for this master thesis can be found in appendix C.1.

For each wave condition in the wavescatter the forces on the crane are calculated. The wave ranges within the scatter are all rounded to the highest number within the range so the vessel motions are not under estimated: 2.25 to 2.5 meter waves become 2.5 meter and 4-5 second periods become 5 seconds.The wave conditions in the wave scatter are: Hs = 0.25 m to Hs = 6 m and Tp = 4 s to Tp = 20 s.

4.5.2. results

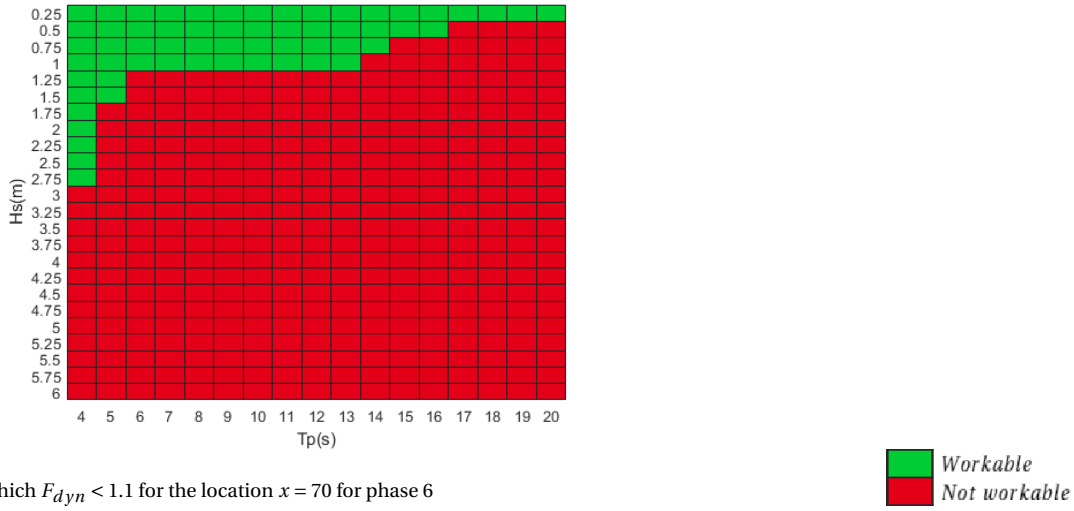

Figure 4.36: Workability which $F_{dyn} < 1.1$ for the location $x = 70$ for phase 6

The conditions that are marked with green rectangles do not cause the wave induced forces on the crane to exceed $F_{dyn} = 1.1$. Although this plot seems to be really negative and the workability seems really low this is not the case. The wave conditions in the north sea are relatively mild, so the wave conditions in the upper left corner of Figure 4.36 are more common then the wave conditions in the lower right corner. The workability during phase 6 is: 34.3 %

5

Hoisting forces and workability

In this chapter the forces on the crane and the motions of the monopile while the vessel is hoisting the monopile are modeled, these forces are then used to calculate the workability of hoisting from a barge next to the vessel.

5.1. Coordinate system

The coordinates for modeling the motions and forces on the monopile are defined in this section:

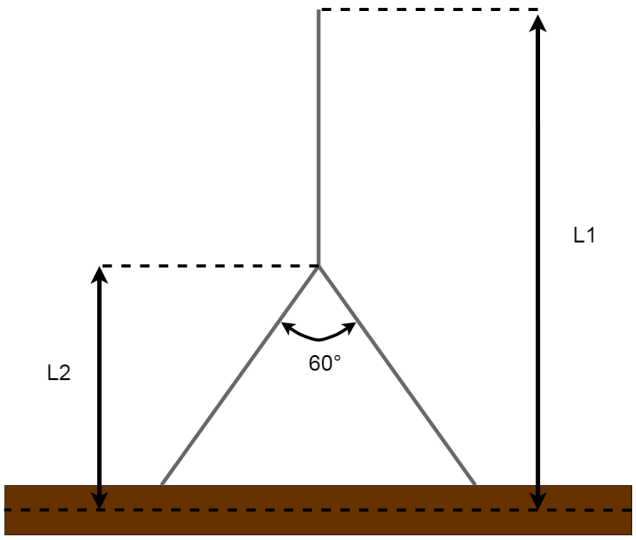

Figure 5.1: Defenition of the lengths l1 and l2

According to an internal rule of Jumbo the angle between the bottom two hoisting cables has a maximum of 60°. $l2$ is fixed at 45.3 m. Length $l1$ varies. When the monopile is hoisted upwards $l1$ will become shorter. When the monopile is just lifted from the barge $l1$ will be 80m. Before the monopile is placed on the gripper it will be on its highest point and then $l1$ will be: 64.4m.

To compute the motions of the monopile a 10 DoF model is made. First a coordinate system is made. There are the six DoF of the vessel as described in section 3.1 and four DoF of the monopile hanging below the crane as seen in Figure 5.2 and Figure 5.3.

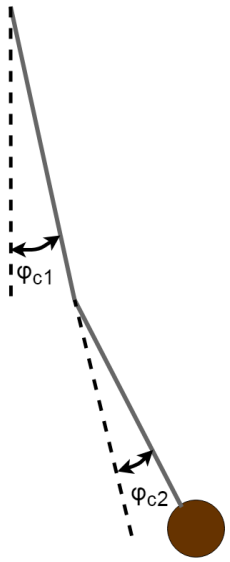

Figure 5.2: Graphical representation of angles ϕ_{c1} and ϕ_{c2}

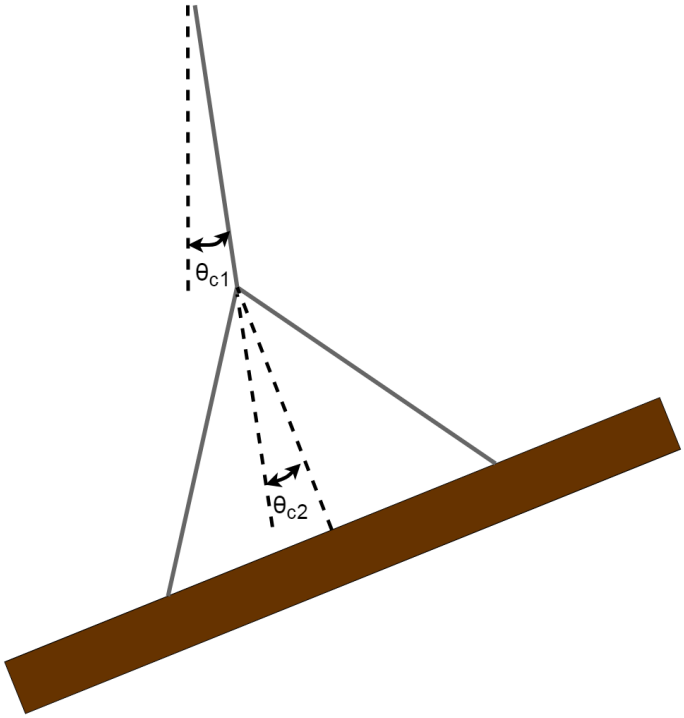

Figure 5.3: Graphical representation of angles θ_{c1} and θ_{c2}

The positive directions of the hoisting cable angles are the same as the vessel. So Figure 5.2 is seen from the front of the vessel so that the monopile is moving towards the vessel with positive ϕ_{c1} and ϕ_{c2} angles. In figure Figure 5.3 the monopile is seen from the vessel so that the monopile is moving towards the front of the vessel for positive angles θ_{c1} and θ_{c2}. ϕ_{c1} is the off-lead angle and θ_{c1} is the side-lead angle. Tuggerlines are used to stop the monopile from rotating square to the θ_{c2} and ϕ_{c2} angles (when all angles are zero this

rotation would be rotation around the global z axis). It is assumed that the tuggerlines are infinetly stiff and that they only influence motions in this direction.

5.2. Displacements of the monopile

Because the vessel will only move with small angles and the maximum off-lead and side-lead angles of the crane are 1°and 2°the small angle estimation is used. This simplifies the calculations so that they become linear and can be used in the frequency domain.
The displacements at the crane tip (x_{ct}, y_{ct}, z_{ct}) are linked to the displacements at the CoG $(x_{CoG}, y_{CoG}, z_{CoG})$:

$$x_{ct} = x_{CoG} + c\sin(\theta) - b\sin(\psi) \approx x_{CoG} + c\theta - b\psi \tag{5.1}$$

$$y_{ct} = y_{CoG} - c\sin(\phi) + a\sin(\psi) \approx y_{CoG} - c\phi + a\psi \tag{5.2}$$

$$z_{ct} = z_{CoG} + b\sin(\phi) - a\sin(\theta) \approx z_{CoG} + b\phi - a\theta \tag{5.3}$$

Where a, b and c are the distances in x, y and z directions from the CoG to the crane tip. The displacements of the monopile can then be described using the displacements of the crane tip:

$$x_m = x_{ct} - l_1\sin(\theta_{c1}) - l_2\sin(\theta_{c2}) \approx x_{CoG} + c\theta - b\psi - l_1\theta_{c1} - l_2\theta_{c2} \tag{5.4}$$

$$y_m = y_{ct} + l_1\sin(\phi_{c1}) + l_2\sin(\phi_{c2}) \approx y_{CoG} - c\phi + a\psi + l_1\phi_{c1} + l_2\phi_{c2} \tag{5.5}$$

$$z_m \approx z_{CoG} + b\phi - a\theta + l_1\frac{\theta_{c1}^2}{2} + l_2\frac{\theta_{c2}^2}{2} + l_1\frac{\phi_{c1}^2}{2} + l_2\frac{\phi_{c2}^2}{2} \tag{5.6}$$

5.3. Monopile hoisting motions and accelerations

$$\begin{aligned}\delta T = {} & \delta x_{mp}\ddot{x}_{mp}m_{mp} + \delta y_{mp}\ddot{y}_{mp}m_{mp} + \delta z_{mp}\ddot{z}_{mp}m_{mp} + \delta\phi_{c1}(\ddot{\phi}_{c1} + \ddot{\phi}_{c2})I_{xx,mp} + \delta\theta_{c1}(\ddot{\theta}_{c1} + \ddot{\theta}_{c2})I_{yy,mp} + \\ & \delta\phi_{c2}(\ddot{\phi}_{c1} + \ddot{\phi}_{c2})I_{xx,mp} + \delta\theta_{c2}(\ddot{\theta}_{c1} + \ddot{\theta}_{c2})I_{yy,mp}\end{aligned} \tag{5.7}$$

$$\delta V = \delta z_{mp}m_{mp}g \tag{5.8}$$

$$\begin{aligned}\delta T + \delta V = m_{mp}\Big(& \\ & \delta x_{CoG}(\ddot{x}_{CoG} + c\ddot{\theta} - b\ddot{\psi} - l_1\ddot{\theta}_{c1} - l_2\ddot{\theta}_{c2}) + \\ & \delta y_{CoG}(\ddot{y}_{CoG} - c\ddot{\phi} + a\ddot{\psi} + l_1\ddot{\phi}_{c1} + l_2\ddot{\phi}_{c2}) + \\ & \delta z_{CoG}(\ddot{z}_{CoG} + b\ddot{\phi} - a\ddot{\theta}) + \\ & \delta\phi(-c(\ddot{y}_{CoG} - c\ddot{\phi} - a\ddot{\psi} + l_1\ddot{\phi}_{c1} + l_2\ddot{\phi}_{c2}) + b(\ddot{z}_{CoG} + b\ddot{\phi} - a\ddot{\theta}) - cg\phi) + \\ & \delta\theta(c(\ddot{x}_{CoG} + c\ddot{\theta} + b\ddot{\psi} - l_1\ddot{\theta}_{c1} - l_2\ddot{\theta}_{c2}) - a(\ddot{z}_{CoG} + b\ddot{\phi} - a\ddot{\theta}) - cg\theta) + \\ & \delta\psi(-b(\ddot{x}_{CoG} + c\ddot{\theta} - b\ddot{\psi} - l_1\ddot{\theta}_{c1} - l_2\ddot{\theta}_{c2}) + a(\ddot{y}_{CoG} - c\ddot{\phi} + a\ddot{\psi} + l_1\ddot{\phi}_{c1} + l_2\ddot{\phi}_{c2}) + \\ & \delta\phi_{c1}(l_1(\ddot{y}_{CoG} - c\ddot{\phi} + a\ddot{\psi} + l_1\ddot{\phi}_{c1} + l_2\ddot{\phi}_{c2}) + r_{xx,mp}^2(\ddot{\phi}_{c1} + \ddot{\phi}_{c2}) + gl_1\phi_{c1}) + \\ & \delta\theta_{c1}(l_1(-\ddot{x}_{CoG} - c\ddot{\theta} + b\ddot{\psi} + l_1\ddot{\theta}_{c1} + l_2\ddot{\theta}_{c2}) + r_{yy,mp}^2(\ddot{\theta}_{c1} + \ddot{\theta}_{c2}) + gl_1\theta_{c1}) \\ & \delta\phi_{c2}(l_2(\ddot{y}_{CoG} - c\ddot{\phi} + a\ddot{\psi} + l_1\ddot{\phi}_{c1} + l_2\ddot{\phi}_{c2}) + r_{xx,mp}^2(\ddot{\phi}_{c1} + \ddot{\phi}_{c2}) + gl_2\phi_{c2}) + \\ & \delta\theta_{c2}(l_2(-\ddot{x}_{CoG} - c\ddot{\theta} + b\ddot{\psi} + l_1\ddot{\theta}_{c1} + l_2\ddot{\theta}_{c2}) + r_{yy,mp}^2(\ddot{\theta}_{c1} + \ddot{\theta}_{c2}) + gl_2\theta_{c2})\Big)\end{aligned} \tag{5.9}$$

From these formulas the mass and stiffness matrices of the monopile are made:

$$\boldsymbol{M_{mp}} = m_{mp}\begin{bmatrix} 1 & 0 & 0 & 0 & c & -b & 0 & -l_1 & 0 & -l_2 \\ 0 & 1 & 0 & -c & 0 & a & l_1 & 0 & l_2 & 0 \\ 0 & 0 & 1 & b & -a & 0 & 0 & 0 & 0 & 0 \\ 0 & -c & b & c^2+b^2 & -ab & -ac & -l_1c & 0 & -l_2c & 0 \\ c & 0 & -a & -ab & c^2+a^2 & -bc & 0 & -l_1c & 0 & -l_2c \\ -b & a & 0 & -ac & -bc & b^2+a^2 & l_1a & l_1b & l_2a & l_2b \\ 0 & l_1 & 0 & -l_1c & 0 & l_1a & l_1^2+r_{xx}^2 & 0 & l_1l_2+r_{xx}^2 & 0 \\ -l_1 & 0 & 0 & 0 & -l_1c & l_1b & 0 & l_1^2+r_{yy}^2 & 0 & l_1l_2+r_{yy}^2 \\ 0 & l_2 & 0 & -l_2c & 0 & l_2a & l_1l_2+r_{xx}^2 & 0 & l_2^2+r_{xx}^2 & 0 \\ -l_2 & 0 & 0 & 0 & -l_2c & l_2b & 0 & l_1l_2+r_{yy}^2 & 0 & l_2^2+r_{yy}^2 \end{bmatrix} \tag{5.10}$$

$$\boldsymbol{C_{mp}} = m_{mp}\begin{bmatrix} 0 & 0 & 0 & 0 & 0 & 0 & 0 & 0 & 0 & 0 \\ 0 & 0 & 0 & 0 & 0 & 0 & 0 & 0 & 0 & 0 \\ 0 & 0 & 0 & 0 & 0 & 0 & 0 & 0 & 0 & 0 \\ 0 & 0 & 0 & 0 & 0 & 0 & 0 & 0 & 0 & 0 \\ 0 & 0 & 0 & 0 & 0 & 0 & 0 & 0 & 0 & 0 \\ 0 & 0 & 0 & 0 & 0 & 0 & 0 & 0 & 0 & 0 \\ 0 & 0 & 0 & 0 & 0 & 0 & l_1 g & 0 & 0 & 0 \\ 0 & 0 & 0 & 0 & 0 & 0 & 0 & l_1 g & 0 & 0 \\ 0 & 0 & 0 & 0 & 0 & 0 & 0 & 0 & l_2 g & 0 \\ 0 & 0 & 0 & 0 & 0 & 0 & 0 & 0 & 0 & l_2 g \end{bmatrix} \tag{5.11}$$

$\boldsymbol{C_{mp}}(4,4) = \boldsymbol{C_{mp}}(5,5) = -cm_{mp}g$ these terms are removed from the stiffness matrix of the model because they are the result of the load getting further away from the CoG when the vessel is heeling. This effect is already taken into account in GM. The z coordiante of the CoG of the monopile is assumed to be at the crane tip when calculating GM of the vessel with the monopile attached to the crane. In the following formulas it is proven that both methods give the same results:

$$C_{44} = \rho g \nabla GM_T = g m_{total} GM_T \tag{5.12}$$

$$GM_T = KB + BM - KG = KB + \frac{I_T}{\nabla} - KG \tag{5.13}$$

$$\Delta KG = \frac{cm_{mp}}{m_{total}} \tag{5.14}$$

from this it can be concluded that:

$$\Delta C_{44} = -cm_{mp}g \tag{5.15}$$

which is the same. Taking this into account in GM is common practice at offshore lifting companies.
The mass matrix of the double pendulum monopile is added to the mass matrix of the vessel obtained from subsection 3.2.1 and the stiffness matrix of the double pendulum monopile is added to the stiffness matrix of the vessel calculated in subsection 3.2.2:

$$\boldsymbol{M_{total}} = \boldsymbol{M_{mp}} + \boldsymbol{M} \tag{5.16}$$

$$\boldsymbol{C_{total}} = \boldsymbol{C_{mp}} + \boldsymbol{C} \tag{5.17}$$

Using this the RAOs can be computed:

$$\boldsymbol{RAO}(\omega,\mu) = \frac{\boldsymbol{L}^T H_{FZ}(\omega,\mu)}{\boldsymbol{L}^T(-\omega^2(\boldsymbol{M_{total}} + \boldsymbol{A}(\omega)) + i\omega(\boldsymbol{B}(\omega) + \boldsymbol{B_{add}}) + \boldsymbol{C_{total}})\boldsymbol{L}} \tag{5.18}$$

where $\boldsymbol{L}$ is filled in using the coordinates of the crane tip (a,b,c)(see subsection 3.3.1:

$$\boldsymbol{L} = \begin{bmatrix} 1 & 0 & 0 & 0 & c & -b & 0 & 0 & 0 & 0 \\ 0 & 1 & 0 & -c & 0 & a & 0 & 0 & 0 & 0 \\ 0 & 0 & 1 & b & -a & 0 & 0 & 0 & 0 & 0 \\ 0 & 0 & 0 & 1 & 0 & 0 & 0 & 0 & 0 & 0 \\ 0 & 0 & 0 & 0 & 1 & 0 & 0 & 0 & 0 & 0 \\ 0 & 0 & 0 & 0 & 0 & 1 & 0 & 0 & 0 & 0 \\ 0 & 0 & 0 & 0 & 0 & 0 & 1 & 0 & 0 & 0 \\ 0 & 0 & 0 & 0 & 0 & 0 & 0 & 1 & 0 & 0 \\ 0 & 0 & 0 & 0 & 0 & 0 & 0 & 0 & 1 & 0 \\ 0 & 0 & 0 & 0 & 0 & 0 & 0 & 0 & 0 & 1 \end{bmatrix} \tag{5.19}$$

5.4. Results

The natural frequencies and eigenvectors of the system are calculated using:

$$(\boldsymbol{C_{total}} - \lambda(\boldsymbol{M_{total}} + \boldsymbol{A}))\,v = 0 \tag{5.20}$$

Where λ are the eigenvalues squared and v is the eigenvector. Because the added mass matrix $\boldsymbol{A}$ is dependent on the wave frequency the natural frequencies are calculated for all 100 frequencys that are previously used in the model. Then the resulting natural frequencies are compared to the frequency of the added mass matrix. The natural frequencies that are the closest to the frequency of the added mass are the natural frequencies of the system. One problem of using this method is that natural frequencies outside of the analysed frequency range are not found.

This gives the following undamped natural frequencies with their eigenvectors:

Table 5.1: Natural frequencies of the vessel lifting a monopile

Natural-frequency	Hertz	Eigenmode
1	0.119	z
2	0.083	y, z, ϕ, ϕ_c and ϕ_{c2}
3	0.088	y, z, ϕ, ϕ_c and ϕ_{c2}
4	0.045	x, θ_c and θ_{c2}
5	0.018	y , ϕ

Then the RAOs for a wave coming from $\mu = 15$ degrees are displayed in the same graphs as the naturalfrequencies (the dashed lines), note that for the first six degrees of freedom this are the RAOs at the crane tip.

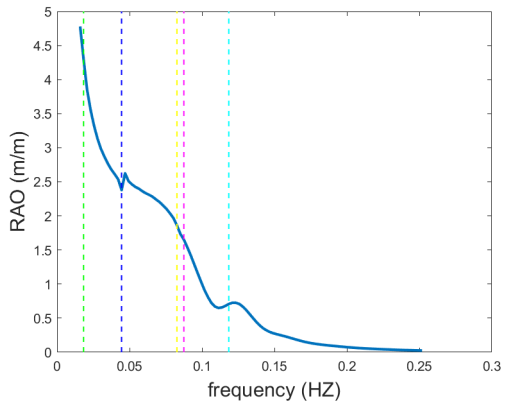

Figure 5.4: The RAO for the first degree of freedom: surge(blue line), compared to the naturalfrequencies(dashed lines)

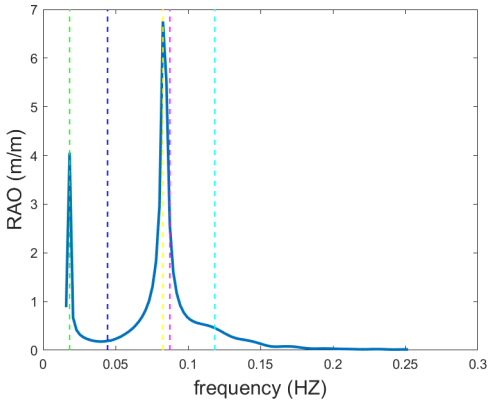

Figure 5.5: The RAO for the second degree of freedom: sway(blue line), compared to the naturalfrequencies(dashed lines)

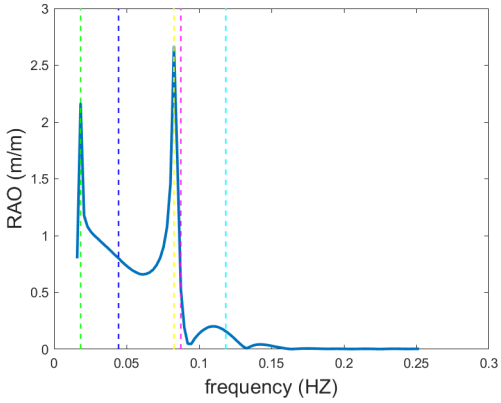

Figure 5.6: The RAO for the third degree of freedom: heave(blue line), compared to the naturalfrequencies(dashed lines)

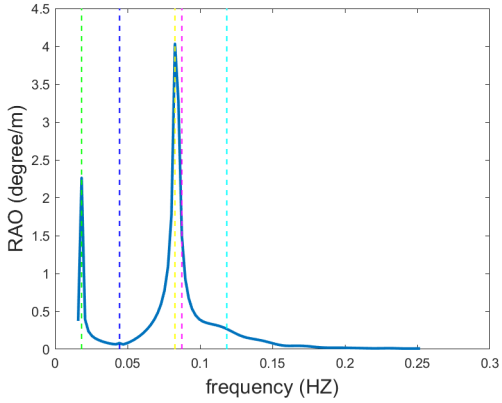

Figure 5.7: The RAO for the fourth degree of freedom: roll(blue line), compared to the naturalfrequencies(dashed lines)

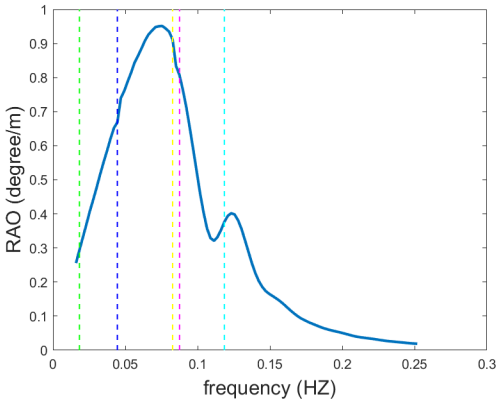

Figure 5.8: The RAO for the fifth degree of freedom: pitch(blue line), compared to the naturalfrequencies(dashed lines)

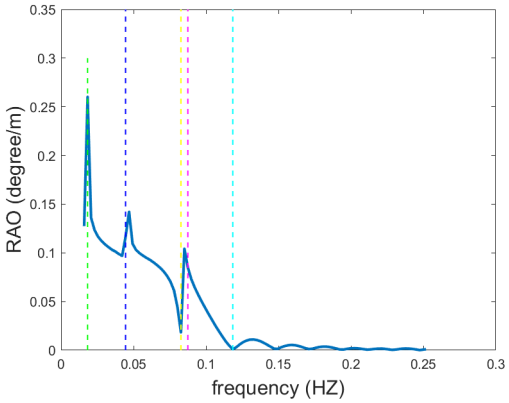

Figure 5.9: The RAO for the sixth degree of freedom: yaw(blue line), compared to the naturalfrequencies(dashed lines)

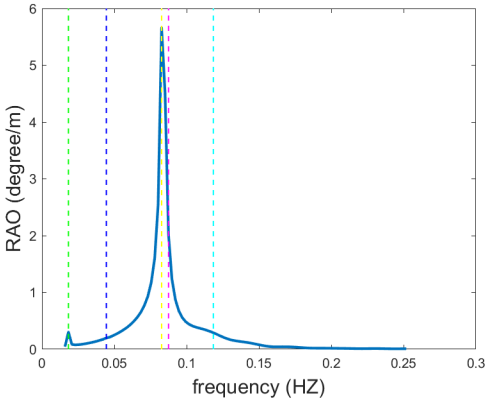

Figure 5.10: The RAO for the seventh degree of freedom: the off-lead angle of the upper hoisting cable(blue line), compared to the naturalfrequencies(dashed lines)

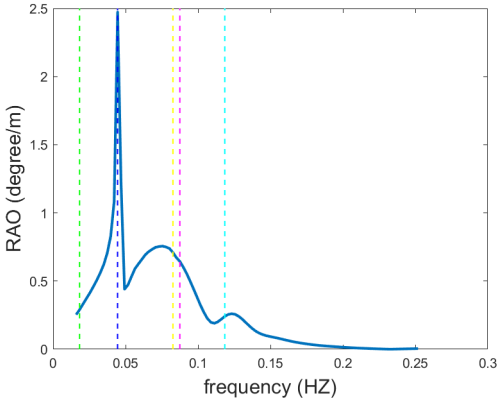

Figure 5.11: The RAO for the eighth degree of freedom: the side-lead angle of the upper hoisting cable(blue line), compared to the naturalfrequencies(dashed lines)

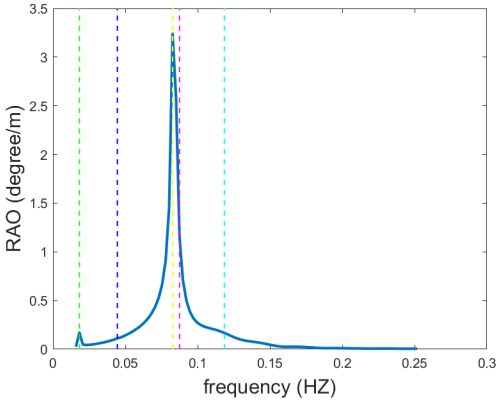

Figure 5.12: The RAO for the ninth degree of freedom: the off-lead angle of the lower hoisting cable(blue line), compared to the naturalfrequencies(dashed lines)

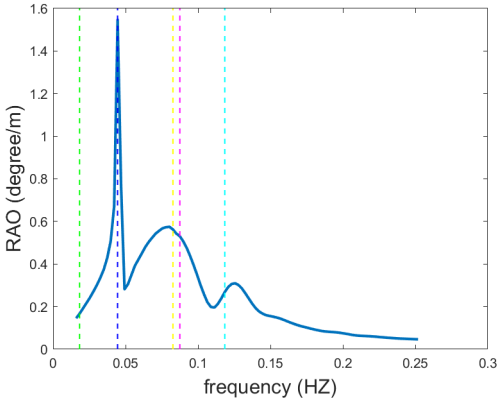

Figure 5.13: The RAO for the tenth degree of freedom: the side-lead angle of the lower hoisting cable(blue line), compared to the naturalfrequencies(dashed lines)

A clear relation between the calculated naturalfrequencies and RAOs can be seen. The off-lead angles (degrees of freedom 8 and 10) have the same peak at arround 0.8 Hertz as roll, heave and sway. This is because the naturalfrequency at 0.83 Hertz has an eigenmode in which these degrees of freedom are dominant. Because the monopile is not placed in the center of the vessel both side-lead angles (degrees of freedom 9 and

10 influence the yaw motions of the vessel and vice versa. This can also be seen in the peak and natural frequency at 0.45 Hertz. The eigenmode of this natural frequency is also dominated by yaw and the side-lead angles as expected. This are the RAOs for a wave direction of 15 degrees(the same direction as the the waves will be coming from at the workability analysis). The RAOs are calculated for all wave directions as seen in Figure 5.14 and Figure 5.15.

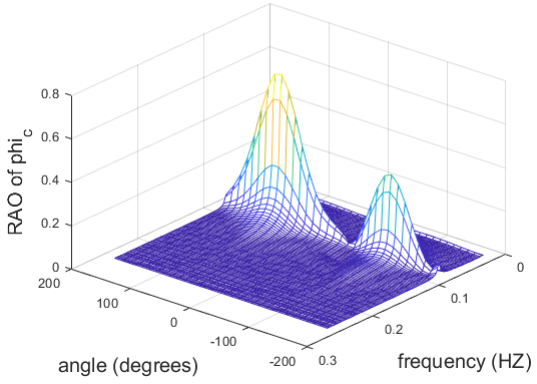

Figure 5.14: The RAO for the seventh degree of freedom: the off-lead angle of the hoisting cable varying over angles and frequencies

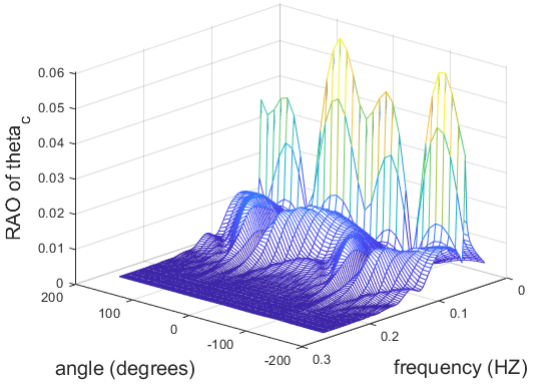

Figure 5.15: The RAO for the seventh degree of freedom: the side-lead angle of the hoisting cable varying over angles and frequencies

The RAOs of the off-lead angle off the hoisting cable are as expected a lot higher with beam waves. The side-lead angles are the lowest with beam waves. Also the natural frequencys as seen in Table 5.1 can clearly be seen in these 3D plots of the RAOs.

5.5. Workability

The limiting factors for the hoisting process are:

- the dynamic amplification factor should not exceed 1.1: $F_{dyn} \leq 1.1$
- the off-lead angle should not exceed one degree $OL \leq 1°$
- the side-lead angle should not exceed two degrees $SL \leq 2°$

All the three factors are checked for every wave height and wave frequency combination in the wave scatter diagram (subsection 4.5.1). If they exceed the limits they are marked red and if they stay within the limit they are marked green. To see the influence of changing the limmiting factors that are displayed above the following limiting factors have been tested:

- $OL \leq 1°$, $OL \leq 2°$ and $OL \leq 3°$
- $SL \leq 1°$, $SL \leq 2°$ and $SL \leq 3°$
- $F_{dyn} \leq 1.05$, $F_{dyn} \leq 1.1$ and $F_{dyn} \leq 1.15$

The limiting factors from low to high are displayed in colors from light green to dark green as can be seen in the legends next to the workability plots. Below every workablitiy plot the workability of the limiting factors is shown in a bar graph. This shows on the left the workability if the limiting factor was the only limiting factor and on the right the workability for all three limiting factors combined, where the other two limiting factors are kept at there standard ($OL \leq 1°$, $SL \leq 2°$ and $F_{dyn} \leq 1.1$). The workability percentage is calculated by adding up the occurrence percentage of all wave conditions that are still workable. The occurrence of the wave conditions can be seen in: section C.1.
First the workability for $l1 = 80m$ is displayed:

Dynamic amplification factor:

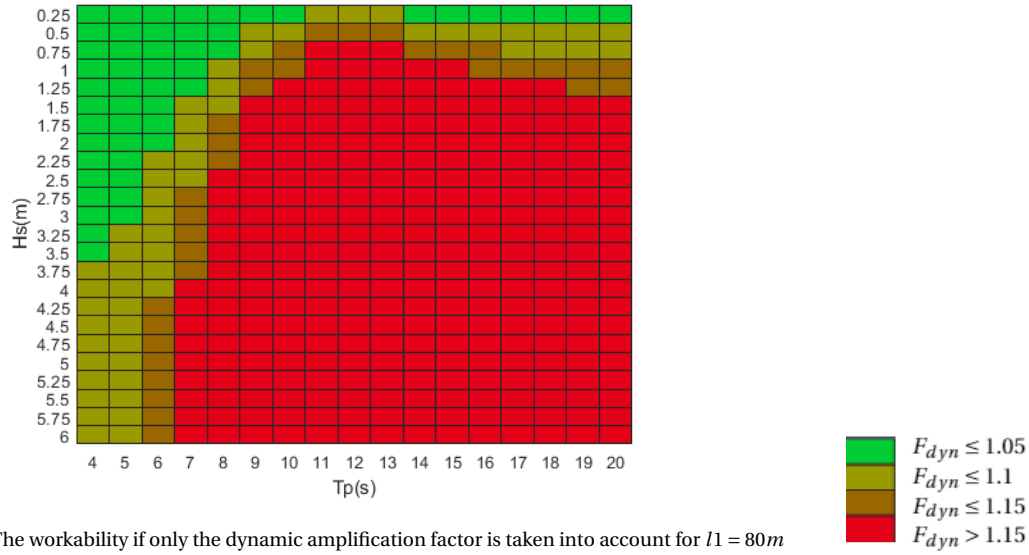

Figure 5.16: The workability if only the dynamic amplification factor is taken into account for $l1 = 80m$

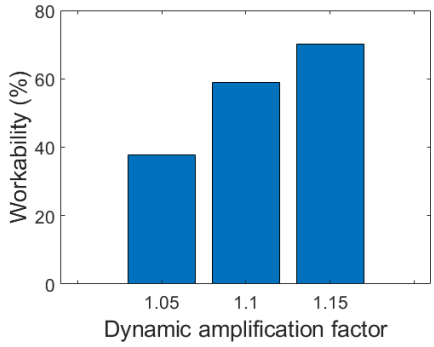

Figure 5.17: The workability when only the Dynamic amplification factor is taken into account, $l1 = 80m$

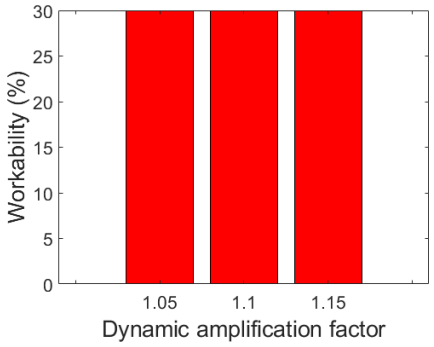

Figure 5.18: Comparing the workability for different dynamic amplification factors, $l1 = 80m$

As seen in Figure 5.17 the workability, when only the dynamic amplification factor is taken into account, does change significantly when it would be increased to 1.15. In Figure 5.18 can be seen that changing the dynamic amplification factor would not influence the total workability. When the tuggerlines can also be used to keep the off-lead and side-lead angle limited the workability displayed in Figure 5.16 will be the total workability for the hoisting process.

side-lead angle:

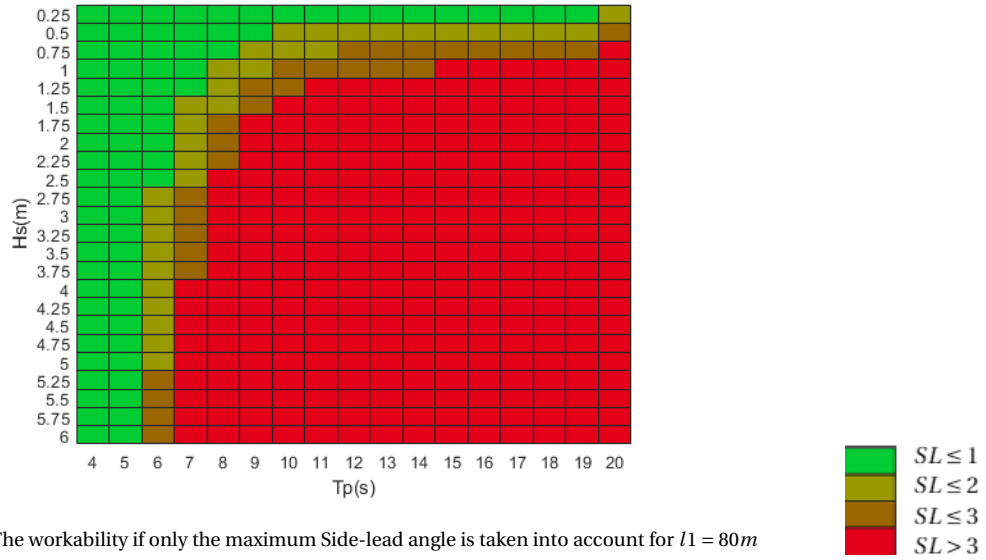

Figure 5.19: The workability if only the maximum Side-lead angle is taken into account for $l1 = 80m$

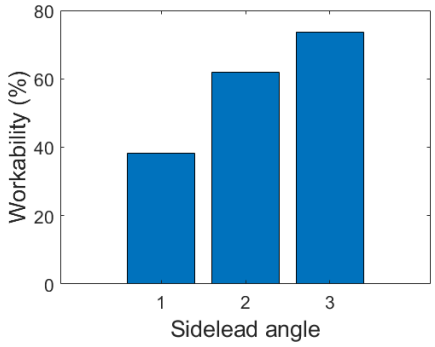

Figure 5.20: The workability when only maximum side-lead angle is taken into account, $l1 = 80m$

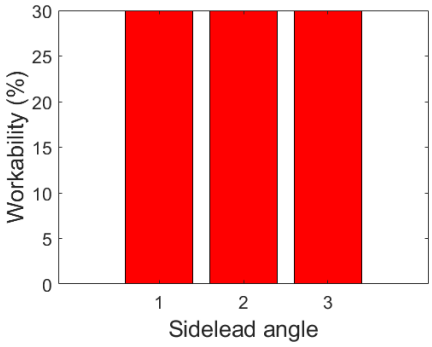

Figure 5.21: Comparing the workability for different maximum side-lead angles, $l1 = 80m$

For the same reason as with the dynamic amplification factor increasing the side-lead angle will not increase the total workability.

off-lead angle:

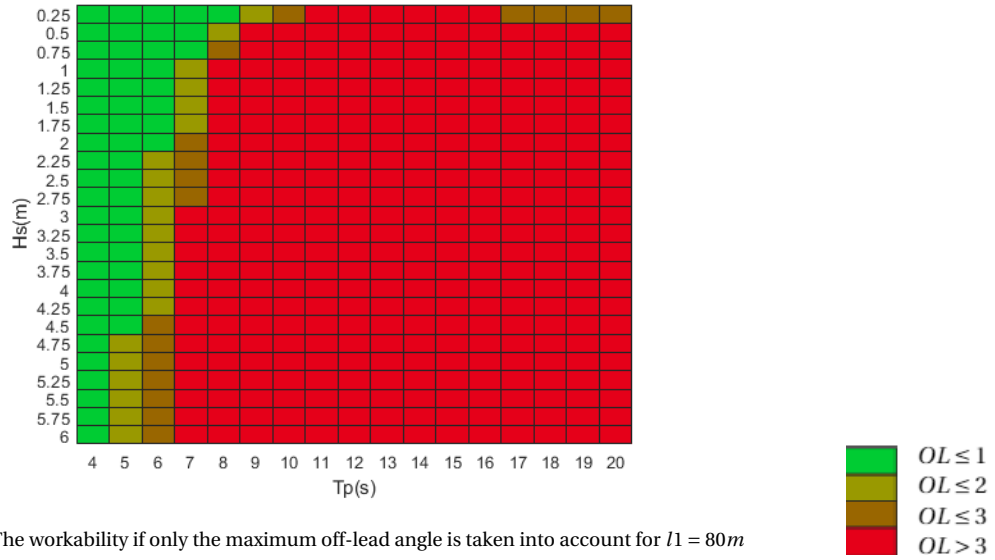

Figure 5.22: The workability if only the maximum off-lead angle is taken into account for $l1 = 80m$

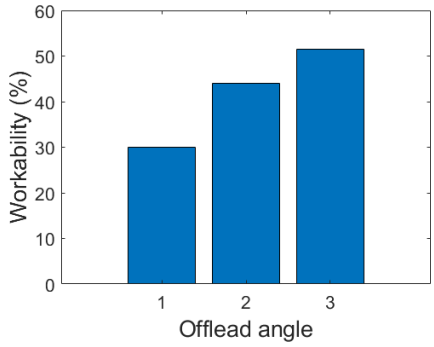

Figure 5.23: The workability when only maximum off-lead angle is taken into account, $l1 = 80m$

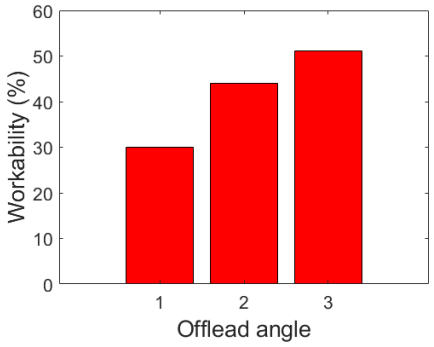

Figure 5.24: Comparing the workability for different maximum off-lead angles, $l1 = 80m$

As seen in Figure 5.24 increasing the off-lead angle will increase the total workability. This does mean that the maximum off-lead angle is limiting the workability for a hoisting cable length of 80m.

Total workability

The workability of all the limiting factors is combined so that the total workability only is positive when all three factors all positive. If one or more of the limiting factors are exceeded for a certain condition it will not be workable for that condition. This is done for the limiting factors of the crane ($OL \leq 1°$, $SL \leq 2°$ and $F_{dyn} \leq 1.1$).

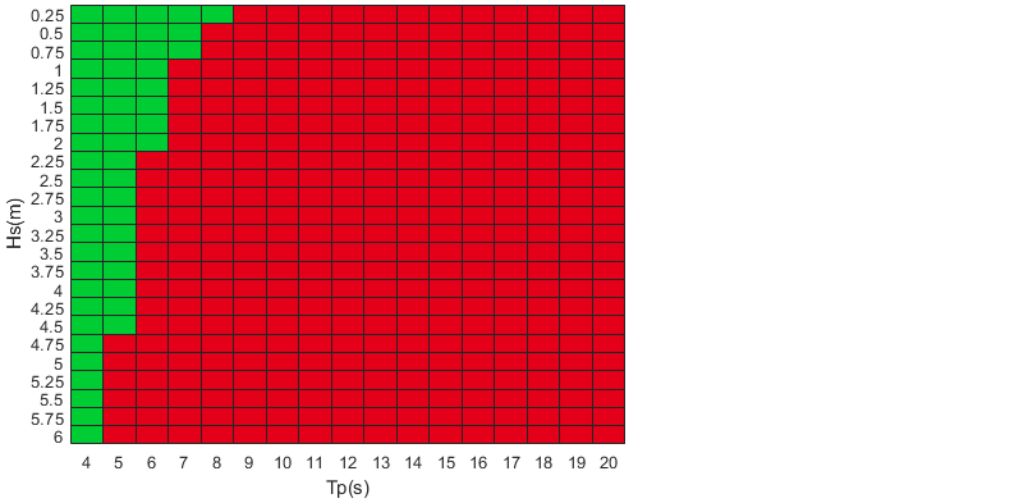

Figure 5.25: The total workability (combining Off-lead angle, Side-lead angle and cable tension workabilitys) for $l1 = 80m$

The same is done for $l1 = 64.4m$:

Dynamic amplification factor:

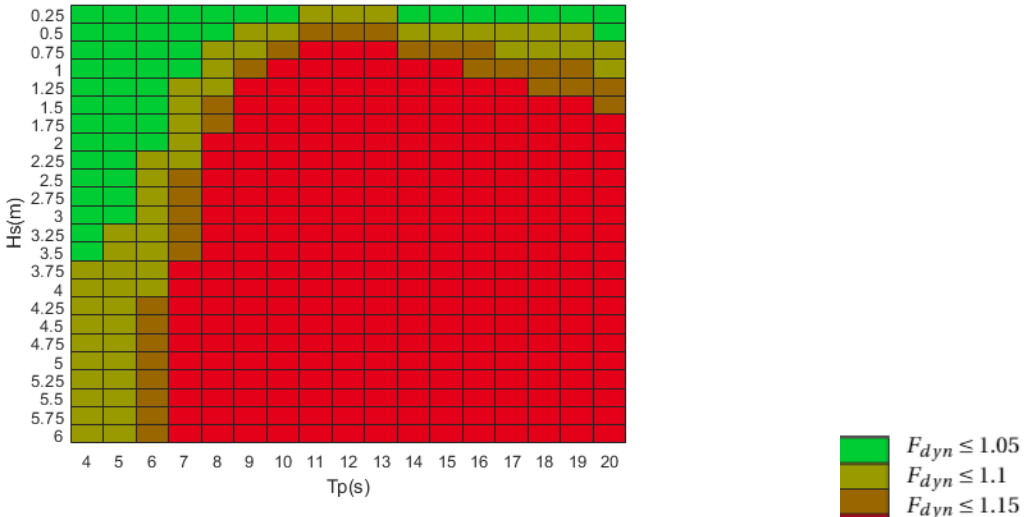

Figure 5.26: The workability if only the maximum cable tension is taken into account for $l1 = 64m$

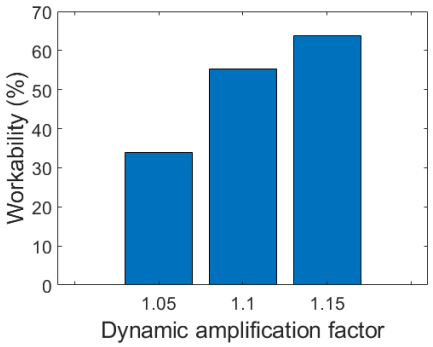

Figure 5.27: The workability when only the Dynamic amplification factor is taken into account, $l1 = 64m$

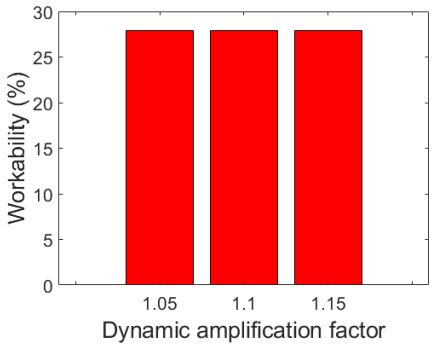

Figure 5.28: Comparing the workability for different dynamic amplification factors, $l1 = 64m$

side-lead angle:

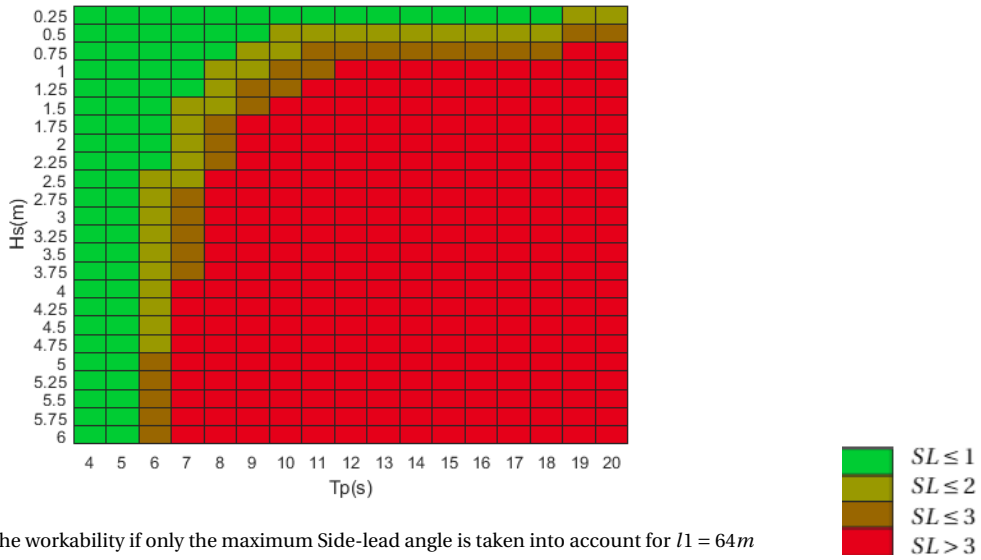

Figure 5.29: The workability if only the maximum Side-lead angle is taken into account for $l1 = 64m$

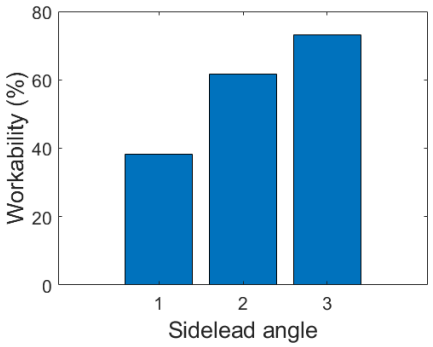

Figure 5.30: The workability when only maximum side-lead angle is taken into account, $l1 = 64m$

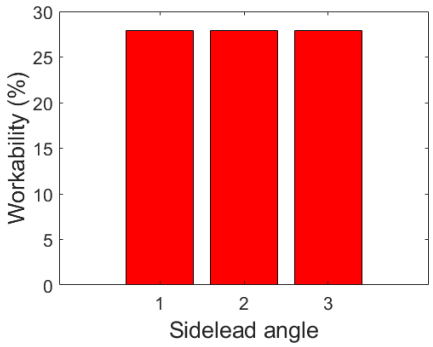

Figure 5.31: Comparing the workability for different maximum side-lead angles, $l1 = 64m$

off-lead angle:

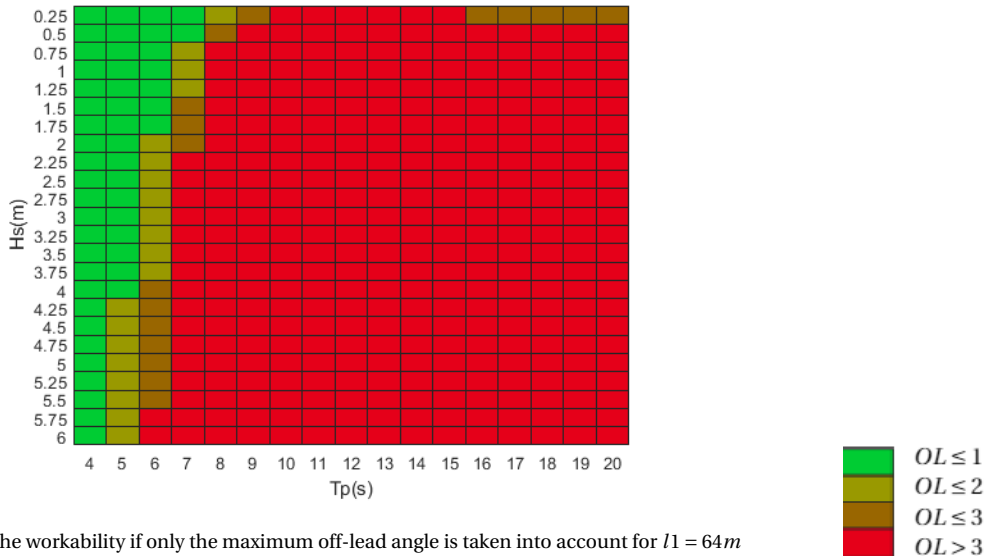

Figure 5.32: The workability if only the maximum off-lead angle is taken into account for $l1 = 64m$

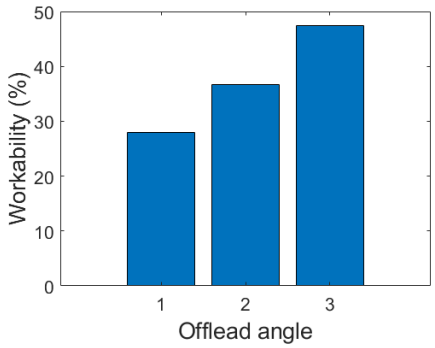

Figure 5.33: The workability when only maximum off-lead angle is taken into account, $l1 = 64m$

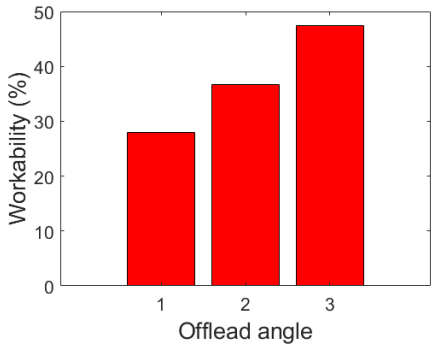

Figure 5.34: Comparing the workability for different maximum off-lead angles, $l1 = 64m$

Total workability

The workability of the limiting factors is combined again to give the total workability for $l1 = 64m$

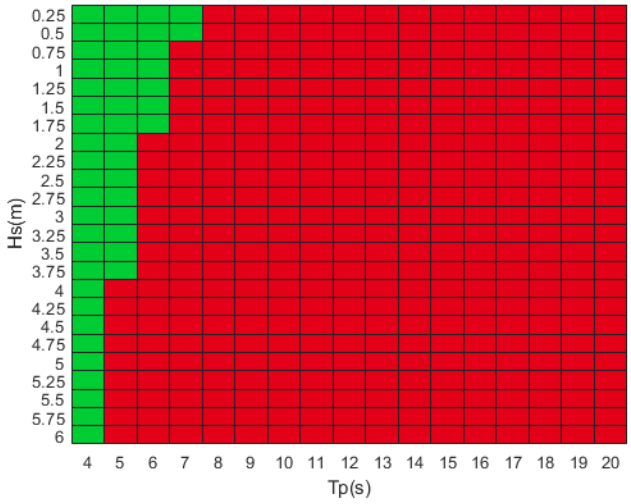

Figure 5.35: The total workability (combining Off-lead angle, Side-lead angle and cable tension workabilitys) for $l1 = 64m$

Also for $l1 = 64m$ the off-lead angle is the limiting factor. Adding up the occurrence percentage of all wave conditions that passed all three limiting factors leads to the total workability of the hoisting at $l1 = 64m$. The occurrence of the wave conditions can be seen in: Appendix C.1.

The total workability for $L1 = 80m$ is: 29.9% and for $L1 = 64m$ the workability is: 27.9%. To increase the workability the three limiting factors are observed and it becomes clear that increasing the off-lead angle from one to two degrees will have the biggest impact on the workability. Increasing the off-lead angle from one to two degrees will increase the workability for $L1 = 80m$ to 44.0% and for $L1 = 64m$ to: 36.7%. Therefor it is advised to increase the maximum off-lead angle of the main crane to two degrees.

5.6. linear model small angle estimation

The linear model used turns out to be accurate enough because during all cases where $F_{dyn} \leq 1.2$ the lower and upper off-lead and side-lead angles as well as the roll, pitch and sway angles are smaller then ten degrees. At an angle of ten degrees the small angle approximation for sinus is 99.5% accurate and the cosinus small angle estimation is almost 100 % accurate as seen in Figure 5.36 [T. Bennison, 2018] The conditions at which the vessel will not exceed ten degrees roll, pitch and yaw can be seen in section D.1.

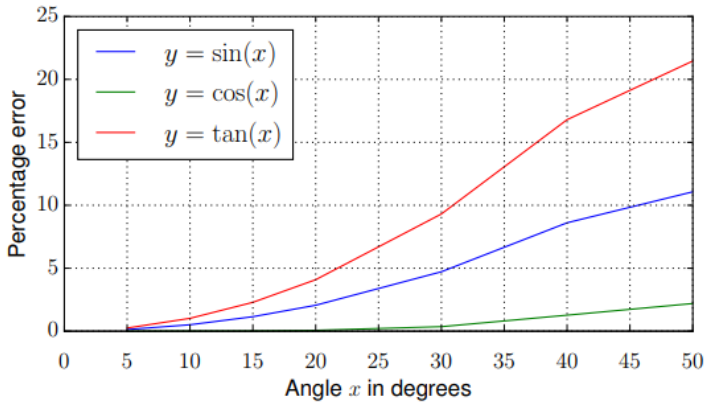

Figure 5.36: The difference between the small angle estimation and the cosinus, sinus and tangens

The crane of the Stella Synergy will have a crane with $F_{dyn} \leq 1.1$ for loads of 2500 ton. Therefor all results that are close to $F_{dyn} = 1.1$ are accurate using this model. When the motions become to severe and the linear model will not be accurate anymore the conditions will not be workable on this vessel anyway. Therefor it is concluded that using small angle estimation in the modelis accurate enough for this problem.

6

Conclusion and recommendations

In this chapter the results and recommendations are discussed.

6.1. Gripper and upending methods and equipment

Upending using the gripper would be the fastest and safest way to upend monopiles with the Stella Synergy. When monopiles are heavier then the maximum lifting capability of the crane the monopiles can be upended in water to reduce the loads on the crane.

The best gripper design for the Stella Synergy will be a motion compensated gripper that is capable of upending. Two good examples of gripper design are the gripper of the Oleg Strasnov and the Huisman two arm gripper. Both are motion compensated and can be made so that they are capable of upending monopiles. The two grippers should be analysed with more detail to make a final decision. The gripper should be capable of gripping the monopile close to the CoG of the monopile so the Stella Synergy will be able to upend the monopiles.

6.2. Vessel motions

Using Aqwa the vessels added mass, damping and undisturbed wave and diffraction forces are calculated. This is done using a 3D model of the vessel. A mesh is made, the mesh size is determined by making the mesh smaller in steps of 1m until the results converge to a constant value. In Matlab the RAOs have been calculated using the hydrodynamic data from Aqwa in combination with the hydro-static properties of the vessel and the viscous roll damping. The calculated RAOs are really close to the measured RAOs from MARIN, only the amplitude off the roll RAO around the roll naturalfrequency is higher. When there are waves in this frequency the motions will be to severe and the difference between 15 and 22 °/m does not matter. However when the model is used for other applications this should be reconsidered. When the viscous roll damping is made higher the calculated and measured RAOs are exactly the same. Jumbo has experienced before that the viscous roll damping measured by MARIN is lower then the real roll damping. This can be because the roll damping measured by MARIN is linearised while it actually is dependent on the roll angular velocity squared.

Using the RAOs the MPM of the vessels motions are calculated. This is done using a Rayleigh distribution. When the crane load curve of the Stella Synergy is taken into account there are only two possible location for the center of the gripper left: $(42,-25)$ and $(70,-25)$. The motions at $(70,-25)$ are far less severe then on $(42,-25)$. The disadvantage is that only monopiles with lengths up to $105m$ can be upended at $(70,-25)$ without coming to close to the secondary crane while it is hoisting the monopiles from a barge into the gripper. Therefor it is advised to place the gripper at $(70,-25)$ unless the monopiles for the upcoming job are getting bigger then 105 m.

6.3. Upending forces and workability

To calculate the forces exerted by the monopile on the gripper and crane a model of the vessel with the monopile attached to it is made. To do this first some simplifications are made. The naturalfrequency of the

monopile on the upending frame is calculated using the stiffness of the hoisting cable. The naturalfrequency of the hoisting cable is between $0.81Hz$ and $1.13Hz$ which is outside of the frequency range of excitation forces. Therefor the hoisting cables are modeled infinitely stiff. To be more certain of this it is advised that the natural frequency is calculated with more detail, for example taking into account the stiffness of the crane itself. When the stiffness of the crane is not assumed to be infinitely stiff the overall stiffness will be lower and therefor the natural frequency will be lower because $f \propto \sqrt{c/m}$. Lifting a lighter monopile will increase the naturalfrequency and therefor the difference between naturalfrequency and excitation frequencies will become bigger, so for lighter monopiles the hoisting cable can also be assumed to be infinitely stiff.

The upending process has been split up into 6 phases. The forces on the crane and gripper are calculated for these phases. First the mass, added mass, diffraction and undisturbed wave forces are calculated using AQWA. The vessel is modeled with the monopile next to it for the phases where the monopile is partly submerged. The vessel is kept statically up straight and at the same draft by using ballasting. The needed ballast is calculated and the changes in the mass matrix because of ballasting and the location of the monopile on the vessel are taken into account, also GM and therefor the stiffness matrix changes from phase to phase. The viscous damping of the monopile is modeled using the drag coefficient of a cylinder, for a Reynolds number of 10^7 C_D is around 1. C_D has also been computed using the Keulegan and Carpenter number, which had the same results. Then the viscous roll and pitch damping coefficients are calculated using stochastic linearisation.

The $\boldsymbol{M}$, $\boldsymbol{A}$, $\boldsymbol{B}$, $\boldsymbol{B_{add}}$ $\boldsymbol{C}$ and $\boldsymbol{L}$ matrices change every phase. Therefor the RAOs are obtained for every phase. Then the forces and moments at the center of gravity of the monopile are calculated using the model. The buoyancy and gravitational forces on the monopile are combined to calculate the static forces and moments on the gripper and crane. Although some similarities are seen between the phases the dynamic forces differ so much that two extra phases have been added with $\theta_u = 45°$ and $\theta_u = 75°$. With the extra phases the transition between the phases has become a lot smaller and more understandable. The dynamic forces in all directions are the biggest during phase 3. Because the graph shape of phase 3 has the least similar shape compared to the other phases it might be use-full to add another phase in between phase 3 and 3.5. Also the moment that the monopile just touches the water can cause high forces and needs to be studied in more detail. The statical forces on the crane during phase one to five are less then 10% of the maximum lifting capacity of the crane. Therefor the workability is only calculated for phase six where the forces on the static forces on the crane are almost 100% of the lifting capacity. The total workability for phase six is calculated using a wave scatter diagram from the central North Sea. The workability for upending during phase six is: 34.3%.

6.4. Hoisting forces and workability

A model is made from the Stella Synergy while it is hoisting a monopile from a barge next to the vessel. The monopile is modeled as a hollow cylinder and the hoisting cable is split up in two parts: the top part which is a single cable and the bottom part which are two cables 60° apart from each other. The cable is allowed to hinge between part one and part two. The cable is assumed to be infinitely stiff. This results in a 10 degree of freedom system: the six degrees of freedom from the vessel plus two angles for each part of cable. The system is modeled using virtual displacement. This results in new mass and damping matrices. Using these the RAOs of the vessel and monopile are calculated. Then the MPM of the motions are calculated.

The crane has three main limiting factors: The maximum dynamic amplification factor, the off-lead angle and the side-lead angle. The MPM off these three factors are calculated using the RAOs and a Rayleigh distribution. Then the workability is calculated by doing the previous calculation over for all wave conditions displayed in the wavescatter sheet. This is done for a $L1 = 64m$ and a $L1 = 80m$ because this is the minimum and maximum cable length used while hoisting the monopile. It becomes clear that the maximum off-lead angle is the limiting factor for the workability. The total workability for $L1 = 80m$ is: 29.9% and for $L1 = 64m$ the workability is: 27.9% Increasing the off-lead angle from one to two degrees will increase the workability for $L1 = 80m$ to 44.0% and for $L1 = 64m$ to: 36.7% The linear model with small angle estimation is checked to be accurate enough to be used in this model

6.5. Total workability

To be able to know the total workability of installing a monopile using the Stella Synergy further research has to be done in the dynamic positioned gripper that might be used. The companies that make the gripper all claim it will be workable with waves up to: $Hs = 3m$. This is a really unreliable statement since the motions at $Hs = 3m$ are different for every vessel and wave period. The grippers are still in an experimental state and although it sounds like a great solution for the Stella Synergy more proof of concept has to be given by the companies who make and design the gripper.

To understand the limitations of the workability better it is advised to calculate the seasonal workability for the monopile installation. In some areas it is not allowed to install monopiles during the seal breading season. If these months have more workable conditions then the other months it is possible that the total workability of the vessel is a lot lower.

When monopiles in other areas are installed other wave spectra should be analysed. A JONSWAP spectrum will not work for areas with a lot of swell. Because the long period swell waves cause larger excitation of the vessel swell will cause the workability to be lower. In areas with a lot of swell the wave directions can also differ a lot. Two waves can come from totally different directions. This should also be analysed when monopiles are planned to be installed in swell prone areas.

A

Vessel Motions Appendix

A.1. radiation potential

The velocity potential function Φ describes the potential of a fluid at a certain location. The derivative of Φ in a direction is the velocity of the fluid flow in that direction.

$$u = \frac{\partial \Phi}{\partial x}; \quad v = \frac{\partial \Phi}{\partial y}; \quad w = \frac{\partial \Phi}{\partial z} \tag{A.1}$$

The velocity potential is split up in:

- Φ_0 is the potential of the incoming undisturbed wave
- Φ_7 is the diffraction potential
- Φ_1 to Φ_6 are the radiation potentials for every degree of freedom

To calculate the radiation forces water is assumed to be non viscous and incompressable and irrotational.

$$\frac{\partial u}{\partial x} + \frac{\partial v}{\partial y} + \frac{\partial w}{\partial z} = 0 \tag{A.2}$$

This results in the Laplace equation:

$$\frac{\partial^2 \Phi}{\partial x^2} + \frac{\partial^2 \Phi}{\partial y^2} + \frac{\partial^2 \Phi}{\partial z^2} = 0 \tag{A.3}$$

Using Bernoulli the pressure can be calculated with the velocity potentials.

$$p = -\rho \frac{\partial \Phi}{\partial t} - \frac{1}{2}(u^2 + v^2 + w^2) - \rho g z \tag{A.4}$$

$-\frac{1}{2}(u^2 + v^2 + w^2)$ is small enough to be neglected (second order). To obtain the forces and moments on the surface, the pressure is integrated over the submerged surface:

$$F = \iint_S (pf)\, dS = \iint_S \left(\rho \frac{\partial \Phi}{\partial t} f\right) dS \tag{A.5}$$

Where f is the motion in the normal direction of the surface of the vessel compared to a motion in the global coordinate system.

$$\begin{vmatrix} f_1 \\ f_2 \\ f_3 \\ f_4 \\ f_5 \\ f_6 \end{vmatrix} = \begin{vmatrix} \cos(n,x) \\ \cos(n,y) \\ \cos(n,z) \\ y\cos(n,z) - z\cos(n,y) \\ z\cos(n,x) - x\cos(n,z) \\ x\cos(n,y) - y\cos(n,x) \end{vmatrix} \tag{A.6}$$

Splitting Φ up in a time and space dependent part results in:

$$\Phi_n = Re\left\{\phi_n v_a e^{-i\omega t}\right\} = Re\left\{\phi_n s_a(-i\omega)e^{-i\omega t}\right\} \quad for \quad n = 1,...,6 \tag{A.7}$$

where v_a is the complex amplitude of velocity and s_a is the complex amplitude of displacement

$$F_{r,j,k} = Re\left\{-\rho\omega^2 s_{a,k}\iint_S (\phi_k n_j)\, dS\, e^{-i\omega t}\right\} = Re\left\{-a\dot{v}_{a,k}e^{-i\omega t} - bv_{a,k}e^{-i\omega t}\right\} = Re\left\{a\omega^2 s_{a,k}e^{-i\omega t} + ib\omega s_{a,k}e^{-i\omega t}\right\} \tag{A.8}$$

from this we find the following formulas for a and b:

$$a_{j,k} = -\rho Re\left\{\iint_S (\phi_k f_j)\, dS\right\} \quad for \quad j = 1,...,6 \tag{A.9}$$

$$b_{j,k} = -\rho\omega Im\left\{\iint_S (\phi_k f_j)\, dS\right\} \quad for \quad j = 1,...,6 \tag{A.10}$$

$\Phi_1,...,\Phi_6$ are calculated using a panel method like Aqwa (chapter3.2.6)

A.2. undisturbed incoming wave and difraction forces

.

The flow potential due to an undisturbed wave in deep water is:

$$\Phi_0 = -\frac{\zeta_a g}{\omega} e^{kz}\sin(\omega t - kxcos(\mu) - kysin(\mu)) \tag{A.11}$$

where μ is the direction which the wave goes and k is the wave number.
from this we can calculate the pressure:

$$p_{\Phi_0+\Phi_7} = -\rho\frac{\partial(\Phi_0+\Phi_7)}{\partial t} \tag{A.12}$$

using this pressure the force can be calculated by integrating over the surface.

$$F_D + F_W = \iint_S \left(p_{\Phi_0+\Phi_7} f\right) dS \tag{A.13}$$

A.3. panelmethod

To be able to calculate the radiation and diffraction potentials for the whole vessel the vessel is split up in a a lot of small surfaces; panels. Every panel has a source strength σ which generates a potential square to the panel. Every panel is influenced by the sources of the other panels as well as the boundary conditions of the bottom and the surface of the ocean. Because the bottom of the ocean is assumed rigid the ocean water can not flow into the bottom so the boundary condition is:

$$\left(\frac{\partial\phi}{\partial z}\right)_{z=-h} = 0 \tag{A.14}$$

where h is the water depth. At the free surface the boundary conditions are:

$$\left(\frac{\partial^2\phi}{\partial t^2}\right)_{z=0} + g\left(\frac{\partial\phi}{\partial z}\right)_{z=0} = 0, \quad \left(\frac{\partial\phi}{\partial z}\right)_{z=-h} = \frac{\partial\zeta}{\partial t} \tag{A.15}$$

To find the diffraction potential the following formula needs to be solved for every panel m taking into account every panel n on the vessel.

$$-\frac{1}{2}\sigma_{m7} + \frac{1}{4\pi}\frac{\partial G_{mn}}{\partial n}\Delta S_n = -\left(\frac{\partial\Phi_0}{\partial n}\right)_m \tag{A.16}$$

This leads to the following formula:

$$\begin{bmatrix} A_{11} & ... & A_{1N} \\ ... & ... & ... \\ A_{N1} & ... & A_{NN} \end{bmatrix} \begin{vmatrix} \sigma_{1,7} \\ ... \\ \sigma_{N,7} \end{vmatrix} = \begin{vmatrix} -\left(\frac{\partial(\phi_0)}{\partial n}\right)_1 \\ ... \\ -\left(\frac{\partial(\phi_0)}{\partial n}\right)_N \end{vmatrix} \tag{A.17}$$

Where A_{mn} is the influence of panel n on $\frac{\partial \phi_7}{\partial n}$ at panel m: $A_{mn} = \frac{1}{4\pi}\frac{\partial G_{mn}}{\partial n}\Delta S_n$ and $\sigma_{n,7}$ is the unknown source strength of the diffraction potential at panel n. N are the number of panels that are used to describe the surface of the vessel.

To find the radiation potentials the boundary conditions at the hull are needed:

$$\frac{\partial \Phi_j}{\partial n} = \frac{\partial \phi_j}{\partial n}(-i\omega s_a e^{-i\omega t}) = v_n = f_j(-i\omega s_a e^{-i\omega t}) \quad for \quad j = 1,...,6 \tag{A.18}$$

Where v_n is the local body velocity in normal direction. From this can be concluded that:

$$\frac{\partial \phi_j}{\partial n} = f_j \quad for \quad j = 1,...,6 \tag{A.19}$$

Using the boundary conditions the radiation potential is calculated as follows for every panel:

$$-\frac{1}{2}\sigma_{mj} + \frac{1}{4\pi}\sum_{n=1}^{N}\sigma_{nj}\frac{\partial G_{mn}}{\partial n}\Delta S_n = f_{mj} \quad for \quad j = 1,...,6 \tag{A.20}$$

This can be written using matrices as:

$$\begin{bmatrix} A_{11} & ... & A_{1N} \\ ... & ... & ... \\ A_{N1} & ... & A_{NN} \end{bmatrix} \begin{vmatrix} \sigma_{1,j} \\ ... \\ \sigma_{N,j} \end{vmatrix} = \begin{vmatrix} f_{j1} \\ ... \\ f_{jN} \end{vmatrix} \quad for \quad j = 1,...,6 \tag{A.21}$$

Where j indicates the radiation potential that is being calculated.
These formulas are solved in Aqwa.

B

Upending Forces Appendix

B.1. Dynamic forces on gripper and crane

B.1.1. phase 1

The dynamicalforces and moments of phase 1 per meter wave amplitude dependent on the wave period are:

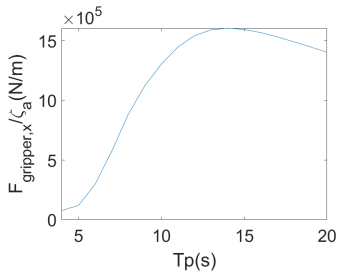

Figure B.1: Phase 1: forces on gripper in x direction per meter wave height

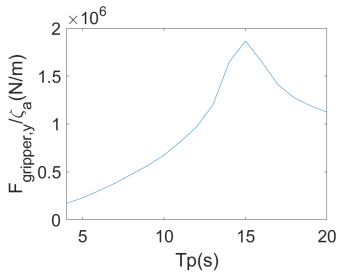

Figure B.2: Phase 1: forces on gripper in y direction per meter wave height

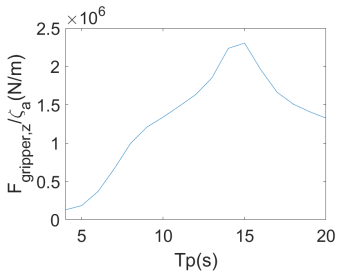

Figure B.3: Phase 1: forces on gripper in z direction per meter wave height

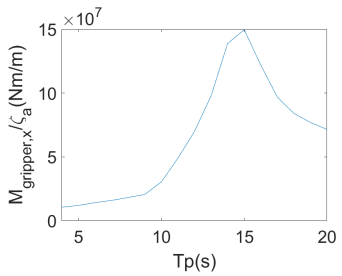

Figure B.4: Phase 1: moments on gripper around the x axis per meter wave height

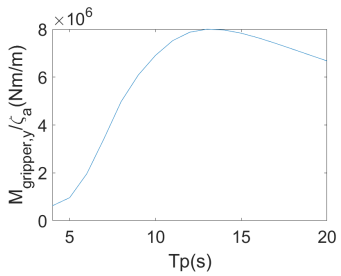

Figure B.5: Phase 1: moments on gripper around the y axis per meter wave height

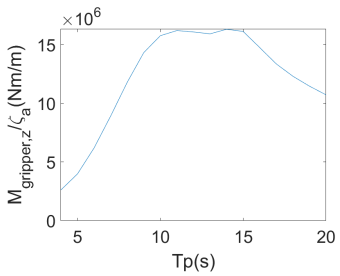

Figure B.6: Phase 1: moments on gripper around the z axis per meter wave height

B.1.2. phase 2

The dynamical forces and moments of phase 2 per meter wave amplitude dependent on the wave period are:

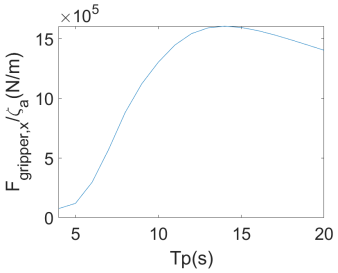

Figure B.7: Phase 2: forces on gripper in x direction per meter wave height

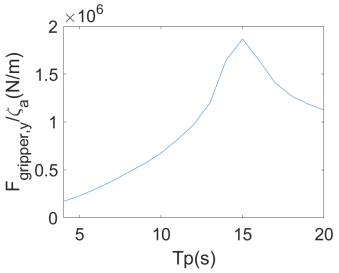

Figure B.8: Phase 2: forces on gripper in y direction per meter wave height

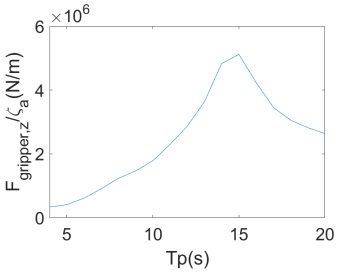

Figure B.9: Phase 2: forces on gripper in z direction per meter wave height

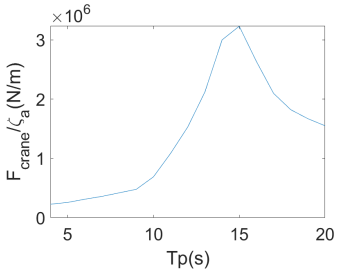

Figure B.10: Phase 2: Forces on crane in z direction per meter wave height

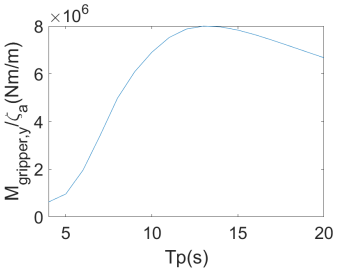

Figure B.11: Phase 2: moments on gripper around the y axis per meter wave height

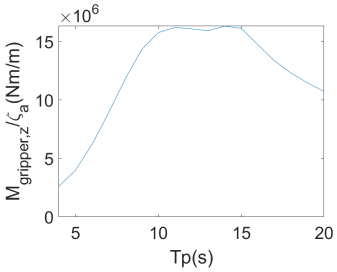

Figure B.12: Phase 2: moments on gripper around the z axis per meter wave height

B.1.3. phase 3

The dynamical forces and moments of phase 3 per meter wave amplitude dependent on the wave period are:

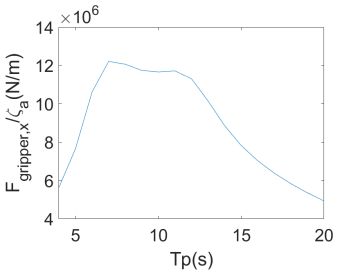

Figure B.13: Phase 3: forces on gripper in x direction per meter wave height

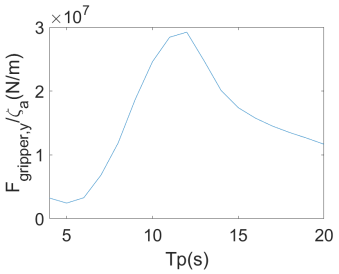

Figure B.14: Phase 3: forces on gripper in y direction per meter wave height

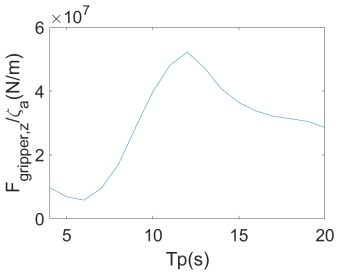

Figure B.15: Phase 3: forces on gripper in z direction per meter wave height

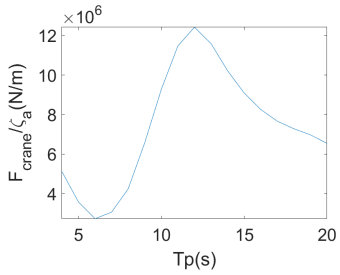

Figure B.16: Phase 3: Forces on crane in z direction per meter wave height

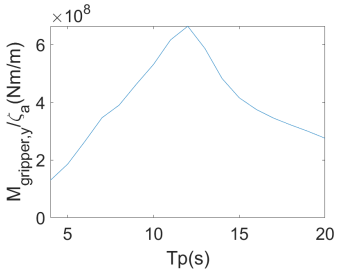

Figure B.17: Phase 3: moments on gripper around the y axis per meter wave height

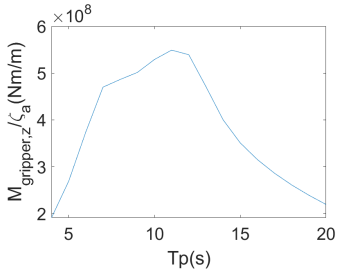

Figure B.18: Phase 3: moments on gripper around the z axis per meter wave height

B.1.4. phase 4

The dynamical forces and moments of phase 4 per meter wave amplitude dependent on the wave period are:

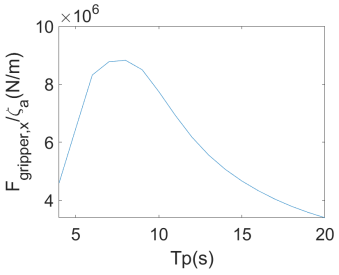

Figure B.19: Phase 4: forces on gripper in x direction per meter wave height

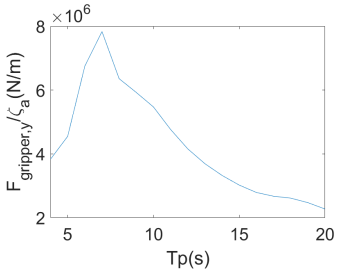

Figure B.20: Phase 4: forces on gripper in y direction per meter wave height

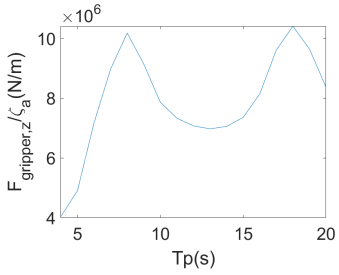

Figure B.21: Phase 4: forces on gripper in z direction per meter wave height

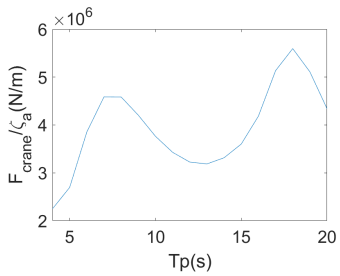

Figure B.22: Phase 4: Forces on crane in z direction per meter wave height

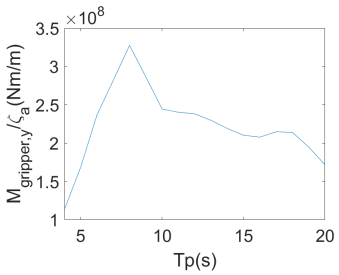

Figure B.23: Phase 4: moments on gripper around the y axis per meter wave height

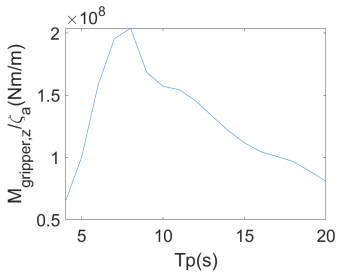

Figure B.24: Phase 4: moments on gripper around the z axis per meter wave height

B.1.5. phase 5

The dynamical forces and moments of phase 5 per meter wave amplitude dependent on the wave period are:

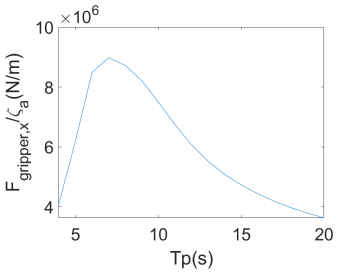

Figure B.25: Phase 5: forces on gripper in x direction per meter wave height

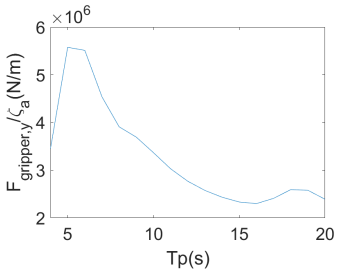

Figure B.26: Phase 5: forces on gripper in y direction per meter wave height

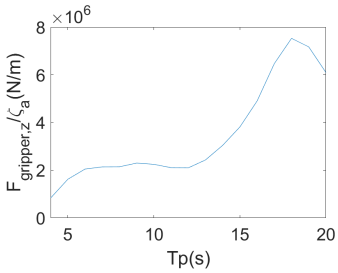

Figure B.27: Phase 5: forces on gripper in z direction per meter wave height

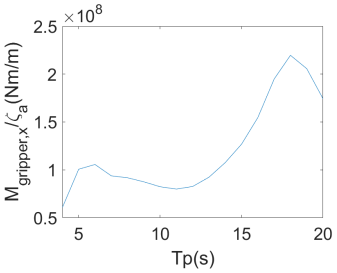

Figure B.28: Phase 5: moments on gripper around the x axis per meter wave height

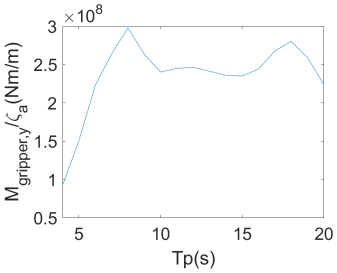

Figure B.29: Phase 5: moments on gripper around the y axis per meter wave height

B.1.6. phase 6

The dynamical forces and moments of phase 6 per meter wave amplitude dependent on the wave period are:

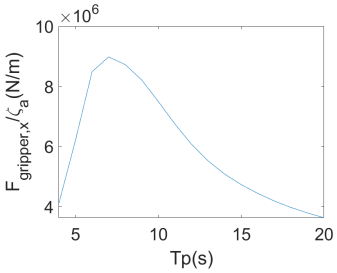

Figure B.30: Phase 6: forces on gripper in x direction per meter wave height

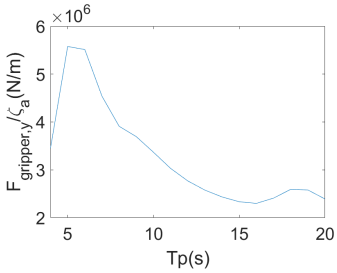

Figure B.31: Phase 6: forces on gripper in y direction per meter wave height

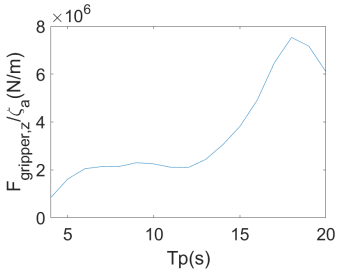

Figure B.32: Phase 6: Forces on crane in z direction per meter wave height

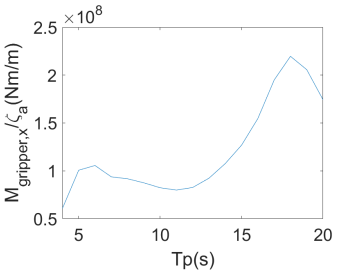

Figure B.33: Phase 6: moments on gripper around the x axis per meter wave height

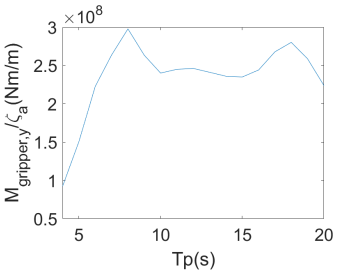

Figure B.34: Phase 6: moments on gripper around the y axis per meter wave height

B.1.7. phase 3.5

The dynamical forces and moments of phase 3.5 per meter wave amplitude dependent on the wave period are:

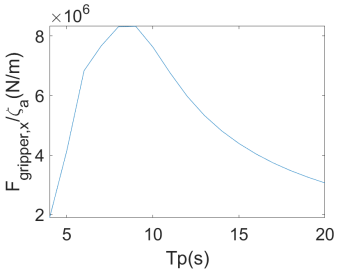

Figure B.35: Phase 3.5: forces on gripper in x direction per meter wave height

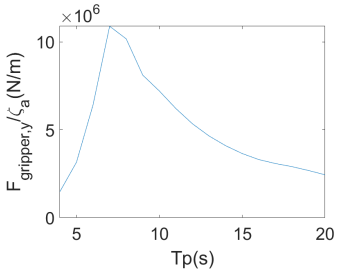

Figure B.36: Phase 3.5: forces on gripper in y direction per meter wave height

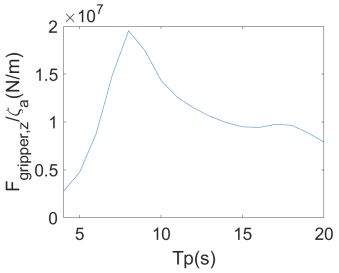

Figure B.37: Phase 3.5: forces on gripper in z direction per meter wave height

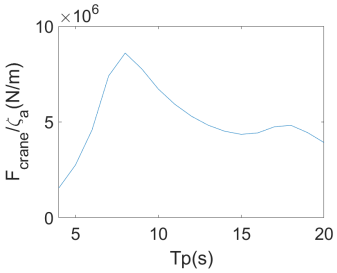

Figure B.38: Phase 3.5: Forces on crane in z direction per meter wave height

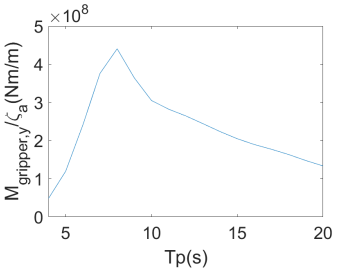

Figure B.39: Phase 3.5: moments on gripper around the y axis per meter wave height

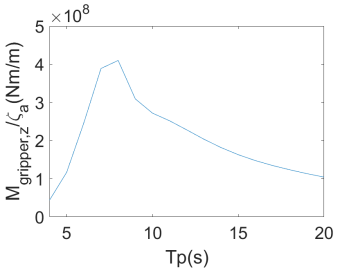

Figure B.40: Phase 3.5: moments on gripper around the z axis per meter wave height

B.1.8. phase 4.5

The dynamical forces and moments of phase 4.5 per meter wave amplitude dependent on the wave period are:

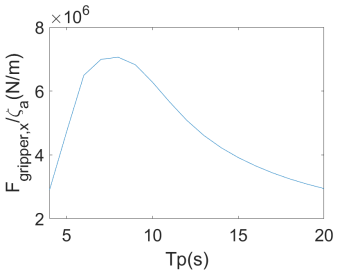

Figure B.41: Phase 4.5: forces on gripper in x direction per meter wave height

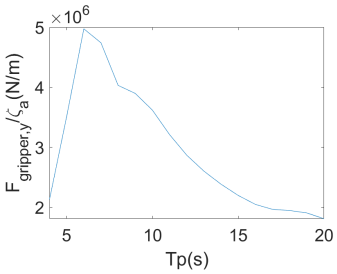

Figure B.42: Phase 4.5: forces on gripper in y direction per meter wave height

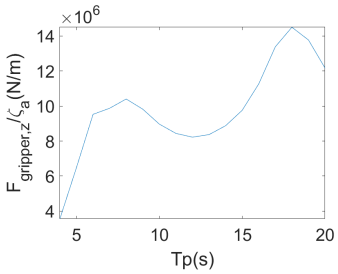

Figure B.43: Phase 4.5: forces on gripper in z direction per meter wave height

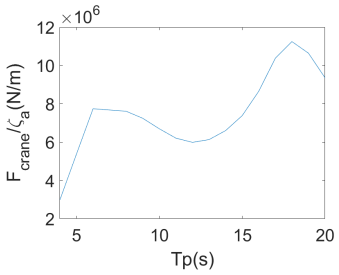

Figure B.44: Phase 4.5: Forces on crane in z direction per meter wave height

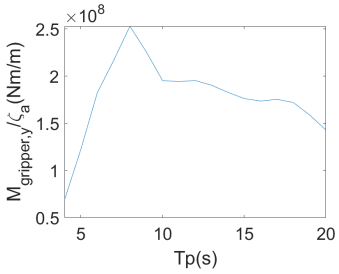

Figure B.45: Phase 4.5: moments on gripper around the y axis per meter wave height

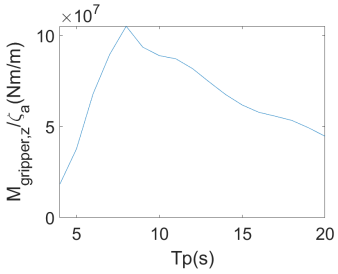

Figure B.46: Phase 4.5: moments on gripper around the z axis per meter wave height

C

Workability Appendix

C.1. wavescatter

Hs(m)		Tp [s] 2 - 3	3 - 4	4 - 5	5 - 6	6 - 7	7 - 8	8 - 9	9 - 10	10 - 11	11 - 12	12 - 13	13 - 14	14 - 15	15 - 16	16 - 17	17 - 18	18 - 19	19 - 20
0.00	0.25	0.0%	0.2%	0.0%	0.0%	0.1%	0.1%	0.0%	0.0%	0.0%	0.0%	0.0%	0.0%	0.0%	0.0%	0.0%	0.0%	0.0%	0.0%
0.25	0.50	0.0%	0.6%	2.0%	0.6%	0.6%	0.3%	0.4%	0.3%	0.2%	0.1%	0.1%	0.0%	0.0%	0.0%	0.0%	0.0%	0.0%	0.0%
0.50	0.75	0.0%	0.5%	2.3%	2.1%	1.2%	0.8%	0.8%	0.4%	0.2%	0.1%	0.1%	0.0%	0.0%	0.0%	0.0%	0.0%	0.0%	0.0%
0.75	1.00	0.0%	0.3%	3.0%	5.4%	3.7%	1.9%	1.8%	1.1%	0.3%	0.3%	0.1%	0.1%	0.0%	0.0%	0.0%	0.0%	0.0%	0.0%
1.00	1.25	0.0%	0.0%	1.2%	3.1%	2.8%	1.9%	1.1%	0.8%	0.3%	0.1%	0.1%	0.0%	0.0%	0.0%	0.0%	0.0%	0.0%	0.0%
1.25	1.50	0.0%	0.0%	0.4%	3.7%	4.3%	2.4%	1.4%	1.2%	0.6%	0.2%	0.1%	0.0%	0.0%	0.0%	0.0%	0.0%	0.0%	0.0%
1.50	1.75	0.0%	0.0%	0.0%	1.2%	2.6%	1.6%	0.9%	0.7%	0.4%	0.2%	0.1%	0.0%	0.0%	0.0%	0.0%	0.0%	0.0%	0.0%
1.75	2.00	0.0%	0.0%	0.0%	0.7%	3.3%	2.4%	1.3%	0.7%	0.7%	0.3%	0.1%	0.0%	0.0%	0.0%	0.0%	0.0%	0.0%	0.0%
2.00	2.25	0.0%	0.0%	0.0%	0.1%	1.6%	1.7%	0.9%	0.4%	0.3%	0.2%	0.0%	0.0%	0.0%	0.0%	0.0%	0.0%	0.0%	0.0%
2.25	2.50	0.0%	0.0%	0.0%	0.0%	1.3%	2.2%	1.1%	0.5%	0.3%	0.2%	0.1%	0.0%	0.0%	0.0%	0.0%	0.0%	0.0%	0.0%
2.50	2.75	0.0%	0.0%	0.0%	0.0%	0.3%	1.1%	0.6%	0.3%	0.1%	0.1%	0.1%	0.0%	0.0%	0.0%	0.0%	0.0%	0.0%	0.0%
2.75	3.00	0.0%	0.0%	0.0%	0.0%	0.2%	1.0%	1.1%	0.4%	0.1%	0.1%	0.1%	0.1%	0.0%	0.0%	0.0%	0.0%	0.0%	0.0%
3.00	3.25	0.0%	0.0%	0.0%	0.0%	0.0%	0.4%	0.7%	0.2%	0.1%	0.1%	0.1%	0.0%	0.0%	0.0%	0.0%	0.0%	0.0%	0.0%
3.25	3.50	0.0%	0.0%	0.0%	0.0%	0.0%	0.2%	0.8%	0.4%	0.1%	0.1%	0.0%	0.0%	0.0%	0.0%	0.0%	0.0%	0.0%	0.0%
3.50	3.75	0.0%	0.0%	0.0%	0.0%	0.0%	0.0%	0.4%	0.3%	0.1%	0.0%	0.0%	0.0%	0.0%	0.0%	0.0%	0.0%	0.0%	0.0%
3.75	4.00	0.0%	0.0%	0.0%	0.0%	0.0%	0.0%	0.3%	0.4%	0.1%	0.0%	0.0%	0.0%	0.0%	0.0%	0.0%	0.0%	0.0%	0.0%
4.00	4.25	0.0%	0.0%	0.0%	0.0%	0.0%	0.0%	0.1%	0.2%	0.1%	0.0%	0.0%	0.0%	0.0%	0.0%	0.0%	0.0%	0.0%	0.0%
4.25	4.50	0.0%	0.0%	0.0%	0.0%	0.0%	0.0%	0.0%	0.3%	0.1%	0.0%	0.0%	0.0%	0.0%	0.0%	0.0%	0.0%	0.0%	0.0%
4.50	4.75	0.0%	0.0%	0.0%	0.0%	0.0%	0.0%	0.0%	0.1%	0.1%	0.0%	0.0%	0.0%	0.0%	0.0%	0.0%	0.0%	0.0%	0.0%
4.75	5.00	0.0%	0.0%	0.0%	0.0%	0.0%	0.0%	0.0%	0.1%	0.1%	0.0%	0.0%	0.0%	0.0%	0.0%	0.0%	0.0%	0.0%	0.0%
5.00	5.25	0.0%	0.0%	0.0%	0.0%	0.0%	0.0%	0.0%	0.0%	0.1%	0.1%	0.0%	0.0%	0.0%	0.0%	0.0%	0.0%	0.0%	0.0%
5.25	5.50	0.0%	0.0%	0.0%	0.0%	0.0%	0.0%	0.0%	0.0%	0.1%	0.0%	0.0%	0.0%	0.0%	0.0%	0.0%	0.0%	0.0%	0.0%
5.50	5.75	0.0%	0.0%	0.0%	0.0%	0.0%	0.0%	0.0%	0.0%	0.0%	0.0%	0.0%	0.0%	0.0%	0.0%	0.0%	0.0%	0.0%	0.0%
5.75	6.00	0.0%	0.0%	0.0%	0.0%	0.0%	0.0%	0.0%	0.0%	0.0%	0.0%	0.0%	0.0%	0.0%	0.0%	0.0%	0.0%	0.0%	0.0%

D

Conclusion Appendix

D.1. small angle estimation

The conditions at which the vessel will not exceed a roll angle of ten degrees are marked green:

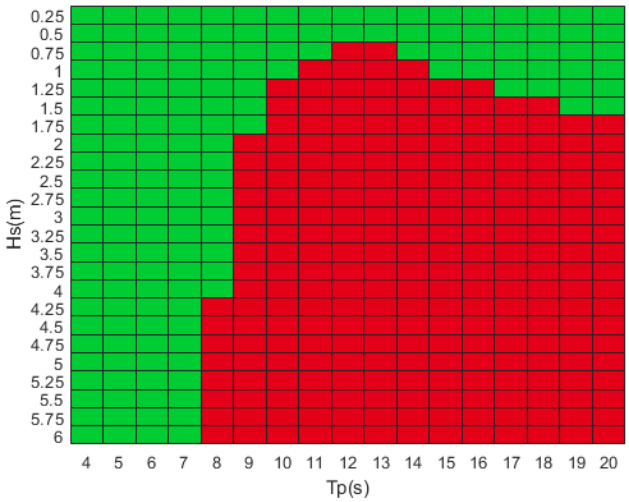

Figure D.1: The conditions at which the vessel does not exceed a roll angle of ten degrees

The conditions at which the vessel will not exceed a pitch angle of ten degrees areare marked green:

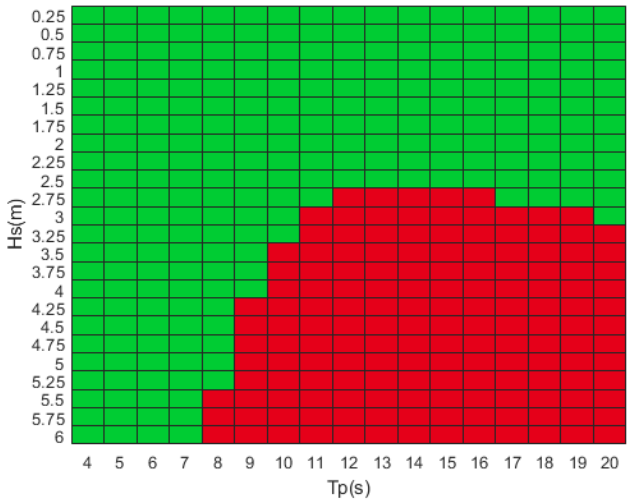

Figure D.2: The conditions at which the vessel does not exceed a pitch angle of ten degrees

The conditions at which the vessel will not exceed a yaw angle of ten degrees areare marked green:

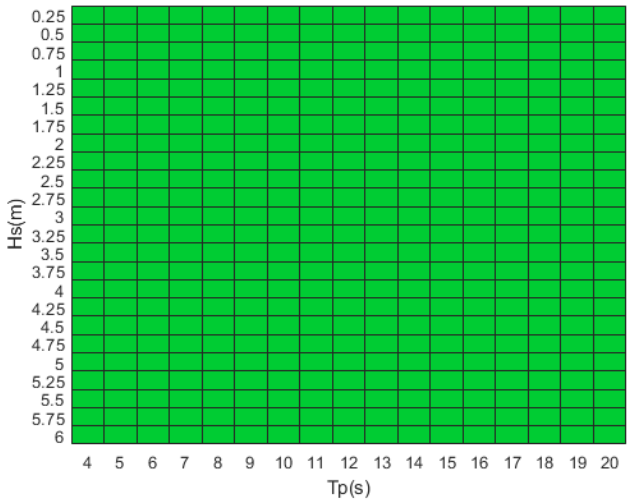

Figure D.3: The conditions at which the vessel does not exceed a yaw angle of ten degrees

Bibliography

4c offshore. Concrete monopile weight. *Monopile support structures*, 2013.

A. Bosch. Next generation wtg foundation and wtg installation. *Wind Days presentation*, 2018.

L.G. Buitendijk. Concrete monopile weight. *Floating installation of offshore wind turbine foundations*, 2016.

L. Charles. Chapter 9. *On the probability distribution of wave force and an introduction to t he correlation drag coefficient and the corelation inertial coefficient*, 1964.

General-electric. Haliade-x offshore wind turbine platform. *website GE*, 2018.

L. H. Carpenter G.H. Keulegan. Forces on cylinders and plates in an oscillating fluid. *Journal of Research of the National Bureau of Standards*, 1985.

T. Haver. Roll damping predictions for vessels; sheerlegs and barges. *Noble Denton Research Project and Allen H.Magnuson*, 2016.

Y. Himeno. Prediction of ship roll damping state of the art. 1981.

ir. Joost den Haan. Monopile installation phases. *slides OE44100 Floating Structures and Mooring Systems TU Delft lecture 1a*, 2018.

S. Widnall J. Peraire. Products of inertia in a plane. *3D Rigid Body Dynamics: The Inertia Tensor*, 2008.

J.B.Crol. Upending of a monopile for an offshore wind turbine foundation. *experimental upending of a monopile wind turbine foundation*, 2015.

Jumbo-maritime. Crane curve graph. *confidential Jumbo document*, 2018.

H.E. Krogstad and Ø.A. Arntsen. Random waves and wave statistics. *Linear wave theory*, 2000.

Marin. Marin vessel motions. *confidential Jumbo document*, 2018.

R. May. Multiple wave spectra. *Ansys manual presentation*, 2012.

NorthSee. Next generation wtg foundation and wtg installation. *Increased depth of offshore wind farms/further offshore and increased turbine capacity*, 2018.

E. Hall T. Bennison. Small angle approximations. *A-Level Mathematics Tarquin Year one*, 2018.

University-Strathclyde. Xl monopile weight. *The Practicality and Challenges of Using XL Monopiles for Offshore Wind Turbine Substructures*, 2015.

Alex van der Steen. One m7-a. *website werken in de offshore*, 2017.

M. Dolores Esteban∗ Pablo Alberdi Mario Imaz José-María Serraclara Vicente Negro, José-Santos López-Gutiérrez. Monopiles in offshore wind: Preliminary estimate of main dimensions. *Discussion*, 2015.

Yaguo Lyu Nicolas Boisson Wenjun Gao, Daniel Nelias. Numerical investigations on drag coefficient of circular cylinder with two free ends in roller bearings. *Introduction*, 2018.

J.R. Whelan Y. Drobyshevski. An approximate method for stochastic linearization of viscous roll damping. *ASME 2010 29th International Conference on Ocean, Offshore and Arctic Engineering*, 2018.